TUDelft

Delft University of Technology

Detecting Single Photons with Superconducting Nanowires

Chang, J.

Important note
To cite this publication, please use the final published version (if applicable).
Please check the document version above.

Detecting Single Photons with Superconducting Nanowires

Detecting Single Photons with Superconducting Nanowires

Proefschrift

ter verkrijging van de graad van doctor
aan de Technische Universiteit Delft,
op gezag van de Rector Magnificus Prof.dr.ir. T.H.J.J. van der Hagen,
voorzitter van het College voor Promoties,
in het openbaar te verdedigen op Donderdag 23 September 2021 om 12:30 uur

door

Jin CHANG

Master of Material Engineering, National University of Defense Technology,
Changsha, China
geboren te Zibo, China.

Dit proefschrift is goedgekeurd door de promotoren.

Samenstelling promotiecommissie bestaat uit:

Rector Magnificus,	voorzitter
Prof.dr. H.P. Urbach,	Technische Universiteit Delft, promotor
Prof.dr. V. Zwiller,	KTH Royal Institute of Technology, promotor

Onafhankelijke leden:

Prof.dr. L. You	SIMIT, CAS, China
Prof.dr. R.H. Hadfield	U. Glasgow, UK
Prof.dr. Y.M. Blanter	Technische Universiteit Delft
Dr.ir. D.R. Schaart	Technische Universiteit Delft
Prof.dr. S. Gröblacher	Technische Universiteit Delft, reservelid

To my parents and parents in law, my wife Yun, and our cat Tiny White.

Jin Chang

Contents

Summary

In the past decades, generating single photons on demand with well defined quantum states and detecting them after photon-photon or photon-matter interaction are central to the area of quantum optics and quantum information science. The ability to detect light efficiently at the single photon level offers unprecedented opportunities for a wide range of applications, including long-distance quantum key distribution, light detection and ranging, photonic quantum computing, weak light detection for astronomy and bio-imaging.

In order to register every interesting photon, different approaches and technologies have been developed to realize efficient single photon detection. Since the first inception in 2001, superconducting nanowire single photon detectors (SNSPDs) have become the best available technology nowadays for single photon detection, covering the electromagnetic spectrum form X-ray till mid-infrared. In this thesis, efforts are made from three major aspects: superconducting material optimization and new SNSPDs material exploration (chapter 3 and 4), large-size and mid-infrared SNSPDs system development (chapter 5 and 6), and near-unity system detection efficiency SNSPDs systems solution (chapter 7). In the end, we also offer inspiring perspectives, point out potential challenges and game-changing applications for future SNSPDs systems. (chapter 8)

As a start, **chapter 2** reviews SNSPDs' evolution history since its first demonstration in 2001 from four vital aspects. (i) SNSPDs' development route in the past decades is systematically summarized, including the pursuit of near-unity detection efficiency, methods to overcome practical operation trade-offs, solutions to reduce the dark count rate as well as improvements to push timing jitter to few picosecond level; (ii) Leading theoretical models to explain SNSPDs' working mechanism are discussed to have a better understating of the physics process of photon detection; (iii) State-of-the-art SNSPDs works based on different material platforms are comprehensively presented, besides, device geometrical dimension, targeted detection wavelength range and pixel numbers are also summarized ; (iv) Applications enabled or greatly benefited from high-performance SNSPDs are provided. Thus, chapter 1 offers a complete picture of the SNSPDs development history, underlying physics, current progress, and future game-changing applications.

Then from superconducting material growth aspect, **chapter 3** explores and optimizes the properties of $Nb_xTi_{1-x}N$ by taking advantage of the flexibility of reactive co-sputter deposition. By tailoring the chemical composition of $Nb_xTi_{1-x}N$ superconducting films, we present optimized sputtering recipe and SNSPDs made from the corresponding film achieved a saturation plateau at 1550 nm with 80% system detection efficiency and 19.5 ps timing jitter.

As a following step, **chapter 4** for the first time shows SNSPDs made from novel granular $Nb_{0.15}Re_{0.85}$ superconducting film. The main figures of merit of the NbRe

detectors are extracted from a flood illumination characterization at 2.8 K, featuring a saturated internal efficiency up to 1301 nm, recovery times between 8-19 ns and jitter of ~35 ps. These results confirm that $Nb_{0.15}Re_{0.85}$ is a promising candidate for making fast and high-efficiency SNSPDs in the future.

Based on the results accumulated above, **chapter 5** presents high performance 20, 25 and 50 μm diameter detectors working for visible, near infrared, and telecom wavelengths. A custom-built mode randomizer setup was used to simulate realistic experiments with randomized modes in the fiber. We achieved over 80% SDE with <20 ps timing jitter for 20 μm SNSPDs and 70% SDE with <20 ps timing jitter for 50 μm SNSPDs. The high efficiency multimode fiber coupled SNSPDs with unparalleled time resolution have already benefited many quantum optics experiments and applications in different labs.

Also, in order to extend NbTiN based SNSPDs' detection wavelength range without changing the cost-effective close-cycle Gifford-McMahon (GM) cooler, **chapter 6** shows extensive mid-infrared single photon detection data of SNSPDs fabricated from 7.5-9.5 nm thick NbTiN superconducting film. With optimized sputtering process and device design, fiber coupled devices achieved system detection efficiency of >50% at 1.5-2.0 μm with sub-15 ps timing jitter. Furthermore, devices made from the same batch show saturated quantum detection efficiency up to 3 μm at 2.5-2.8 K. This has significantly extended the working wavelength of NbTiN based SNSPDs to mid-infrared range with unprecedented time resolution.

In order to achieve near-unity system detection efficiency, **chapter 7** shows novel SNSPDs fabricated on a membrane cavity with exceeding 99% SDE at 1350 nm. Detectors from the same batch show 94-98% SDE at 1260-1625 nm with 15-26 ps timing jitter. The SiO_2/Au membrane enables broadband absorption in small SNSPDs (radius of 8 μm), offering high detection efficiency in combination with high timing performance. Prime challenges in optical design, device fabrication as well as accurate and reliable detection efficiency measurements to achieve high performance single-photon detection are also thoroughly analyzed.

In the end, **chapter 8** summarizes the main results of the thesis, points out challenges standing ahead of the SNSPDs community and offers future perspectives in SNSPDs field.

1

Introduction

Jin Chang

It always seems impossible until it's done.

Nelson Mandela

1.1. Theories of light

1.1.1. Classical theory of light

Historically, optics vacillates between the concepts of light as a particle and light as a wave, the former was proposed by Newton, and the latter was developed following seminal works by Huygens, Young, Fresnel, and many other scientists. In the 1800s, Maxwell discovered the electromagnetic field for light and it became prominent late since then, ushering in a century of developments in modern optics. According to electromagnetic theory, accelerated electric charges produce electromagnetic field (EM field) [1]. It consists of synchronized oscillations of electric and magnetic fields, propagates at a fixed speed vacuum (known as the speed of light), and carries radiation energy. From the wavelike perspective, EM waves can be identified as radio waves, microwaves, infrared radiation, visible light, ultraviolet radiation, X-rays, and gamma-rays in the order of increased frequency (decreased wavelength).

1.1.2. Non-classical light

Non-classical light is light that cannot be described using classical electrodynamics; its characteristics are explained by the quantized EM field and quantum electrodynamics. For example, a quantified EM field can be described in two conjugate quadrature components and the uncertainties in the two conjugate variables satisfy the Heisenberg uncertainty principle. It is possible to reduce the fluctuations in one of them well below the quantum limit by enhancing the fluctuation of the other canonically conjugate quadrature while the Heisenberg uncertainty principle is still fulfilled. Such states are known as "squeezed states" or "Squeezed light" [2].

Another example is photon Fock state - a quantum state which is an element of a Fock space with a well-defined number of photons [3]. For example, a single photon represents the quantum of electromagnetic radiation [4], or the one-particle state. Current technologies operating at the single-photon level play a major role because of the explosive growth of quantum information and computation technology [5, 6] as well as quantum optics applications [7], where single photons are used to encode information in different degrees of freedom including polarization, momentum, number state, energy and time. Also, photons travel at the speed of light and interact weakly with the surrounding environment over long distances, which gives lower-noise and low-loss advantages over other types of qubits.

1.2. Single photon generation

Ideally, a single-photon source has the following characteristics: it emits one photon at a time (single-photon emission probability is 100% and there is no multiple-photon emission event), and subsequently emitted photons are indistinguishable. Also, the emission repetition rate is arbitrarily fast and precisely tunable. Though deviations from these ideal characteristics always exist in real-world sources, many approaches are available nowadays to generate single photons: if the emission time of single photons could be at any arbitrary time defined by the user, this type of source is known as "deterministic source", for example, color centers [8, 9], quan-

1

tum dots (QDs) [10, 11], single-ions [12], single-atoms [13], single-molecules [14], atomic ensembles [15]; As a comparison, if the single photons emission time could not be precisely controlled, they are called "probabilistic" single-photon sources, including parametric down conversion [16, 17] and four-wave mixing in fibers[18, 19]. Below we show two representative types of single-photon sources: quantum dots (QDs, deterministic single-photon source) and heralded single photons (probabilistic single-photon source). Additionally, we present the faint laser, a frequently used quasi-single-photon source for single-photon detector characterization.

1.2.1. Quantum dots

Semiconductor quantum dots (QDs) have been systematically studied and used as on-demand single-photon sources in the past years. For example, molecular beam epitaxy methods can grow a structure of tiny smaller-band-gap semiconductor embedded in a larger-band-gap semiconductor [20] and chemical synthesis can produce colloidal quantum dots [21]. The small size of quantum dots leads to a discrete energy structure for the electrons and holes. In the QDs, electron-hole pair (known as exciton) can be produced on demand by either optically or electrically excited. After excitation, the radiative recombination of the electron-hole pair leads to single-photon emission. The photon emission direction can be engineered by fabricating distributed Bragg reflectors on the double-side of the quantum dots. Moreover, QDs can be integrated into micro-cavities to increase the spontaneous emission rate [22–24].

1.2.2. Heralded single photons

There are two types of commonly used heralded single-photon sources: spontaneous parametric down-conversion (SPDC) and spontaneous four-wave mixing. In SPDC, pump lasers are used to illuminate optical crystal (for example, beta barium borate, BaB_2O_4, $LiNbO_3$ or $LiIO_3$) with a $\chi^{(2)}$ nonlinearity to create two photons. The energy and momentum conservation constraints (phase matching) determine the possible wave vector relations between the two down-conversion generated photons [25, 26]. Emission from the SPDC process is highly directional, which is required in most applications, but the inherent dispersion of transparent material is very difficult to control.

In four-wave mixing, a $\chi^{(3)}$ nonlinear process happens where two pump photons are converted into two correlated photons in centrosymmetric materials such as glass. Though the absolute $\chi^{(3)}$ nonlinearity of glass is very small, optical fiber with its long interaction length can be used to produce photon pairs via FWM [27]. When using a FMW as single-photon source, the single-photon background created by Raman scattering must be suppressed or avoided [28].

1.2.3. Faint laser

Instead of using quantum dots or heralded single photons, a faint laser is widely used in labs as a quasi-single-photon source for SNSPDs' efficiency characterization. Previous studies shows that coherent light (laser) with a constant intensity has Poissonian photon statistics [29]. If P(n) represents the possibility of n-photon

1

events and $\bar{n}$ represents the mean photon number per pulse, then P(n) is given by the following formula:

$$P(n) = \frac{\bar{n}^n}{n!}e^{-\bar{n}} \tag{1.1}$$

For example if $\bar{n}$= 0.01, then P(0)=99%, P(1)= 0.99% and P(n≥2) = 0.01%, thus in the case which contains photon(s), a single-photon event is dominant. The Poisson distribution is uniquely characterized by the mean photon number $\bar{n}$ and it is easily adjusted by attenuating the laser to reduce its intensity.

Typically, for SNSPDs system efficiency measurements, lasers are attenuated heavily to reach $\bar{n}$< 0.01 thus multi-photon event probability could be neglected. However, when measuring SNSPDs' system efficiency at a high count rate, the multi-photon events need to be considered for efficiency correction [30].

1.3. Single photon detection

While the single-photon emitters field is growing rapidly, different technologies have been developed to detect light at the single-photon level, including photomultiplier tube, transition edge sensors, single-photon avalanche diode, and superconducting nanowire single-photon detectors. Below we will give a short introduction to each of them.

1.3.1. Photomultiplier tube

Photomultiplier tube (PMT) was the first device to detect light at the single-photon level dates back to the 1930s [31]. There are two fundamental processes behind the operation of a PMT: photoelectric effect [32] and secondary emission [33]. The photoelectric effect refers to the fact what for a range of photoelectric materials if they are illuminated by photons that have energy equals to or exceeding the work function of the material, they will emit electrons. And secondary emission means that incident electron with sufficient energy can knock out more electrons when hitting the surface or passing through a medium.

A PMT typically contains a photocathode, several dynodes, an anode, and read-out circuitry. Initially, an incident single photon excites a photoelectron from the photocathode, the photoelectron is then accelerated by the electric field between the photocathode and the first dynode, knocking out more electrons. Those electrons are subsequently accelerated and hit a second dynode where each electron knocks out more electrons. Multiple dynodes are used to repeat this process and with 10-20 dynodes, about 10^6 electrons will eventually be generated and arrive at the PMT anode. In the end, a current spike will be detected by detection electronics to register the incident photon. PMTs can offer time resolution below ns, but they suffer from a high dark count rate, limited efficiency, and weak response in the infrared region.

1.3.2. Transition edge sensors

Superconducting transition-edge sensors (TES) is a thermal sensor that measures the small amount of input radiation energy by recording the increase of resistance

of a superconducting film biased within its superconducting-to-normal transition region [34]. In this region, the logarithmic sensitivity of a TES device is α = d logR/d logT (R is the device resistance and T is temperature), which is a few orders of magnitude higher than that of a semiconductor-based detector.

The first TES demonstration was shown in 1942 [35], and after more than half a century of development, TES has been successful used in applications including millimeter-wave [36], gamma rays [37], and near-infrared single-photon detection [38]. However, due to its working mechanism, TES usually requires to be operated at mK dilution fridge. Also, in order to read out detected signals, special amplifiers or circuitry are typically needed, for example, superconducting quantum interference device (SQUID) current amplifiers [39]. Also, it is difficult to operate TES within the extremely narrow (a few mK) superconducting-transition regions. Small fluctuations in bath temperature can significantly degrade their performance as well. Due to their thermal detection process, the time resolution of TES usually has a long recovery time and high timing jitter (in the nanosecond regime) [40].

1.3.3. Single Photon Avalanche Diode

Avalanche photodiode (APD) is a highly sensitive semiconductor electronic device that uses the photoelectric effect to convert light into current (or voltage) [41]. They are designed to operate under a low reverse bias voltage and the leakage current changes linearly with the absorption of light. APD exhibits an internal current gain effect (avalanche effect) due to the impact ionization phenomenon thus it provides internal first-stage gain through the avalanche multiplication process [42]. However, since the reverse bias voltage of APD is always lower than the breakdown voltage, APD does not have sensitivity at the single-photon level.

As a comparison, in single-photon avalanche diode (SPAD, also known as Geiger mode APD), the reverse bias is so high that a large avalanche current can be generated and grow exponentially from single photon-initiated carriers. As a result, SPAD can detect low-intensity signals down to single photons [43]. However, due to the large energy bandgap of the semiconductor used for SPAD, they show limited detection efficiency in the infrared wavelength range (for example, Silicon SPADs have limited efficiency at 1100 nm and beyond). Also, they suffer from an after-pulsing issue because, after one detection event, a charge carrier has a certain probability to receives enough energy to be released from the trap level and then triggers a new avalanche process [44].

1.3.4. Superconducting nanowire single-photon detector

In 1911, superconductivity was first observed by Onnes in Leiden University [45]. When mercury is cooled to the temperature of 4K in liquid helium, its resistance sharply dropped to zero. Since then, superconductivity-related research has led to a burgeoning development of fundamental physics and emerge of novel scientific instruments. For example, superconducting quantum interference devices (SQUIDs) [46] were developed to detect extremely weak magnetic fields and hot-electron bolometers [47] were built to measure electromagnetic radiation with high sensitivity.

1

In the late 1990s, Nb [48] and NbN [49] based superconducting devices were systematically studied, including their temperature-dependent electron-phonon interaction process and time-resolved hot-electron energy relaxation behavior. In 1998, NbN fast hot-electron photo-detectors (HEPs) with a responsively of $\sim$ 220 A/W [49] was demonstrated and in 2000 [50], NbN HEPs using an electro-optic sampling method was reported with few-ps quasi-particle thermalization time. These indicated that NbN superconducting devices have the potential to detect light at the single-photon level. Then in 2001 [51], the first NbN superconducting single-photon detector was demonstrated by using NbN stripe at 4.2 K and current-biased close to its critical current. The device exhibited an experimentally measured quantum efficiency of 20% for 0.81 um wavelength photons and negligible dark counts. From 2001 till now, the superconducting nanowire single-photon detection field has experienced rapid development, and its detailed evolution history is summarized in the next chapter.

Here, we will briefly introduce the key parameters of an SNSPD, including

- System detection efficiency (SDE) System detection efficiency η_{SDE} is one of the most performance metrics for SNSPDs. It represents the possibility of generating a measurable electric signal from an incident single-photon. SDE can be calculated by the following equation

$$\eta_{SDE} = \eta_{intrinsic} \times \eta_{absorption} \times \eta_{coupling} \qquad (1.2)$$

  where $\eta_{intrinsic}$ is the internal efficiency (the possibility to generate a detectable electric pulse for an absorbed photon), $\eta_{absorption}$ is the optical absorption efficiency in the nanowire, and $\eta_{coupling}$ is optical coupling efficiency of the SNSPD system. For SDE measurement details and experiment setup, see chapter 7.

- Dark count rate (DCR) The dark count represents the detection events when there is no input optical signal. Based on the origin, the dark count can be divided into internal and external dark count. The former is caused by an internal physics process (for example, unbinding of vortex-antivortex pairs) and the latter can be caused by black-body radiation or background light in the lab. More discussion of DCR is presented in chapter 2.

- Dead time Dean time of an SNSPD shows how fast the detector recovers to its initial status after detecting an incident photon. During the dead time of an SNSPD, its efficiency is not absolute zero and the efficiency recovery speed is related to both the detector itself (kinetic inductance) and readout circuitry. For more detailed dead time characterization (auto-correlation measurement), see chapter 7.

- Timing jitter Low timing jitter, (or high time resolution), is one of the most distinctive merits of SNSPDs when compared to other types of single-photon detectors. For each photon absorbed by the superconducting nanowire, it takes a certain time δ_t to generate a detectable electric signal. The histogram of δ_t

typically has a Gaussian-type distribution and its full-width-at-half-maximum (FWHM) can be defined as the timing jitter of a device. For more jitter analysis, see chapter 2.

1.4. Scope of this thesis

The scope of this thesis includes:

Chapter 2 reviews SNSPDs' evolution history since its first demonstration in 2001. This intensive review chapter includes SNSPDs' development route in the past decades, discusses leading theoretical models to explain SNSPDs' working mechanism, presents the state-of-the-art SNSPDs works, and provides representative applications enabled by high performance SNSPDs.

Chapter 3 explores and optimizes the properties of $Nb_xTi_{1-x}N$ by taking advantage of the flexibility of reactive co-sputter deposition. By tailoring the chemical composition of $Nb_xTi_{1-x}N$ superconducting films, we present an optimized sputtering recipe for NbTiN based SNSPDs and carried out several material property studies to verify the film quality. We also present high-performance fiber-couped SNSPDs from the optimized films.

Chapter 4 we firstly show SNSPDs made from novel granular $Nb_{0.15}Re_{0.85}$ superconducting thin film. It confirms that $Nb_{0.15}Re_{0.85}$ is a candidate for making infrared SNSPDs in the future.

Chapter 5 demonstrates the role of polarization on the efficiency of SNSPDs and presents high efficiency multimode fiber-coupled SNSPDs with unparalleled time resolution from visible to telecom wavelengths.

Chapter 6 shows fabricated SNSPDs from 5-9.5 nm thick NbTiN superconducting film with saturated quantum detection efficiency up to 3 μm at 2.8 K. It shows that NbTiN based SNSPDs have the ability of working in the mid-infrared range with unprecedented time resolution.

Chapter 7 shows SNSPDs fabricated on a novel membrane cavity with exceeding 99% SDE at telecom wavelengths. We also discussed in detail the challenges in achieving such high system detection efficiency.

Chapter 8 summarizes the main results of the thesis, points out challenges standing ahead of us, and offers future perspectives in the SNSPDs field.

References

[1] R. P. Feynman, R. B. Leighton, and M. Sands, *The feynman lectures on physics; vol. i,* American Journal of Physics **33**, 750 (1965).

[2] R. Slusher, L. Hollberg, B. Yurke, J. Mertz, and J. Valley, *Observation of squeezed states generated by four-wave mixing in an optical cavity,* Physical review letters **55**, 2409 (1985).

[3] P. Bertet, A. Auffeves, P. Maioli, S. Osnaghi, T. Meunier, M. Brune, J.-M. Raimond, and S. Haroche, *Direct measurement of the wigner function of a one-photon fock state in a cavity,* Physical Review Letters **89**, 200402 (2002).

[4] A. Einstein, *″U on a heuristic point of view concerning the generation and transformation of light,* annals of physics **4** (1905).

[5] D. Bouwmeester and A. Zeilinger, *The physics of quantum information: basic concepts,* in *The physics of quantum information* (Springer, 2000) pp. 1–14.

[6] C. H. Bennett and D. P. DiVincenzo, *Quantum information and computation,* nature **404**, 247 (2000).

[7] M. O. Scully and M. S. Zubairy, *Quantum optics,* (1999).

[8] M. D. Eisaman, J. Fan, A. Migdall, and S. V. Polyakov, *Invited review article: Single-photon sources and detectors,* Review of scientific instruments **82**, 071101 (2011).

[9] E. Wu, J. Rabeau, G. Roger, F. Treussart, H. Zeng, P. Grangier, S. Prawer, and J.-F. Roch, *Room temperature triggered single-photon source in the near infrared,* New Journal of Physics **9**, 434 (2007).

[10] S. Kako, C. Santori, K. Hoshino, S. Götzinger, Y. Yamamoto, and Y. Arakawa, *A gallium nitride single-photon source operating at 200 K,* Nature materials **5**, 887 (2006).

[11] A. J. Shields, *Semiconductor quantum light sources,* Nanoscience And Technology: A Collection of Reviews from Nature Journals , 221 (2010).

[12] C. Maurer, C. Becher, C. Russo, J. Eschner, and R. Blatt, *A single-photon source based on a single ca+ ion,* New journal of physics **6**, 94 (2004).

[13] M. Hennrich, T. Legero, A. Kuhn, and G. Rempe, *Photon statistics of a non-stationary periodically driven single-photon source,* New Journal of Physics **6**, 86 (2004).

[14] M. Steiner, A. Hartschuh, R. Korlacki, and A. J. Meixner, *Highly efficient, tunable single photon source based on single molecules,* Applied physics letters **90**, 183122 (2007).

[15] S. Chen, Y.-A. Chen, T. Strassel, Z.-S. Yuan, B. Zhao, J. Schmiedmayer, and J.-W. Pan, *Deterministic and storable single-photon source based on a quantum memory,* Physical review letters **97**, 173004 (2006).

[16] E. Waks, E. Diamanti, and Y. Yamamoto, *Generation of photon number states,* New Journal of Physics **8**, 4 (2006).

[17] A. Soujaeff, T. Nishioka, T. Hasegawa, S. Takeuchi, T. Tsurumaru, K. Sasaki, and M. Matsui, *Quantum key distribution at 1550 nm using a pulse heralded single photon source,* Optics express **15**, 726 (2007).

[18] J. Fan and A. Migdall, *A broadband high spectral brightness fiber-based two-photon source,* Optics express **15**, 2915 (2007).

[19] E. A. Goldschmidt, M. D. Eisaman, J. Fan, S. V. Polyakov, and A. Migdall, *Spectrally bright and broad fiber-based heralded single-photon source,* Physical Review A **78**, 013844 (2008).

[20] D. Leonard, M. Krishnamurthy, C. Reaves, S. P. DenBaars, and P. M. Petroff, *Direct formation of quantum-sized dots from uniform coherent islands of ingaas on gaas surfaces,* Applied Physics Letters **63**, 3203 (1993).

[21] X. Brokmann, E. Giacobino, M. Dahan, and J.-P. Hermier, *Highly efficient triggered emission of single photons by colloidal cdse/ zns nanocrystals,* Applied Physics Letters **85**, 712 (2004).

[22] A. Kress, F. Hofbauer, N. Reinelt, M. Kaniber, H. J. Krenner, R. Meyer, G. Böhm, and J. J. Finley, *Manipulation of the spontaneous emission dynamics of quantum dots in two-dimensional photonic crystals,* Physical Review B **71**, 241304 (2005).

[23] S. Laurent, S. Varoutsis, L. Le Gratiet, A. Lemaître, I. Sagnes, F. Raineri, A. Levenson, I. Robert-Philip, and I. Abram, *Indistinguishable single photons from a single-quantum dot in a two-dimensional photonic crystal cavity,* Applied Physics Letters **87**, 163107 (2005).

[24] D. Press, S. Götzinger, S. Reitzenstein, C. Hofmann, A. Löffler, M. Kamp, A. Forchel, and Y. Yamamoto, *Photon antibunching from a single quantum-dot-microcavity system in the strong coupling regime,* Physical Review Letters **98**, 117402 (2007).

[25] L. Mandel and E. Wolf, *Optical coherence and quantum optics* (Cambridge university press, 1995).

[26] R. W. Boyd, *Nonlinear optics* (Academic press, 2020).

[27] J. E. Sharping, M. Fiorentino, and P. Kumar, *Observation of twin-beam-type quantum correlation in optical fiber,* Optics letters **26**, 367 (2001).

[28] S. D. Dyer, M. J. Stevens, B. Baek, and S. W. Nam, *High-efficiency, ultra low-noise all-fiber photon-pair source,* Optics express **16**, 9966 (2008).

[29] M. Fox, *Quantum optics: an introduction*, Vol. 15 (OUP Oxford, 2006).

[30] I. Esmaeil Zadeh, J. W. N. Los, R. B. M. Gourgues, V. Steinmetz, G. Bulgarini, S. M. Dobrovolskiy, V. Zwiller, and S. N. Dorenbos, *Single-photon detectors combining high efficiency, high detection rates, and ultra-high timing resolution,* APL Photonics **2**, 111301 (2017).

[31] V. Zworykin, G. Morton, and L. Malter, *The secondary emission multiplier-a new electronic device,* Proceedings of the Institute of Radio Engineers **24**, 351 (1936).

[32] A. Einstein, *Zur elektrodynamik bewegter körper,* Annalen der physik **4** (1905).

1

1

[33] A. Dekker, *Secondary electron emission,* in *Solid state physics*, Vol. 6 (Elsevier, 1958) pp. 251–311.

[34] K. D. Irwin and G. C. Hilton, *Transition-edge sensors,* Cryogenic particle detection , 63 (2005).

[35] D. H. Andrews, W. Brucksch Jr, W. Ziegler, and E. Blanchard, *Attenuated superconductors i. for measuring infra-red radiation,* Review of Scientific Instruments **13**, 281 (1942).

[36] D. Schwan, F. Bertoldi, S. Cho, M. Dobbs, R. Guesten, N. Halverson, W. Holzapfel, E. Kreysa, T. Lanting, A. Lee, *et al.*, *Apex-sz a sunyaev–zel'dovich galaxy cluster survey,* New Astronomy Reviews **47**, 933 (2003).

[37] T. Miyazaki, J. N. Ullom, M. F. Cunningham, and S. E. Labov, *Noise analysis of gamma-ray TES microcalorimeters with a demonstrated energy resolution of 52 ev at 60 kev,* IEEE transactions on applied superconductivity **13**, 630 (2003).

[38] B. Cabrera, R. Clarke, P. Colling, A. Miller, S. Nam, and R. Romani, *Detection of single infrared, optical, and ultraviolet photons using superconducting transition edge sensors,* Applied Physics Letters **73**, 735 (1998).

[39] J. Clarke and A. I. Braginski, *The SQUID Handbook, 1: Fundamentals and Technology of SQUIDs and SQUID Systems*, Vol. 1 (Wiley-Vch, 2004).

[40] A. Lamas-Linares, B. Calkins, N. A. Tomlin, T. Gerrits, A. E. Lita, J. Beyer, R. P. Mirin, and S. Woo Nam, *Nanosecond-scale timing jitter for single photon detection in transition edge sensors,* Applied Physics Letters **102**, 231117 (2013).

[41] S. Cova, M. Ghioni, A. Lacaita, C. Samori, and F. Zappa, *Avalanche photodiodes and quenching circuits for single-photon detection,* Applied optics **35**, 1956 (1996).

[42] M. A. Saleh, M. M. Hayat, P. P. Sotirelis, A. L. Holmes, J. C. Campbell, B. E. Saleh, and M. C. Teich, *Impact-ionization and noise characteristics of thin iii-v avalanche photodiodes,* IEEE Transactions on Electron Devices **48**, 2722 (2001).

[43] F. Zappa, S. Tisa, A. Tosi, and S. Cova, *Principles and features of single-photon avalanche diode arrays,* Sensors and Actuators A: Physical **140**, 103 (2007).

[44] S. Cova, M. Ghioni, A. Lotito, I. Rech, and F. Zappa, *Evolution and prospects for single-photon avalanche diodes and quenching circuits,* journal of modern optics **51**, 1267 (2004).

[45] H. Kamerlingh Onnes, *The resistance of pure mercury at helium temperatures,* Commun. Phys. Lab. Univ. Leiden, b **120** (1911).

[46] R. Kleiner, D. Koelle, F. Ludwig, and J. Clarke, *Superconducting quantum interference devices: State of the art and applications,* Proceedings of the IEEE **92**, 1534 (2004).

[47] D. W. Floet, E. Miedema, T. Klapwijk, and J. Gao, *Hotspot mixing: A framework for heterodyne mixing in superconducting hot-electron bolometers,* Applied physics letters **74**, 433 (1999).

[48] E. Gershenzon, M. Gershenzon, G. Gol'tsman, A. Lyul'kin, A. Semenov, and A. Sergeev, *Electron-phonon interaction in ultrathin Nb films,* Sov. Phys. JETP **70**, 505 (1990).

[49] K. Il'in, I. Milostnaya, A. Verevkin, G. Gol'tsman, E. Gershenzon, and R. Sobolewski, *Ultimate quantum efficiency of a superconducting hot-electron photodetector,* Applied physics letters **73**, 3938 (1998).

[50] K. Il'in, M. Lindgren, M. Currie, A. Semenov, G. Gol'Tsman, R. Sobolewski, S. Cherednichenko, and E. Gershenzon, *Picosecond hot-electron energy relaxation in NbN superconducting photodetectors,* Applied Physics Letters **76**, 2752 (2000).

[51] G. N. Gol'tsman, O. Okunev, G. Chulkova, A. Lipatov, A. Semenov, K. Smirnov, B. Voronov, A. Dzardanov, C. Williams, and R. Sobolewski, *Picosecond superconducting single-photon optical detector,* Applied Physics Letters **79**, 705 (2001).

1

2

SNSPDs Overview: evolution history, background theory, state-of-the-art detectors and applications

Two decades after their demonstration, Superconducting Nanowire Single-Photon Detectors (SNSPDs) have become indispensable tools for quantum photonics as well as for many other photon-starved applications. This invention has not only led to a burgeoning academic field with a wide range of applications but also triggered industrial efforts. Current state-of-the-art SNSPDs combine near-unity detection efficiency over a wide spectral range, low dark counts, short dead times and picosecond time resolution. The present perspective discusses important milestones and progress of SNSPDs research, emerging applications, future challenges and gives an outlook on technological developments required to bring SNSPDs to the next level: a photon-counting, fast time-tagging imaging and multi-pixel technology that is also compatible with quantum photonic integrated circuits.

2.1. Brief introduction of SNSPDs

2.1.1. Single-photon detection and the emergence of SNSPDs

Technologies operating at the single-photon level, the quantum of the electromagnetic field [1], are crucial for communication, sensing and computation [2, 3]. Photons can encode information using different degrees of freedom including polarization, momentum, number state, energy and time. For instance, quantum key distribution was demonstrated over a distance exceeding 4600 km [4], potentially forming the backbone of a quantum internet [5]. As crucial as the single photon carriers, are the high-performance single-photon detectors to perform measurements on the quantum bits. They were instrumental in recent demonstration of large-scale Boson sampling [6], showing a computational advantage over conventional supercomputers. Furthermore, in a number of other fields including bio-imaging, light detection and ranging (LiDAR) [7–9], optical time domain reflectometry [10, 11], single-molecule detection [12], semiconductor circuits inspection [13], star light correlation spectroscopy [14], diffuse optical tomography [15], positron emission tomography [16], mass spectroscopy and quantum metrology measurements [17] single photon/particle detectors are essential. For these applications, tremendous efforts have been made to produce single-photon detectors combining near unity system detection efficiencies (SDE), low dark count rates (DCR), short timing jitters, high maximum count rates, photon number resolution capabilities, and large active areas.

Single Photon Avalanche Diode (SPAD) [18, 19] and Photomultiplier Tubes (PMTs) [20, 21] were first used to detect single photons. However, combining high detection efficiency with high time-resolution and low noise in SPADs and PMTs remains a challenge. In addition, a limited spectral response (limited at 1100 nm for Silicon) and afterpulsing further limit their use for quantum technologies. With two decades of development since their inception [22], superconducting nanowire single photon detectors (SNSPDs) offer unrivalled detection metrics with an unprecedented combination of performance, for a comparison of SPADs and PMTs with SNSPDs see [23].

2.1.2. A brief history of SNSPDs development

Before the inception and maturity of SNSPDs, other superconducting devices such as Josephson-junctions [24], Superconducting Quantum Interference Devices (SQUIDs) [25], hot electron bolometers [26, 27], and Transition Edge Sensors (TES) [28–30] already achieved high performances. The first demonstration of single-photon detection with current-biased superconducting microbridges was reported in 2001 at a wavelength of 0.81 μm [22]. After that, the acronyms SNSPD and SSPD are widely used in the research community to describe devices originated by Gol'tsman *et al*. The field of SNSPDs then underwent fast development and was driven by applications requirements. In 2002 meandering nanowires were introduced to increase the active area [31]. In 2033, the first commercial use of SNSPD, for integrated circuit fault testing, was reported [32]. A key driver pushing SNSPD early development was Quantum Key Distribution (QKD) that made commercialization viable. The first SNSPD based QKD was reported in 2006 [33] and was followed by a world record 200 km QKD experiment [34] doubling the previous distance achieved with InGaAs SPADs and matched the loss threshold for space to ground QKD of 40 dB. Soon after these pioneering works, fiber-coupled SNSPDs reached a detection efficiency of 24% at 1550 nm [35] and were further improved to 47% with antenna structures [36]. Optical cavities were integrated with SNSPDs to boost the detection efficiency to 57% at 1550 nm [37]. In 2012, by stacking two WSi SNSPDs and connecting them in parallel, the system detection efficiency (SDE) was improved to over 87% [38]. Another important development in 2011 and 2012 was the integration of SNSPDs with photonic waveguides [39, 40] which made high on-chip detection efficiency possible and delivered a key element to the toolbox of integrated quantum photonics (see Section 2.3.1). In 2013, WSi SNSPDs in an integrated cavity reached an SDE of 93% at 1550 nm [41], 92-93% SDE was subsequently demonstrated with other material platforms [42, 43]. In 2020, three independent groups reported >98% SDE based on three different material systems: MoSi with distributed Bragg reflectors [44], dual-layer NbN meanders [45] and NbTiN with a membrane cavity [46].

Beside a high detection efficiency, detectors with low dark count rates, i.e. undesired detection events generated without illumination or due to black-body radiation, are vital in many photon-starved applications. Early works [47] showed intrinsic dark counts to originate from vortices crossing the nanowire cross-section, which may be triggered by thermal fluctuations or current-assisted unbinding of vortex-antivortex pairs [48]. Additionally, black-body radiation can be a major source of dark counts, especially for large area SNSPDs and particularly at longer wavelengths [49]. To suppress black-body induced dark counts, cold filters [50] or fibers with end-face coatings can be used [51]. It has also been shown that the dark count rate increases under illumination due to the suppression of switching current by incident light [52]. As of 2021, a dark count rate as low as 10^{-4} per second has been demonstrated [50, 53], further studies are required to determine the origin of the remaining dark counts.

High time resolution is one of the distinctive advantages of SNSPDs. Time jitter represents the time interval statistics between photons impinging the detector

2

and the generation of the electrical detection signal. Early experimental works [54, 55] showed that besides time jitter of the detector itself (briefly discussed in Section 2.1.3) several other experimental parameters such as electrical noise, fiber dispersion, and the accuracy of laser synchronization signals all contribute to the overall system time jitter. Experimentally, in 2006 a sub-30 ps time jitter was demonstrated by making SNSPDs from a 4 nm-thick NbN film [56]. In 2016, a timing jitter of 17.8 ps was achieved using an ultrafast time-correlated single-photon counting setup [57]. In 2017, by employing a cryogenic amplifier, a 14.8 ps jitter was demonstrated [42] with NbTiN SNSPDs. In the same year, by optimizing experimental measurement setup, a 12 ps timing jitter was demonstrated with NbN SNSPDs [58]. Recently, the fiber-coupled SNSPD's timing jitter was pushed down to 7.7 ps [59]. As of April 2021, the best reported time jitter belongs to short straight nanowires and is <3 ps for NbN [60] and 4.8 ps for WSi[61].

2.1.3. Understanding SNSPDs' performance optimization and trade-offs

To date, the theoretical understanding of the exact detection mechanism in SNSPDs is still under development. We discuss some of the leading models in Section 2.2.1. Here we briefly hint at some basic observations to discuss the operation limits of SNSPDs.

Generally speaking, the detection efficiency of a SNSPD is influenced by two parameters: its optical absorption, i.e. what fraction of photons incident on the SNSPD is absorbed in the detector and the internal efficiency, the probability that an absorbed photon generates a measurable detection event. Small constrictions along the nanowires (due to nano-fabrication and/or variation in the superconducting film) were shown to be one limiting factor for the critical current as well as for the internal detection efficiency [62, 63]. It was also demonstrated that bends in a meandering nanowire can lead to a noticeable reduction of the critical current as shown in [64–66], this current crowding issue can be addressed by optimizing the bend geometry [67] or with spiral SNSPDs [68]. As for the absorption efficiency, the optical absorption of typical superconductors used for SNSPD fabrication have been studied [69] and the polarization dependence of SDE and nanowire designs (fill factor, linewidth, device size) are well-understood and comprehensively discussed in [70, 71]. To minimize polarization dependence, three-dimensional architecture [38], near-field optics [72], dielectric capping layers [73] or fractal-shape nanowires [74, 75] were demonstrated.

The operation temperature dependence of SNSPDs is, at least experimentally, well understood: If the internal detection efficiency at a specific temperature and for a specific photon energy is unsaturated (no plateau in the detection rate versus bias current curve), the detection efficiency reduces as the temperature increases. Additionally, both intrinsic and blackbody induced dark counts are temperature dependent [76]. The former, independent of the applicable model or exact origin of DCR, is due to the fact that potential barriers (for example for vortex crossing or vortex-antivortex depairing) or electron/photon interaction time constants are all temperature dependent. The intrinsic darkcount, for a fixed bias to switching

current ratio, often increases with higher temperature. Extrinsic darkcount may decrease with temperature as the detection efficiency for photons (for example long wavelength blackbody photons) is reduced as the temperature increases [76]. Therefore, in a system in which blackbody radiation is well filtered out, the signal to noise ratio often decreases as the temperature is increased.

The timing properties of SNSPDs (recovery time and time jitter) have been thoroughly studied: Early on, the recovery time of NbN SNSPDs was found to be limited by their kinetic inductance [77], revealing an intrinsic trade-off between large-area devices and fast recovery times. A more systematic electro-thermal model [78] was presented to better explain the detection dynamics with a practical solution to shorten recovery time by adding a resistor in series to SNSPDs. However, in the same work it was demonstrated that there is a limit to reducing SNSPDs recovery times, this limit is dictated by electrothermal feedback and hence depends on the substrate material, on the superconductor, temperature, bias, critical current, as well as on the SNSPD's kinetic inductance. While detectors with very fast electrical recovery time (<1ns) have been demonstrated, it has also been shown that the electrical recovery time (extracted from the pulse traces) is not necessarily the same as the detector recovery time [79]. Alternatively, multi-pixel [56] and multi-element structures [80] were proposed and demonstrated to increase the active area without sacrificing time performance and even offering photon number resolution prospects[81].

Since SNSPDs typically cover areas of hundreds of square microns and the electrical signal propagates through the detector with finite speed, photons detected at different locations generate detection pulses that reach the readout circuit at different times, leading to a geometrical jitter [82]. In 2017 [83], the influence of Fano fluctuations on timing jitter was also reported. In the same year, timing jitter caused by distributed electronic and geometric inhomogeneity of a superconducting nanowire [84] was analyzed. Also, vortex-crossing-induced jitter was systematically studied and the theoretical limit of SNSPDs' intrinsic timing jitter was estimated to be around 1 ps [85]. Another study, based on the two-temperature model coupled with the modified time-dependent Ginzburg-Landau equation, argued that photon absorption location on a current-carrying superconducting strip has direct influence on the minimal achievable time jitter. The minimum jitter was shown to depend on the critical temperature of the superconducting film. This was calculated to be of the order 0.8 ps for a nanowire with a width of 130 nm made from a typical NbN superconducting films with a critical temperature of 10 K [86]. Narrower nanowires can potentially improve the minimum achievable jitter. If no other fundamental limitation for time jitter is discovered, ultimately, the time jitter would be limited by the dynamics of suppression of superconductivity (pair breaking) which depends on material, temperature and the optical excitation density [87].

2.1.4. Content of this chapter

After summarizing the history and development of SNSPDs over the past two decades, we highlight the leading theories to explain the operation mechanism and provide the status quo and state-of-the-art in SNSPD technology (Section 2.2). A selected

number of current and potential future applications are discussed in Section 2.3. Finally, we provide an outlook for future development (Section 2.4). For a more in-depth and technical review of SNSPD's working principle, intrinsic limitations, and design solutions, we refer the readers to ref. [88].

2.2. SNSPD detection mechanisms and state-of-the-art

2.2.1. SNSPD detection mechanisms

This section gives an overview of the leading physical models of the detection mechanisms in SNSPDs, providing a qualitative description to understand basic working principles and device physics. We consider the most common SNSPD implementation, based on a superconducting nanowire (width 50-100 nm) patterned from a thin film (thickness 5-10 nm) using a top-down nanofabrication process. The nanowire, often designed as a meandering structure, is biased with a DC current close to the device's critical current via a bias tee, low noise amplifiers and counting electronics are used to detect single-photon events and register corresponding voltage pulses. A phenomenological model of the detection process was proposed in the initial reports on SNSPDs[22, 89] and has been revised in the following two decades. To allow for quantitative modelling and design optimizations, the detection process[90] was divided into subsequent steps (see Figure 2.1): (I) photon absorption; (II) creation of quasiparticles and phonons combined with their diffusion; (III) emergence of a non-superconducting nanowire segment; (IV) re-direction of bias current in readout circuitry, leading to a voltage pulse; (V) detector recovery.
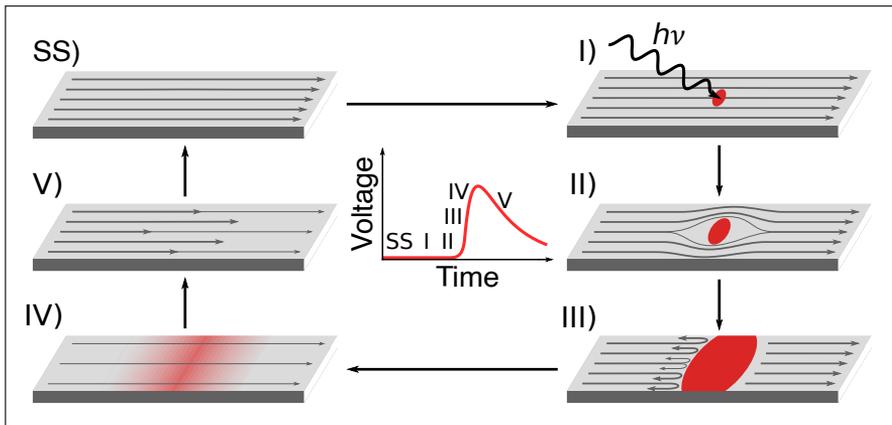
Figure 2.1: Macroscopic explanation of the detection mechanism (based on [22, 78, 89, 91]). In Steady State (SS), the superconducting thin-film strip is current biased. Photon absorption (I) leads to the creation of quasi-particles and phonons (II). This leads to the formation of a normal-conducting part of the strip (III). Redirection of the current towards the read-out electronics allows a recovery of the superconducting state (IV), which leads to a return of the current (V) to its initial value. This reset dynamics are limited by the kinetic inductance of the device. Center: The voltage readout signal with each step labeled.

(I) The initial absorption of a single photon within the active detector area is well described by classical electromagnetic theory. This allows for the use of established modelling tools [92] to optimize optical absorption in the superconducting layer for a desired wavelength range. The absorption of a visible or near-infrared photon results in (II) the formation and expansion of a cloud of quasiparticles, which is initiated by the relaxation of the photo-excited electron and followed by the creation, multiplication and diffusion of quasiparticles and phonons. These processes are governed by electron-electron, electron-phonon as well as phonon-phonon interactions and their characteristic timescales,[93] whereas the diffusion constants as well as the ratio of the heat capacities of electrons and phonons are crucial for the spatio-temporal relaxation dynamics. This down-conversion process is modeled through deterministic kinetic equations for electrons and phonons [94] or through a stochastic loss of excitation energy into the substrate [83]. An instability of the superconducting state emerges due to the quasiparticle cloud, linked with a local reduction of the superconducting order parameter, re-distribution of the current density and lowering of the effective critical current density. Combining ideas from deterministic and stochastic models allows to describe a complete set of measurements qualitatively [95, 96] but these existing models require further developments to be able to fully describe the physical processes quantitatively. This instability can lead to a photon detection event, associated with (III) parts of the nanowire transitioning to a non-superconducting state. Following initial descriptions relying on a normal-conducting 'hotspot', models of the SNSPD detection mechanism have been refined, underlining the importance of magnetic vortices [47, 97, 98]. For further details on the mechanisms governing the local emergence of a non-superconducting segment of the detector area, we refer to Engel et al.[90]. Subsequently, the resistive region of the nanowire grows due to internal Joule heating [78]. The increasing resistance, on the order of several kilo Ohms [78], leads to (IV) the re-direction of the bias current from the nanowire towards the read-out electronics. The circuit behavior can be described using lumped element models[99, 100] or planar microwave simulations. Once the resistive area has sufficiently cooled down, (V) superconductivity is restored and the current flowing through the nanowire returns to its initial value, whereas the dynamics are governed by the kinetic inductance of the device.[77, 78] In cases where the resistive domain does not cool-down rapidly enough, the detector latches due to thermal runaway and no further photons can be detected until the device is actively reset [101].

While models for step (I), (IV) and (V) can be used to predict and develop successful designs, models for step (II) and (III) are missing such capabilities. The fluctuations beyond the initial down-conversion cascade, the non-equilibrium state of electron-phonon baths and the missing element of intrinsic dark counts are examples for open problems and challenges for the future.

2.2.2. State-of-the-art SNSPDs

In the section below we discuss advances with regards to the superconducting materials used for production of SNSPDs, nanofabrication, multi-pixel detectors, the nano- and micro-wire SNSPDs, wavelength range, state-of-the-art performance,

and characterization of SNSPDs that has led to detectors with >98% SDE [44, 46, 102].

Superconducting materials and nano-fabrication of SNSPDs

A variety of superconducting materials have been explored for SNSPDs. The material selection for the superconducting film can be based on various factors but the motivations for specific choices can mainly be divided into two groups: optical properties such as absorption at different wavelengths, and superconducting properties such as critical temperature and critical current density. In practice, other parameters may also be taken into account, for example for photons with higher energy the use of higher critical temperature superconductors might be preferred to simplify the cryo-cooling system while for mid-infrared detectors (beyond 2-3 μm), low-gap amorphous superconductors such as MoSi and WSi have so far been the main option. In Table 2.1 we present an overview of some leading results based on different superconducting materials. Beside the highlighted superconducting materials in Table 2.1 another important class of superconducting materials which have been subject of research are the High Tc superconductors. High-Tc SNSPDs is a topic of longstanding discussions with reports of dark counts [103] and signatures of single-photon operation [104] on the one hand and skepticism [105] on the other hand. Therefore, further studies are required to understand the limits and potentially unlock the use of these promising platforms.

Table 2.1: **Overview of some SNSPD leading works on different material platforms**

Material	efficiency / time jitter	temperature	wavelength
NbN [43, 45]	92-98.2%/40-106.1 ps	0.8-2.1 K	1550-1590 nm *
NbTiN [42, 46]	92-99.5% / 14.8-34 ps	2.5-2.8K	1290-1500 nm **
WSi [41, 44]	93-98% / 150 ps	120mK-<2K ***	1550 nm
MoGe [106]	20% / 69-187 ps	250mk-2.5K	1550 nm
MoRe [107]	-/-	9.7K	-
MoSi [108–110]	80-87% / 26-76 ps	0.8-1.2K ****	1550nm
NbRe[111]	-/35 ps	2.8K	500-1550 nm
NbTiN [76]	15-82% /30-70 ps	2.5-6.2K	400-1550nm
NbSi [112]	-/-	300mK	1100-1900 nm
TaN [113]	-/-	0.6-2K	600-1700 nm
MgB$_2$ [114–116]	-/-	3-5K	Visible

* Optimal performance at <1K while an SDE of 90-95% was achieved at 2.1K. Time jitter depends on temperature and design. Errobar for 98.2% was $\pm$1%.
** Errorbar for 99.5% efficiency was (-2.07,+0.5)%.
*** Operation up to $\sim$ 2K possible at the cost of higher time jitter [41], temperature and jitter measurements are not mentioned in [44]. Errorbar for was $\pm$0.5%.
**** In [109] an operating temperature of 2.3 K was demonstrated with added cost of higher time jitter and lower internal efficiency saturation.

Production of high performance SNSPDs involves various nano-fabrication technologies. Starting from a commercial substrate (typically silicon), the first fabrication step involves the deposition of a distributed Bragg reflector to enhance the optical absorption (metal based reflectors are also possible [42, 46] but less common). A superconducting thin film (typically 4-10 nm) is then deposited on top of the mirror layer. The electrical contacts are formed by means of optical or e-beam lithography, metal deposition (evaporation or sputtering), and lift-off. The nanowire detector can be formed using a single electron-beam lithography step followed by reactive ion etching. For detector packaging and to achieve stable and efficient operation, coupling to an optical fiber is crucial, which is typically done with self-aligned schemes requiring additional lithographic steps combined with deep etching of the substrate (micro-machining using a Bosch process). The complete process is illustrated in Figure 2.2.
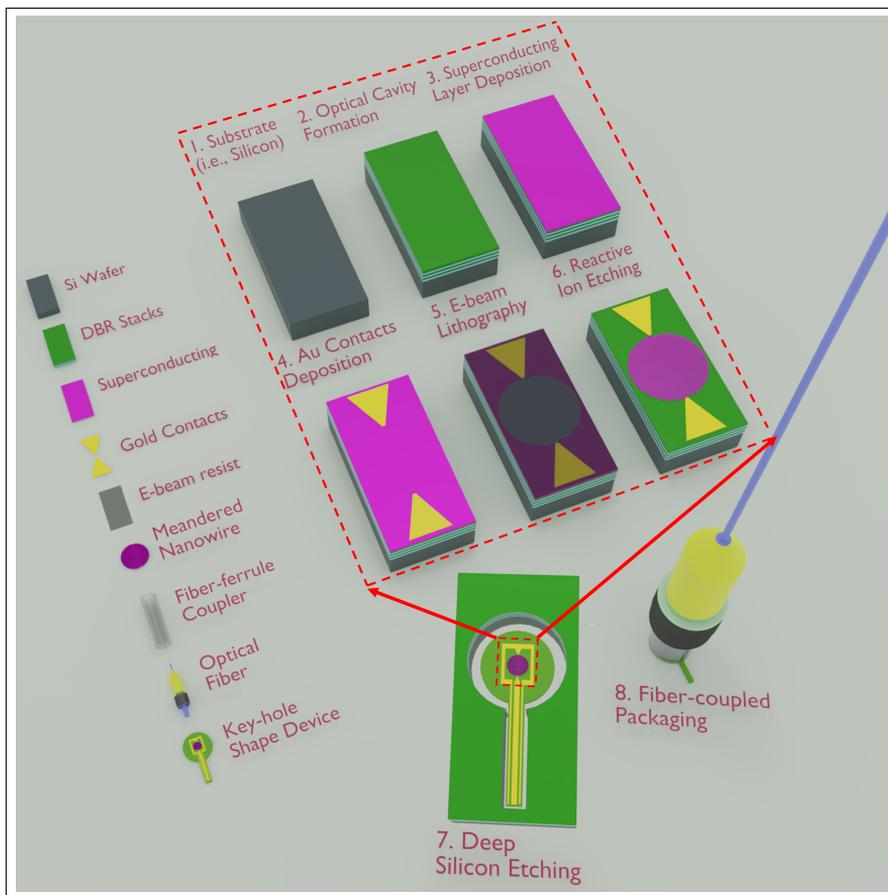

Figure 2.2: Illustration of the process flow for fabricating SNSPDs from a bare silicon substrate to a fiber-coupled device. For details see main text.

Deposition of the superconducting layer is a crucial step and its quality has a direct impact on the detector performance. This is typically performed by magnetron sputtering and can yield nanocrystalline or amorphous layers. Excellent deposition uniformity and nanofabrication processes are required to ensure manufacturing of devices with reproducible and consistent superconducting properties. In this regard, amorphous materials such as WSi and MoSi as well as optimized crystalline films with relatively larger thicknesses (8-12 nm) [59, 117] are considered more forgiving and thus favourable for high-yield detector fabrication. In addition, plasma-enhanced atomic layer deposition [118, 119] and single-crystalline molecular beam epitaxy [120] growth of NbN were recently demonstrated as viable and potentially high-yield alternatives for SNSPD fabrication.

Wavelength range

SNSPDs have been demonstrated to operate from the X-ray to the mid-infrared wavelength range. In 2012, soft X-ray detection was demonstrated[121]. In contrast to the standard detection mechanism, where photons are absorbed in the meander, for X-ray detection the absorbance in thin superconducting layers with thicknesses around 10 nm is low and absorption in the substrate plays a major role [122, 123]. Due to the the significant higher particle energy, X-ray detectors can have saturated intrinsic efficiency at considerably larger geometrical parameters, which can increase X-ray absorption in the superconductor to a few percent [124, 125]. SNSPDs for UV photons have reached efficiencies of $> 85\%$, dark count rates of 0.25 counts per hour and timing jitter <60 ps [126]. By engineering film deposition to optimize energy sensitivity, WSi detectors were shown with a saturated internal efficiency at $10\mu m$ [127] in 2020. Although beyond the scope of single-photon detection, it is worth mentioning that SNSPD structures can also be used to detect α and β particles [128].

Multipixel SNSPDs

In systems with a small number of superconducting single-photon detectors such as fiber-coupled multi-pixel arrays [59], a straightforward way to address individual detection channels is through spatial multiplexing of the biasing and RF detection signals through several coaxial lines. As multi-pixel arrays scale in size, a limit on the number of coaxial lines is set by the cryostat cooling power [129]. Multi-pixel readout techniques for SNSPDs are under development, a row-column readout of pixels for a 32×32 detector-array using only 64 electrical connections was demonstrated [130]. This method is very attractive as the number of required RF lines is only $2N$, for arrays consisting of N^2 detectors, though this approach does not allow for simultaneous readout of all pixels. Time-domain multiplexing is another approach, where a single superconducting transmission line is used to address several detectors on the same chip [131–135]. One of the main challenges of this approach is the fast propagation speed of the electrical signal in the superconducting transmission-lines, approaching the speed of light, which limits the possibility for dense packing of detectors[132]. Dispersion engineering was recently used to reduce group velocity of the detection signal in the superconducting transmission-line by orders of magnitude. Both planar and multi-layered structures were used

to control the group velocity of the detection signals [131, 133–135]. Another promising route for scalable readout of multipixel SNSPDs is the use of Single flux quantum (SFQ) logic [136–141]. Frequency multiplexing was also demonstrated for SNSPDs [142], where several resonant cavities operating at different radio frequencies are coupled to individual detectors on a single transmission-line. For the latter, a challenge in large scale systems is the complexity involved with matching resonant frequencies of the cavities to the driving radio-frequency tones. Alternatively, amplitude coding of the detection signals of SNSPDs provides another approach for multiplexing[143, 144]. The advantage is the simplicity of fabrication and readout method using a voltage division circuit. On the other hand, the drawback is the need for on-chip resistors to set different amplitude levels, which dissipate heat, and additionally the size of the array is limited by the leakage current in different branches[134].

Nanowire v.s. microwire detectors

SNSPDs have typical nanowires widths in the range 40-120 nm. These devices show exceptional performance, but require complex nanofabrication. Recently, detectors with wide micrometer lines were reported: Superconducting Microstrip Single-Photon Detectors (SMSPD) [145]. These devices have, compared to SNSPDs, far larger critical currents and lower kinetic inductance, making them suitable for the fabrication of large-area detectors as shown in a number of recent works [146–149]. For example [147] demonstrates devices with meander widths of 1 and 3 micron and active areas up to 400×400 μm^2 with excellent light detection in micro-strips fabricated by conventional optical lithography [149]. Additionally, very recently, high performance single-photon detection (SDE >90%) was demonstrated [68]. Since this a relatively new research direction, there are limited reports on time resolution [150], wavelength limits and high count-rate performances are yet to be reported.

2.3. SNSPD Applications

In this section we review a non-exhaustive number of established and emerging applications of SNSPDs.

2.3.1. Quantum optics, information processing, quantum communication and integrated quantum photonics

SNSPDs have been the detectors of choice in landmark quantum information processing experiments, i.e. on large scale boson sampling [6] and record breaking quantum communication experiments [151–153]. Also high performance SNSPDs played a major role in the loophole-free test of local realism based on Bell experiment [154]. A recent promising direction for application of SNSPDs in quantum information promising is its integration with ion-trap[155]. For an up-to-date review on the use of SNSPDs in quantum technologies we refer to [105].

Complex quantum photonics integrated circuits require many on-chip single-photon detectors. SNSPD in traveling wave geometry [39, 40], with its outstanding

performance and small footprint, serves as an excellent candidate for this function in photonic integrated circuits. Waveguide-integrated SNSPDs have already been used for on-chip single qubit quantum optics experiments [156, 157], to demonstrate on-chip two qubit quantum interference [158], and for on-chip secure quantum communication [159]. SNSPDs were integrated in different nano-photonics platforms such as Si [40, 160–166], SiN [156–158, 167–172], GaAs [39, 172–175], AlN [172, 176], LiNbO3 [172, 177, 178], Ta_2O_5 [179], and diamond [180, 181]. In Ref. [182] the performance of most of these earlier SNSPD nano-photonics platforms is reviewed. Integrated SNSPDs have also demonstrated sub-nanosecond recovery time [163, 179]. Another important aspect in sophisticated integrated quantum photonics circuitry is the reliability of photonics elements. It has been shown [171] that by fabricating traveling wave SNSPDs buried under photonic waveguides, one can determinedly ensure that only the best performing detectors are integrated. Further development of integrated SNSPDs, as envisioned in Section 2.4.2 can significantly enhance the role of SNSPDs in future quantum nanophotonics circuits.

2.3.2. Light detection and ranging (LIDAR)

LIDAR is an optical measurement technique for studying environmental parameters such as the atmosphere, vegetation as well as remote objects. The detector performance influences the resolution, acquisition time and maximum range. It has been shown that SNSPDs outperform conventional Geiger-mode avalanche photodiodes both in low noise environments and, under appropriate operation, in noisy (high background) environments [7, 8]. SNSPDs were used for measuring sea fog in an area 180-km in diameter [183]. Kilometer-range, high resolution imaging at telecom wavelength has also been demonstrated [184]. Another promising direction with encouraging recent results is single-photon LIDAR beyond 2000 nm, a wavelength range with both reduced solar flux and atmospheric absorption [9].

2.3.3. Mass spectrometry

SNSPDs offer excellent potential for applications in the field of mass spectrometry where impacts of single ions can be measured. They show exceptional sensitivity and, additionally, operate at a convenient (particularly considering the size and the heat load of common mass spectrometry chambers) temperature of 2-5 K which is within the operating temperature range of relatively inexpensive Gifford-McMahon and pulsed-tube cryostats. The feasibility of sub-nanosecond detection using these detectors has already been demonstrated [12, 185]. In Addition, proof of principle for detection of neutral and low energy particles was demonstrated [186, 187]. Superconducting nanowire detectors do not rely on the secondary electron mechanism and their detection mechanism is based on the creation of high energy quasiparticles by the impact, allowing for 100% detection efficiency even for macromolecules [188]. While SNSPDs offer excellent performances, until recently their active area had been limited. With the development of SNSPD arrays (employing any of several existing multiplexing techniques), kilo-pixel detectors have been introduced [130] that can cover much larger areas, and by interfacing SNSPD arrays and cryogenically-cooled electronics (see Section 2.4.1), even larger arrays are

expected to become available.

2.3.4. Diffuse correlation spectroscopy

Biological tissues are strongly diffusive media. Diffused optical imaging is a functional medical imaging modality which uses the lower attenuation of near-infrared light to probe physiological parameters in the tissue such as oxy- and deoxyhemoglobin [15].The light transport in these tissues are mainly dominated by scattering and it has been shown that achievable resolution (the half-width of the point-spread function) scales with thickness [189].Recently, SNSPDs have been considered for improving the performance of diffuse correlation spectroscopy [190].

2.3.5. Optical Time Domain Reflectometry (OTDR)

To identify the position of losses and scattering along optical fiber networks, reflection of a laser pulse is measured and timing yields information on the fault position [191]. The ability to operate at the single photon level, with the outstanding time resolution and low dark counts of SNSPDs, allows for OTDR measurements to be carried out over the longest possible distances and yield cm resolution [10, 11, 192]. Additionally, OTDR can be used to implement fiber-optic distributed Raman sensor for absolute temperature measurements [193, 194].

2.3.6. Future applications

In neuromorphic computing, SNSPDs were recently proposed both as a direct platform for neuromorphic computing [195, 196] and in conjunction with on-chip semiconducting photon sources [197, 198]. Neuromorphic computing is the discipline that produces neural-inspired computational platforms and architectures. Carver Mead in the late 80s, has come a long way and has had important results such as beating humans in the game of Go [199].

In astronomy, SNSPD are finding uses for exoplanet transit spectroscopy, in deep space optical communication, as well as in the search for dark matter. Detecting such particles places stringent requirements on the detector, SNSPDs have been shown to be suitable candidates for direct detection of dark-matter particles from the halo of Milky Way directly creating an excitation in a detector on Earth of sub-GeV particles [53]. Another application is wide band optical communication to satellites. The limited power available on satellites places stringent requirements on the downlink detectors, with yet stronger requirements if the emitter is further away, as for a deep space probe. These requirements have shed light on SNSPDs [200–204] for downlink, and possibly for uplink.

Nearly 70 years after the pioneering intensity correlation experiments by Hanbury-Brown and Twiss [205], there is growing interest in temporal correlation spectroscopy to achieve high angular resolution in studies of celestial light sources with star light correlation spectroscopy. Temporal intensity interferometry in comparison with conventional direct interferometry has the advantages of having a simplified implementation. This is because no light recombination or physical delay lines are needed and as a result the correlation will be insensitive to environmental turbulences. Recently, using avalanche photodiodes with an active area of $100\,\mu m^2$,

2

time jitter of 500 ps and integrating for 70.5 hours, temporal intensity interferom-
etry (photon bunching) experiments were carried on three bright stars. Currently
available SNSPD technology readily offers ~5 folds improvements of SNR as com-
pared to [14]. Future SNSPD developments will push the boundaries of this field
even further.

Advances in single-photon detection at mid-infrared wavelengths [206, 207] has
led to a growing interest in mid-infrared spectroscopy with SNSPDs [208, 209]. Re-
cently, Wollman et. al. [210], for the Origins Space Telescope concept, studied the
potentials of SNSPDs as a tool to probe bio-signatures in exoplanets atmospheres:
using a mid-infrared spectrometer they will study small spectral changes in a star
light due to the absorption or emission from a transiting exoplanet atmosphere.
The wavelengths range from $2.8\,\mu m$ to $20\,\mu m$ is of particular interest because it
contains absorption lines of many important molecules vital for life, SNSPD based
sensors are promising candidates for exoplanet transit spectroscopy.

Positron emission tomography (PET) [16] is a routinely used functional imaging
technology to visualize changes in metabolic and physiological activities as well as
chemical regional composition inside the body. PET is an important tool in cancer
therapy and with the help of radiotracers, it can retrieve quantitative information
about location and concentration of tumor cells. The high time-resolution of SNSPDs
integrated with scintillators [211] will allow to reach the 10-picosecond PET chal-
lenge [212, 213]. Combining SNSPDs with various types of scintillators (particularly
cryogenic scintillators) is an exciting research field for SNSPD and PET but also for
the broader high-energy physics community.

In biomedical imaging, SNSPDs open new possiblities: the weak emission from
oxygen singlet at 1270 nm can readily be measured, operation further in the in-
frared allows for deeper imaging in biological samples where scattering is lower and
specific molecules can be tracked [214].

For some quantum computation implementations, an important challenge is to
funnel large amounts of data in and out of cryostats operating at mK temperatures
with limited cooling power. This limits the classical approach of using coaxial lines,
the use of optical fibers to communicate at the single photon level using SNSPDs
with systems operating at mK offers the prospects of very large data bandwidth
with very low thermal loads.

2.4. Outlook

After a review of current and future applications of SNSPDs in Section 2.3, we
present two important envisioned SNSPD developments which could further boost
the impact of SNSPDs in science and technology.

2.4.1. Large SNSPD arrays with integrated cryogenic electron-
ics

Addressing the readout challenge of large SNSPD arrays, i.e. accessing and pro-
cessing large amounts of data generated at cryogenic temperatures, is imperative
for high-end imaging applications. As discussed in Section 2.2.2, each readout tech-

nique has specific advantages and disadvantages. We envision future large-scale systems with hybrid cryogenic RF readout techniques utilizing different readout schemes in different sub-systems. Additionally, dispersion engineering is a powerful tool that can be used to tailor the properties of the superconducting transmission lines for better footprints or to boost the operating bandwidth [215, 216].

2
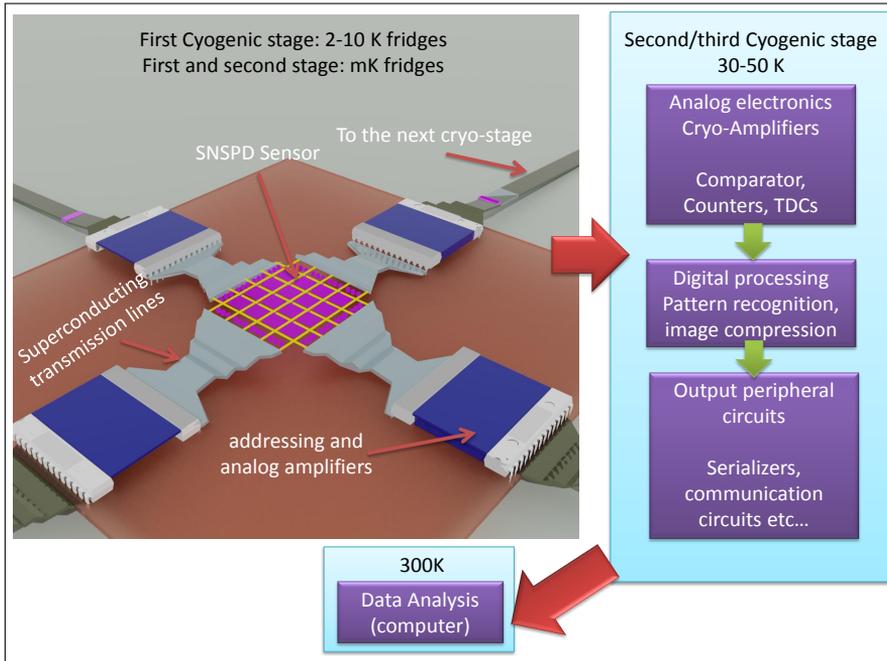
Figure 2.3: Concept illustration of a large SNSPD based imaging sensor: the pixels are addressed and the SNSPD pulses are amplified using the first cryogenic stage readout circuitry connected to the sensor via superconducting transmission lines. The pre-amplified analog signals are then passed to the second cryogenic stage for further processing which includes pulse counting, time to digital converters (TDC), data compression and finally serializers. A processing unit at room temperature receives and analyzes the pre-processed data.

For applications requiring large SNSPD arrays (e.g. high resolution imaging and spectroscopy), it is essential to integrate cryogenic readout circuits close to the SNSPD and separate them from processing units (comparators, counters, time to digital converters, and digital processing units) operating at higher temperatures. Connections among these units must have high RF transmission while providing high thermal isolation (i.e. low thermal conduction, see for example [217]). Such an envisioned system is illustrated in Figure 2.3: The array sensor is connected via superconducting transmission lines to the pixel addressing and pulse pre-amplification electronics (illustrated as addressing and analog amplifiers in the figure) within the first cryogenic stage. Low thermal conductivity coaxial links are used to connect the first cryogenic stage to the second stage (30-50K). The second cryogenic stage is where further complex processing are performed which may include (but be not

2

limited to) triggering, pulse counting, time to digital converters for time stamping, data compression and serializers able to handle the large data stream. We foresee successful implementation of large area, high density imaging sensors such as the one shown in Figure 2.3 can bring about a step change to many imaging applications discussed in Section 2.3. A further step could be the integration of such a sensor in compact cryo-coolers [218], making it even more attractive for applications where size and power consumption are important decision making factors such as equipment integrated in satellites.

2.4.2. SNSPD-based re-configurable integrated quantum photonics

Using SNSPDs for conditional reconfiguration of quantum photonics circuits based on detection events, as illustrated in Figure 2.4, can facilitate quantum communication schemes such as teleportation, entanglement swapping, quantum repeaters, etc. Such schemes rely on performing a (Bell-state) measurement on a photonic qubit, then feed-forward the resulting detection electrical signal to conditionally modify another photonic qubit on the same or a different chip. This comes as a challenge though, the time-scale for the voltage signal of SNSPDs is on the order of nanoseconds, necessitating delaying optical signals on the chip by a similar time-scale to allow for conditional reconfiguration of the circuit based on detection events. To overcome such a challenge, ultra-fast on-chip SNSPDs must be implemented, in combination with heat-free fast re-configurable photonic circuits and ultra-low loss optical delay lines to match the electrical signal delay. An important step toward such a goal was recently demonstrated by realizing waveguide integrated SNSPDs with thin-film lithium niobate circuits, which can deliver the needed modulation for fast routing of single photons on-chip [219]. Another interesting application for such re-configurable circuits are quantum simulators for implementing sampling problems, quantum transport simulations or disordered quantum systems. The integration of efficient sources and detectors with low-loss optical waveguides on the same chip will significantly advance the scalability prospects for photonic quantum simulators.

2.5. Conclusion

In this perspective, we reviewed the evolution of SNSPDs, the state-of-the-art, working mechanisms, fabrication methods, material platforms, readout schemes, applications and disruptive enabled technologies. Our goal is to provide a dynamic multidisciplinary picture targeted toward both the community of SNSPD researchers and scientists working on overlapping lines of research where this technology can have important impact. An outlook for future developments of SNSPD is also provided along with two key envisioned enabling developments to boost the impact of SNSPD in science and technology.
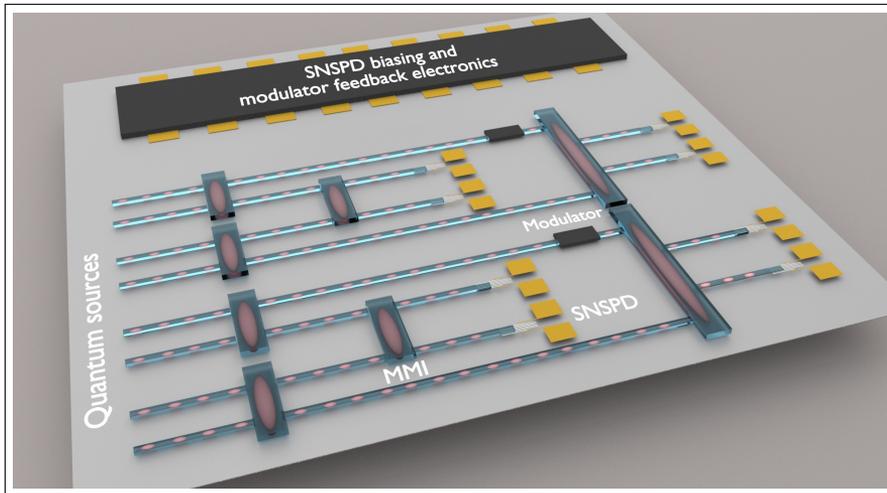
Figure 2.4: Concept illustration of a single photon reconfigurable quantum photonic circuit consisting of quantum sources, beam splitters that are implemented here using multimode interferometers (MMI), electro-optic modulators, and SNSPDs. Detection signals from quantum interference outcome between different qubits are processed by the feedback-electronics module to apply qubit rotations on-chip.

References

[1] A. Einstein, *on a heuristic point of view concerning the generation and transformation of light,* annals of physics **4** (1905).

[2] D. Bouwmeester and A. Zeilinger, *The physics of quantum information: basic concepts,* in *The physics of quantum information* (Springer, 2000) pp. 1–14.

[3] C. H. Bennett and D. P. DiVincenzo, *Quantum information and computation,* nature **404**, 247 (2000).

[4] Y.-A. Chen, Q. Zhang, T.-Y. Chen, W.-Q. Cai, S.-K. Liao, J. Zhang, K. Chen, J. Yin, J.-G. Ren, Z. Chen, S.-L. Han, Q. Yu, K. Liang, F. Zhou, X. Yuan, M.-S. Zhao, T.-Y. Wang, X. Jiang, L. Zhang, W.-Y. Liu, Y. Li, Q. Shen, Y. Cao, C.-Y. Lu, R. Shu, J.-Y. Wang, L. Li, N.-L. Liu, F. Xu, X.-B. Wang, C.-Z. Peng, and J.-W. Pan, *An integrated space-to-ground quantum communication network over 4,600 kilometres,* Nature **589**, 214 (2021).

[5] H. J. Kimble, *The quantum internet,* Nature **453**, 1023 (2008).

[6] H. Zhong, Han-Senand Wang, Y.-H. Deng, M.-C. Chen, L.-C. Peng, Y.-H. Luo, J. Qin, D. Wu, X. Ding, Y. Hu, P. Hu, X.-Y. Yang, W.-J. Zhang, H. Li, Y. Li, X. Jiang, L. Gan, G. Yang, L. You, Z. Wang, L. Li, N.-L. Liu, C.-Y. Lu, and J.-W. Pan, *Quantum computational advantage using photons,* Science **370**, 1460 (2020).

2

[7] D. Salvoni, M. Ejrnaes, L. Parlato, A. Sannino, A. Boselli, G. P. Pepe, R. Cristiano, and X. Wang, *Lidar techniques for a SNSPD-based measurement,* Journal of Physics: Conference Series **1182**, 012014 (2019).

[8] C. Wu, W. Xing, L. Xia, H. Huang, and C. Xu, *Receiver performance characteristics of single-photon lidar in a strong background environment,* Appl. Opt. **58**, 102 (2019).

[9] G. G. Taylor, D. Morozov, N. R. Gemmell, K. Erotokritou, S. Miki, H. Terai, and R. H. Hadfield, *Photon counting lidar at 2.3 μm wavelength with superconducting nanowires,* Optics express **27**, 38147 (2019).

[10] J. Hu, Q. Zhao, X. Zhang, L. Zhang, X. Zhao, L. Kang, and P. Wu, *Photon-counting optical time-domain reflectometry using a superconducting nanowire single-photon detector,* Journal of Lightwave Technology **30**, 2583 (2012).

[11] C. Schuck, W. H. P. Pernice, X. Ma, and H. X. Tang, *Optical time domain reflectometry with low noise waveguide-coupled superconducting nanowire single-photon detectors,* Applied Physics Letters **102**, 191104 (2013).

[12] N. Zen, A. Casaburi, S. Shiki, K. Suzuki, M. Ejrnaes, R. Cristiano, and M. Ohkubo, *1 mm ultrafast superconducting stripline molecule detector,* Applied Physics Letters **95**, 172508 (2009).

[13] R. Sobolewski, A. Verevkin, G. Gol'Tsman, A. Lipatov, and K. Wilsher, *Ultrafast superconducting single-photon optical detectors and their applications,* IEEE Transactions on applied superconductivity **13**, 1151 (2003).

[14] W. Guerin, A. Dussaux, M. Fouché, G. Labeyrie, J.-P. Rivet, D. Vernet, F. Vakili, and R. Kaiser, *Temporal intensity interferometry: photon bunching in three bright stars,* Monthly Notices of the Royal Astronomical Society **472**, 4126 (2017).

[15] I. Nissila, T. Noponen, J. Heino, T. Kajava, and T. Katila, *Diffuse Optical Imaging. In: Lin J.C. (eds) Advances in Electromagnetic Fields in Living Systems. Advances in Electromagnetic Fields in Living Systems* (Springer, Boston, MA., 2005).

[16] D. L. Bailey, D. W. Townsend, P. Valk, and M. Maisy, *Positron emission tomography: basic sciences* (Springer, 2005).

[17] D. Twerenbold, J. Vuilleumier, D. Gerber, A. Tadsen, B. van den Brandt, and P. M. Gillevet, *Detection of single macromolecules using a cryogenic particle detector coupled to a biopolymer mass spectrometer,* Applied Physics Letters **68**, 3503 (1996), https://doi.org/10.1063/1.115772 .

[18] D. Renker, *Geiger-mode avalanche photodiodes, history, properties and problems,* Nuclear Instruments and Methods in Physics Research Section A:

Accelerators, Spectrometers, Detectors and Associated Equipment **567**, 48 (2006).

[19] D. Renker and E. Lorenz, *Advances in solid state photon detectors,* Journal of Instrumentation **4**, P04004 (2009).

[20] R. Foord, R. Jones, C. Oliver, and E. Pike, *The use of photomultiplier tubes for photon counting,* Applied optics **8**, 1975 (1969).

[21] P. Cushman and R. Rusack, *A photomultiplier tube incorporating an avalanche photodiode,* Nuclear Instruments and Methods in Physics Research Section A: Accelerators, Spectrometers, Detectors and Associated Equipment **333**, 381 (1993).

[22] G. N. Gol'tsman, O. Okunev, G. Chulkova, A. Lipatov, A. Semenov, K. Smirnov, B. Voronov, A. Dzardanov, C. Williams, and R. Sobolewski, *Picosecond superconducting single-photon optical detector,* Applied Physics Letters **79**, 705 (2001).

[23] R. H. Hadfield, *Single-photon detectors for optical quantum information applications,* Nature Photonics **3**, 696 (2009).

[24] Y. Makhlin, G. Schön, and A. Shnirman, *Quantum-state engineering with josephson-junction devices,* Reviews of modern physics **73**, 357 (2001).

[25] J. Clarke and A. I. Braginski, *The SQUID handbook*, Vol. 1 (Wiley Online Library, 2004).

[26] J. Zmuidzinas and P. L. Richards, *Superconducting detectors and mixers for millimeter and submillimeter astrophysics,* Proceedings of the IEEE **92**, 1597 (2004).

[27] S. Seliverstov, S. Maslennikov, S. Ryabchun, M. Finkel, T. Klapwijk, N. Kaurova, Y. Vachtomin, K. Smirnov, B. Voronov, and G. Goltsman, *Fast and sensitive terahertz direct detector based on superconducting antenna-coupled hot electron bolometer,* IEEE Transactions on Applied Superconductivity **25**, 1 (2014).

[28] D. H. Andrews, W. F. Brucksch, W. T. Ziegler, and E. R. Blanchard, *Attenuated superconductors i. for measuring infra☐red radiation,* Review of Scientific Instruments **13**, 281 (1942), https://doi.org/10.1063/1.1770037 .

[29] A. J. Miller, S. W. Nam, J. M. Martinis, and A. V. Sergienko, *Demonstration of a low-noise near-infrared photon counter with multiphoton discrimination,* Applied Physics Letters **83**, 791 (2003).

[30] K. D. Irwin and G. C. Hilton, *Transition-edge sensors,* Cryogenic particle detection , 63 (2005).

2

[31] A. Verevkin, J. Zhang, R. Sobolewski, A. Lipatov, O. Okunev, G. Chulkova, A. Korneev, K. Smirnov, G. Gol'tsman, and A. Semenov, *Detection efficiency of large-active-area nbn single-photon superconducting detectors in the ultraviolet to near-infrared range,* Applied Physics Letters **80**, 4687 (2002).

[32] J. Zhang, N. Boiadjieva, G. Chulkova, H. Deslandes, G. Goltsman, A. Korneev, P. Kouminov, M. Leibowitz, W. Lo, R. Malinsky, O. Okunev, A. Pearlman, W. Slysz, K. Smirnov, C. Tsao, A. Verevkin, B. Voronov, K. Wilsher, and R. Sobolewski, *Noninvasive cmos circuit testing with nbn superconducting single-photon detectors,* Electronics Letters **39**, 1086 (2003).

[33] R. H. Hadfield, J. L. Habif, J. Schlafer, R. E. Schwall, and S. W. Nam, *Quantum key distribution at 1550nm with twin superconducting single-photon detectors,* Applied Physics Letters **89**, 241129 (2006), https://doi.org/10.1063/1.2405870 .

[34] H. Takesue, S. W. Nam, Q. Zhang, R. H. Hadfield, T. Honjo, K. Tamaki, and Y. Yamamoto, *Quantum key distribution over a 40-db channel loss using superconducting single-photon detectors,* Nature Photonics **1**, 343 (2007).

[35] X. Hu, T. Zhong, J. E. White, E. A. Dauler, F. Najafi, C. H. Herder, F. N. Wong, and K. K. Berggren, *Fiber-coupled nanowire photon counter at 1550 nm with 24% system detection efficiency,* Optics letters **34**, 3607 (2009).

[36] X. Hu, E. A. Dauler, R. J. Molnar, and K. K. Berggren, *Superconducting nanowire single-photon detectors integrated with optical nano-antennae,* Optics Express **19**, 17 (2011).

[37] K. M. Rosfjord, J. K. Yang, E. A. Dauler, A. J. Kerman, V. Anant, B. M. Voronov, G. N. Gol'Tsman, and K. K. Berggren, *Nanowire single-photon detector with an integrated optical cavity and anti-reflection coating,* Optics express **14**, 527 (2006).

[38] V. B. Verma, F. Marsili, S. Harrington, A. E. Lita, R. P. Mirin, and S. W. Nam, *A three-dimensional, polarization-insensitive superconducting nanowire avalanche photodetector,* Applied Physics Letters **101**, 251114 (2012).

[39] J. P. Sprengers, A. Gaggero, D. Sahin, S. Jahanmirinejad, G. Frucci, F. Mattioli, R. Leoni, J. Beetz, M. Lermer, M. Kamp, S. Höfling, R. Sanjines, and A. Fiore, *Waveguide superconducting single-photon detectors for integrated quantum photonic circuits,* Applied Physics Letters **99**, 181110 (2011).

[40] W. H. P. Pernice, C. Schuck, O. Minaeva, M. Li, G. N. Goltsman, A. V. Sergienko, and H. X. Tang, *High-speed and high-efficiency travelling wave single-photon detectors embedded in nanophotonic circuits,* Nature Communications **3**, 1325 (2012).

[41] F. Marsili, V. B. Verma, J. A. Stern, S. Harrington, A. E. Lita, T. Gerrits, I. Vayshenker, B. Baek, M. D. Shaw, R. P. Mirin, *et al.*, *Detecting single infrared photons with 93% system efficiency,* Nature Photonics **7**, 210 (2013).

[42] I. Esmaeil Zadeh, J. W. N. Los, R. B. M. Gourgues, V. Steinmetz, G. Bulgarini, S. M. Dobrovolskiy, V. Zwiller, and S. N. Dorenbos, *Single-photon detectors combining high efficiency, high detection rates, and ultra-high timing resolution,* APL Photonics **2**, 111301 (2017).

[43] W. Zhang, L. You, H. Li, J. Huang, C. Lv, L. Zhang, X. Liu, J. Wu, Z. Wang, and X. Xie, *Nbn superconducting nanowire single photon detector with efficiency over 90% at 1550 nm wavelength operational at compact cryocooler temperature,* Science China Physics, Mechanics & Astronomy **60**, 120314 (2017).

[44] D. V. Reddy, R. R. Nerem, S. W. Nam, R. P. Mirin, and V. B. Verma, *Superconducting nanowire single-photon detectors with 98% system detection efficiency at 1550nm,* Optica **7**, 1649 (2020).

[45] P. Hu, H. Li, L. You, H. Wang, Y. Xiao, J. Huang, X. Yang, W. Zhang, Z. Wang, and X. Xie, *Detecting single infrared photons toward optimal system detection efficiency,* Optics Express **28**, 36884 (2020).

[46] J. Chang, J. Los, J. Tenorio-Pearl, N. Noordzij, R. Gourgues, A. Guardiani, J. Zichi, S. Pereira, H. Urbach, V. Zwiller, *et al.*, *Detecting telecom single photons with 99.5- 2.07+ 0.5% system detection efficiency and high time resolution,* APL Photonics **6**, 036114 (2021).

[47] L. N. Bulaevskii, M. J. Graf, and V. G. Kogan, *Vortex-assisted photon counts and their magnetic field dependence in single-photon superconducting detectors,* Phys. Rev. B **85**, 014505 (2012).

[48] T. Yamashita, S. Miki, K. Makise, W. Qiu, H. Terai, M. Fujiwara, M. Sasaki, and Z. Wang, *Origin of intrinsic dark count in superconducting nanowire single-photon detectors,* Applied Physics Letters **99**, 161105 (2011).

[49] J. Chang, I. E. Zadeh, J. W. Los, J. Zichi, A. Fognini, M. Gevers, S. Dorenbos, S. F. Pereira, P. Urbach, and V. Zwiller, *Multimode-fiber-coupled superconducting nanowire single-photon detectors with high detection efficiency and time resolution,* Applied optics **58**, 9803 (2019).

[50] H. Shibata, K. Shimizu, H. Takesue, and Y. Tokura, *Ultimate low system dark-count rate for superconducting nanowire single-photon detector,* Optics letters **40**, 3428 (2015).

[51] W. Zhang, X. Yang, H. Li, L. You, C. Lv, L. Zhang, C. Zhang, X. Liu, Z. Wang, and X. Xie, *Fiber-coupled superconducting nanowire single-photon detectors integrated with a bandpass filter on the fiber end-face,* Superconductor Science and Technology **31**, 035012 (2018).

2

[52] S. Chen, L. You, W. Zhang, X. Yang, H. Li, L. Zhang, Z. Wang, and X. Xie, *Dark counts of superconducting nanowire single-photon detector under illumination,* Optics express **23**, 10786 (2015).

[53] Y. Hochberg, I. Charaev, S.-W. Nam, V. Verma, M. Colangelo, and K. K. Berggren, *Detecting sub-gev dark matter with superconducting nanowires,* Phys. Rev. Lett. **123**, 151802 (2019).

[54] L. You, X. Yang, Y. He, W. Zhang, D. Liu, W. Zhang, L. Zhang, L. Zhang, X. Liu, S. Chen, *et al.*, *Jitter analysis of a superconducting nanowire single photon detector,* Aip Advances **3**, 072135 (2013).

[55] Q. Zhao, L. Zhang, T. Jia, L. Kang, W. Xu, J. Chen, and P. Wu, *Intrinsic timing jitter of superconducting nanowire single-photon detectors,* Applied Physics B **104**, 673 (2011).

[56] E. A. Dauler, B. S. Robinson, A. J. Kerman, J. K. Yang, K. M. Rosfjord, V. Anant, B. Voronov, G. Gol'tsman, and K. K. Berggren, *Multi-element superconducting nanowire single-photon detector,* IEEE Transactions on Applied Superconductivity **17**, 279 (2007).

[57] V. Shcheslavskiy, P. Morozov, A. Divochiy, Y. Vakhtomin, K. Smirnov, and W. Becker, *Ultrafast time measurements by time-correlated single photon counting coupled with superconducting single photon detector,* Review of scientific instruments **87**, 053117 (2016).

[58] J. Wu, L. You, S. Chen, H. Li, Y. He, C. Lv, Z. Wang, and X. Xie, *Improving the timing jitter of a superconducting nanowire single-photon detection system,* Applied optics **56**, 2195 (2017).

[59] I. Esmaeil Zadeh, J. W. N. Los, R. B. M. Gourgues, J. Chang, A. W. Elshaari, J. R. Zichi, Y. J. van Staaden, J. P. E. Swens, N. Kalhor, A. Guardiani, Y. Meng, K. Zou, S. Dobrovolskiy, A. W. Fognini, D. R. Schaart, D. Dalacu, P. J. Poole, M. E. Reimer, X. Hu, S. F. Pereira, V. Zwiller, and S. N. Dorenbos, *Efficient single-photon detection with 7.7 ps time resolution for photon-correlation measurements,* ACS Photonics **7**, 1780 (2020).

[60] B. Korzh, Q.-Y. Zhao, J. P. Allmaras, S. Frasca, T. M. Autry, E. A. Bersin, A. D. Beyer, R. M. Briggs, B. Bumble, M. Colangelo, *et al.*, *Demonstration of sub-3 ps temporal resolution with a superconducting nanowire single-photon detector,* Nature Photonics **14**, 250 (2020).

[61] B. Korzh, Q.-Y. Zhao, S. Frasca, D. Zhu, E. Ramirez, E. Bersin, M. Colangelo, A. E. Dane, A. D. Beyer, J. Allmaras, E. E. Wollman, K. K. Berggren, and M. D. Shaw, *Wsi superconducting nanowire single photon detector with a temporal resolution below 5 ps,* in *Conference on Lasers and Electro-Optics* (Optical Society of America, 2018) p. FW3F.3.

[62] R. H. Hadfield, P. A. Dalgarno, J. A. O'Connor, E. Ramsay, R. J. Warburton, E. J. Gansen, B. Baek, M. J. Stevens, R. P. Mirin, and S. W. Nam, *Submicrometer photoresponse mapping of nanowire superconducting single-photon detectors,* Applied Physics Letters **91**, 241108 (2007).

[63] A. J. Kerman, E. A. Dauler, J. K. Yang, K. M. Rosfjord, V. Anant, K. K. Berggren, G. N. Gol'tsman, and B. M. Voronov, *Constriction-limited detection efficiency of superconducting nanowire single-photon detectors,* Applied Physics Letters **90**, 101110 (2007).

[64] J. R. Clem and K. K. Berggren, *Geometry-dependent critical currents in superconducting nanocircuits,* Phys. Rev. B **84**, 174510 (2011).

[65] D. Henrich, P. Reichensperger, M. Hofherr, J. Meckbach, K. Il'in, M. Siegel, A. Semenov, A. Zotova, and D. Y. Vodolazov, *Geometry-induced reduction of the critical current in superconducting nanowires,* Physical Review B **86**, 144504 (2012).

[66] H. Hortensius, E. Driessen, T. Klapwijk, K. Berggren, and J. Clem, *Critical-current reduction in thin superconducting wires due to current crowding,* Applied Physics Letters **100**, 182602 (2012).

[67] M. K. Akhlaghi, H. Atikian, A. Eftekharian, M. Loncar, and A. H. Majedi, *Reduced dark counts in optimized geometries for superconducting nanowire single photon detectors,* Optics express **20**, 23610 (2012).

[68] G.-Z. Xu, W.-J. Zhang, L.-X. You, J.-M. Xiong, X.-Q. Sun, H. Huang, X. Ou, Y.-M. Pan, C.-L. Lv, H. Li, *et al.*, *Superconducting microstrip single-photon detector with system detection efficiency over 90% at 1550 nm,* arXiv preprint arXiv:2101.05407 (2021).

[69] A. Banerjee, R. M. Heath, D. Morozov, D. Hemakumara, U. Nasti, I. Thayne, and R. H. Hadfield, *Optical properties of refractory metal based thin films,* Opt. Mater. Express **8**, 2072 (2018).

[70] V. Anant, A. J. Kerman, E. A. Dauler, J. K. Yang, K. M. Rosfjord, and K. K. Berggren, *Optical properties of superconducting nanowire single-photon detectors,* Optics express **16**, 10750 (2008).

[71] S. Dorenbos, E. Reiger, N. Akopian, U. Perinetti, V. Zwiller, T. Zijlstra, and T. Klapwijk, *Superconducting single photon detectors with minimized polarization dependence,* Applied Physics Letters **93**, 161102 (2008).

[72] F. Zheng, R. Xu, G. Zhu, B. Jin, L. Kang, W. Xu, J. Chen, and P. Wu, *Design of a polarization-insensitive superconducting nanowire single photon detector with high detection efficiency,* Scientific Reports **6**, 1 (2016).

[73] L. Redaelli, V. Zwiller, E. Monroy, and J. Gérard, *Design of polarization-insensitive superconducting single photon detectors with high-index dielectrics,* Superconductor Science and Technology **30**, 035005 (2017).

2

[74] X. Chi, K. Zou, C. Gu, J. Zichi, Y. Cheng, N. Hu, X. Lan, S. Chen, Z. Lin, V. Zwiller, *et al.*, *Fractal superconducting nanowire single-photon detectors with reduced polarization sensitivity,* Optics letters **43**, 5017 (2018).

[75] Y. Meng, K. Zou, N. Hu, X. Lan, L. Xu, J. Zichi, S. Steinhauer, V. Zwiller, and X. Hu, *Fractal superconducting nanowire avalanche photodetector at 1550 nm with 60% system detection efficiency and 1.05 polarization sensitivity,* Optics Letters **45**, 471 (2020).

[76] R. Gourgues, J. W. N. Los, J. Zichi, J. Chang, N. Kalhor, G. Bulgarini, S. N. Dorenbos, V. Zwiller, and I. E. Zadeh, *Superconducting nanowire single photon detectors operating at temperature from 4 to 7 k,* Opt. Express **27**, 24601 (2019).

[77] A. J. Kerman, E. A. Dauler, W. E. Keicher, J. K. W. Yang, K. K. Berggren, G. Gol'tsman, and B. Voronov, *Kinetic-inductance-limited reset time of superconducting nanowire photon counters,* Applied Physics Letters **88**, 111116 (2006).

[78] J. K. W. Yang, A. J. Kerman, E. A. Dauler, V. Anant, K. M. Rosfjord, and K. K. Berggren, *Modeling the Electrical and Thermal Response of Superconducting Nanowire Single-Photon Detectors,* IEEE Transactions on Applied Superconductivity **17**, 581 (2007).

[79] C. Autebert, G. Gras, E. Amri, M. Perrenoud, M. Caloz, H. Zbinden, and F. Bussieres, *Direct measurement of the recovery time of superconducting nanowire single-photon detectors,* Journal of Applied Physics **128**, 074504 (2020).

[80] E. A. Dauler, A. J. Kerman, B. S. Robinson, J. K. Yang, B. Voronov, G. Goltsman, S. A. Hamilton, and K. K. Berggren, *Photon-number-resolution with sub-30-ps timing using multi-element superconducting nanowire single photon detectors,* Journal of Modern Optics **56**, 364 (2009).

[81] A. Divochiy, F. Marsili, D. Bitauld, A. Gaggero, R. Leoni, F. Mattioli, A. Korneev, V. Seleznev, N. Kaurova, O. Minaeva, G. Gol'tsman, K. G. Lagoudakis, M. Benkhaoul, F. Lévy, and A. Fiore, *Superconducting nanowire photon-number-resolving detector at telecommunication wavelengths,* Nature Photonics **2**, 302 (2008).

[82] N. Calandri, Q.-Y. Zhao, D. Zhu, A. Dane, and K. K. Berggren, *Superconducting nanowire detector jitter limited by detector geometry,* Applied Physics Letters **109**, 152601 (2016).

[83] A. Kozorezov, C. Lambert, F. Marsili, M. Stevens, V. Verma, J. Allmaras, M. Shaw, R. Mirin, and S. W. Nam, *Fano fluctuations in superconducting-nanowire single-photon detectors,* Physical Review B **96**, 054507 (2017).

[84] Y. Cheng, C. Gu, and X. Hu, *Inhomogeneity-induced timing jitter of super-conducting nanowire single-photon detectors,* Applied Physics Letters **111**, 062604 (2017).

[85] H. Wu, C. Gu, Y. Cheng, and X. Hu, *Vortex-crossing-induced timing jitter of superconducting nanowire single-photon detectors,* Applied Physics Letters **111**, 062603 (2017).

[86] D. Y. Vodolazov, *Minimal timing jitter in superconducting nanowire single-photon detectors,* Physical Review Applied **11**, 014016 (2019).

[87] J. Demsar, *Non-equilibrium phenomena in superconductors probed by femtosecond time-domain spectroscopy,* Journal of Low Temperature Physics **201**, 676 (2020).

[88] I. Holzman and Y. Ivry, *Superconducting nanowires for single-photon detection: Progress, challenges, and opportunities,* Advanced Quantum Technologies **2**, 1800058 (2019), https://onlinelibrary.wiley.com/doi/pdf/10.1002/qute.201800058 .

[89] A. D. Semenov, G. N. Gol'tsman, and A. A. Korneev, *Quantum detection by current carrying superconducting film,* Physica C: Superconductivity **351**, 349 (2001).

[90] A. Engel, J. J. Renema, K. Il'in, and A. Semenov, *Detection mechanism of superconducting nanowire single-photon detectors,* Superconductor Science and Technology **28**, 114003 (2015).

[91] C. M. Natarajan, M. G. Tanner, and R. H. Hadfield, *Superconducting nanowire single-photon detectors: physics and applications,* Superconductor Science and Technology **25**, 063001 (2012).

[92] K. A. Sunter and K. K. Berggren, *Optical modeling of superconducting nanowire single photon detectors using the transfer matrix method,* Appl. Opt. **57**, 4872 (2018).

[93] A. Engel and A. Schilling, *Numerical analysis of detection-mechanism models of superconducting nanowire single-photon detector,* Journal of Applied Physics **114**, 214501 (2013).

[94] D. Y. Vodolazov, *Single-photon detection by a dirty current-carrying super-conducting strip based on the kinetic-equation approach,* Phys. Rev. Applied **7**, 034014 (2017).

[95] J. Allmaras, A. Kozorezov, B. Korzh, K. Berggren, and M. Shaw, *Intrinsic timing jitter and latency in superconducting nanowire single-photon detectors,* Phys. Rev. Applied **11**, 034062 (2019).

2

[96] J. P. Allmaras, *Modeling and Development of Superconducting Nanowire Single-Photon Detectors*, Ph.D. thesis, California Institute of Technology (2020).

[97] A. N. Zotova and D. Y. Vodolazov, *Photon detection by current-carrying superconducting film: A time-dependent ginzburg-landau approach,* Phys. Rev. B **85**, 024509 (2012).

[98] J. J. Renema, R. Gaudio, Q. Wang, Z. Zhou, A. Gaggero, F. Mattioli, R. Leoni, D. Sahin, M. J. A. de Dood, A. Fiore, and M. P. van Exter, *Experimental test of theories of the detection mechanism in a nanowire superconducting single photon detector,* Phys. Rev. Lett. **112**, 117604 (2014).

[99] A. Semenov, P. Haas, H.-W. Hübers, K. Ilin, M. Siegel, A. Kirste, D. Drung, T. Schurig, and A. Engel, *Intrinsic quantum efficiency and electro-thermal model of a superconducting nanowire single-photon detector,* Journal of Modern Optics **56**, 345 (2009).

[100] Q.-Y. Zhao, D. F. Santavicca, D. Zhu, B. Noble, and K. K. Berggren, *A distributed electrical model for superconducting nanowire single photon detectors,* Applied Physics Letters **113**, 082601 (2018).

[101] A. J. Kerman, J. K. W. Yang, R. J. Molnar, E. A. Dauler, and K. K. Berggren, *Electrothermal feedback in superconducting nanowire single-photon detectors,* Physical Review B **79**, 100509 (2009).

[102] A. Verevkin, C. Williams, G. N. Gol'tsman, R. Sobolewski, and G. Gilbert, *Single-photon superconducting detectors for practical high-speed quantum cryptography,* in *International Conference on Quantum Information* (Optical Society of America, 2001) p. PA3.

[103] M. Ejrnaes, L. Parlato, R. Arpaia, T. Bauch, F. Lombardi, R. Cristiano, F. Tafuri, and G. Pepe, *Observation of dark pulses in 10 nm thick ybco nanostrips presenting hysteretic current voltage characteristics,* Superconductor Science and Technology **30** (2017), 10.1088/1361-6668/aa94b9.

[104] M. Lyatti, M. A. Wolff, I. Gundareva, M. Kruth, S. Ferrari, R. E. Dunin-Borkowski, and C. Schuck, *Energy-level quantization and single-photon control of phase slips in yba2cu3o7–x nanowires,* Nature Communications **11**, 763 (2020).

[105] L. You, *Superconducting nanowire single-photon detectors for quantum information,* Nanophotonics **9**, 2673 (01 Sep. 2020).

[106] V. B. Verma, A. E. Lita, M. R. Vissers, F. Marsili, D. P. Pappas, R. P. Mirin, and S. W. Nam, *Superconducting nanowire single photon detectors fabricated from an amorphous mo0.75ge0.25 thin film,* Applied Physics Letters **105**, 022602 (2014).

[107] I. Milostnaya, A. Korneev, M. Tarkhov, A. Divochiy, O. Minaeva, V. Se-leznev, N. Kaurova, B. Voronov, O. Okunev, G. Chulkova, K. Smirnov, and G. Gol'tsman, *Superconducting single photon nanowire detectors development for ir and thz applications,* Journal of Low Temperature Physics **151**, 591 (2008).

[108] Y. P. Korneeva, M. Y. Mikhailov, Y. P. Pershin, N. Manova, A. Divochiy, Y. B. Vakhtomin, A. Korneev, K. Smirnov, A. Sivakov, A. Y. Devizenko, *et al.*, *Superconducting single-photon detector made of mosi film,* Superconductor Science and Technology **27**, 095012 (2014).

[109] V. B. Verma, B. Korzh, F. Bussières, R. D. Horansky, S. D. Dyer, A. E. Lita, I. Vayshenker, F. Marsili, M. D. Shaw, H. Zbinden, R. P. Mirin, and S. W. Nam, *High-efficiency superconducting nanowire single-photon detectors fabricated from mosi thin-films,* Opt. Express **23**, 33792 (2015).

[110] M. Caloz, M. Perrenoud, C. Autebert, B. Korzh, M. Weiss, C. Schönenberger, R. J. Warburton, H. Zbinden, and F. Bussières, *High-detection efficiency and low-timing jitter with amorphous superconducting nanowire single-photon detectors,* Applied Physics Letters **112**, 061103 (2018).

[111] C. Cirillo, J. Chang, M. Caputo, J. Los, S. Dorenbos, I. Esmaeil Zadeh, and C. Attanasio, *Superconducting nanowire single photon detectors based on disordered nbre films,* Applied Physics Letters **117**, 172602 (2020).

[112] S. N. Dorenbos, P. Forn-Díaz, T. Fuse, A. H. Verbruggen, T. Zijlstra, T. M. Klapwijk, and V. Zwiller, *Low gap superconducting single photon detectors for infrared sensitivity,* Applied Physics Letters **98**, 251102 (2011).

[113] A. Engel, A. Aeschbacher, K. Inderbitzin, A. Schilling, K. Il'in, M. Hofherr, M. Siegel, A. Semenov, and H.-W. Hübers, *Tantalum nitride superconducting single-photon detectors with low cut-off energy,* Applied Physics Letters **100**, 062601 (2012).

[114] H. Shibata, T. Akazaki, and Y. Tokura, *Fabrication of mgb_2 nanowire single-photon detector with meander structure,* Applied Physics Express **6**, 023101 (2013).

[115] S. Cherednichenko, N. Acharya, E. Novoselov, and V. Drakinskiy, *Low kinetic inductance superconducting mgb_2 nanowire photon detectors with a 100 picosecond relaxation time,* (2019), arXiv:1911.01480 .

[116] S. Cherednichenko, N. Acharya, E. Novoselov, and V. Drakinskiy, *Ir- and visible- light single photon detection in superconducting mgb_2 nanowires,* (2019), arXiv:1911.01652 .

[117] J. Zichi, J. Chang, S. Steinhauer, K. Von Fieandt, J. W. Los, G. Visser, N. Kalhor, T. Lettner, A. W. Elshaari, I. E. Zadeh, *et al.*, *Optimizing the stoichiometry of ultrathin nbtin films for high-performance superconducting nanowire single-photon detectors,* Optics Express **27**, 26579 (2019).

2

[118] R. Cheng, S. Wang, and H. Tang, *Superconducting nanowire single-photon detectors fabricated from atomic-layer- deposited nbn,* Applied Physics Letters **115**, 241101 (2019).

[119] E. Knehr, A. Kuzmin, D. Y. Vodolazov, M. Ziegler, S. Doerner, K. Ilin, M. Siegel, R. Stolz, and H. Schmidt, *Nanowire single-photon detectors made of atomic layer-deposited niobium nitride,* Superconductor Science and Technology **32**, 125007 (2019).

[120] R. Cheng, J. Wright, H. G. Xing, D. Jena, and H. X. Tang, *Epitaxial niobium nitride superconducting nanowire single-photon detectors,* Applied Physics Letters **117**, 132601 (2020), https://doi.org/10.1063/5.0018818 .

[121] K. Inderbitzin, A. Engel, A. Schilling, K. Il'in, and M. Siegel, *An ultra-fast superconducting nb nanowire single-photon detector for soft x-rays,* Applied Physics Letters **101**, 162601 (2012).

[122] D. Perez, de Lara, M. Ejrnaes, A. Casaburi, M. Lisitskiy, R. Cristiano, S. Pagano, A. Gaggero, R. Leoni, G. Golt'sman, and B. Voronov, *Feasibility investigation of nbn nanowires as detector in time-of-flight mass spectrometers for macromolecules of interest in biology (proteins),* Journal of Low Temperature Physics **151**, 771 (2008).

[123] A. Branny, P. Didier, J. Zichi, I. E. Zahed, S. Steinhauer, V. Zwiller, and U. Vogt, *X-ray induced secondary particle counting with thin nbtin nanowire superconducting detector,* IEEE Transactions on Applied Superconductivity , 1 (2021).

[124] K. Inderbitzin, A. Engel, and A. Schilling, *Soft x-ray single-photon detection with superconducting tantalum nitride and niobium nanowires,* IEEE Transactions on Applied Superconductivity **23**, 2200505 (2013).

[125] X. Zhang, Q. Wang, and A. Schilling, *Superconducting single x-ray photon detector based on w0.8si0.2,* AIP Advances **6**, 115104 (2016).

[126] E. E. Wollman, V. B. Verma, A. D. Beyer, R. M. Briggs, B. Korzh, J. P. Allmaras, F. Marsili, A. E. Lita, R. P. Mirin, S. W. Nam, and M. D. Shaw, *Uv superconducting nanowire single-photon detectors with high efficiency, low noise, and 4 k operating temperature,* Opt. Express **25**, 26792 (2017).

[127] V. Verma, B. Korzh, A. Walter, A. Lita, R. Briggs, M. Colangelo, Y. Zhai, E. Wollman, A. Beyer, J. Allmaras, *et al.*, *Single-photon detection in the mid-infrared up to 10 micron wavelength using tungsten silicide superconducting nanowire detectors,* arXiv preprint arXiv:2012.09979 (2020).

[128] H. Azzouz, S. N. Dorenbos, D. De Vries, E. B. Ureña, and V. Zwiller, *Efficient single particle detection with a superconducting nanowire,* AIP Advances **2**, 032124 (2012).

[129] S. Steinhauer, S. Gyger, and V. Zwiller, *Progress on large-scale super-conducting nanowire single-photon detectors,* Applied Physics Letters **118**, 100501 (2021).

[130] E. E. Wollman, V. B. Verma, A. E. Lita, W. H. Farr, M. D. Shaw, R. P. Mirin, and S. W. Nam, *Kilopixel array of superconducting nanowire single-photon detectors,* Opt. Express **27**, 35279 (2019).

[131] R. Cheng, C.-L. Zou, X. Guo, S. Wang, X. Han, and H. X. Tang, *Broadband on-chip single-photon spectrometer,* Nature communications **10**, 1 (2019).

[132] M. Hofherr, M. Arndt, K. Il'In, D. Henrich, M. Siegel, J. Toussaint, T. May, and H.-G. Meyer, *Time-tagged multiplexing of serially biased superconducting nanowire single-photon detectors,* IEEE transactions on applied super-conductivity **23**, 2501205 (2013).

[133] Q.-Y. Zhao, D. Zhu, N. Calandri, A. E. Dane, A. N. McCaughan, F. Bellei, H.-Z. Wang, D. F. Santavicca, and K. K. Berggren, *Single-photon imager based on a superconducting nanowire delay line,* Nature Photonics **11**, 247 (2017).

[134] D. Zhu, Q.-Y. Zhao, H. Choi, T.-J. Lu, A. E. Dane, D. Englund, and K. K. Berggren, *A scalable multi-photon coincidence detector based on superconducting nanowires,* Nature nanotechnology **13**, 596 (2018).

[135] A. W. Elshaari, A. Iovan, S. Gyger, I. E. Zadeh, J. Zichi, L. Yang, S. Steinhauer, and V. Zwiller, *Dispersion engineering of superconducting waveguides for multi-pixel integration of single-photon detectors,* APL Photonics **5**, 111301 (2020), https://doi.org/10.1063/5.0019734 .

[136] S. Miki, H. Terai, T. Yamashita, K. Makise, M. Fujiwara, M. Sasaki, and Z. Wang, *Superconducting single photon detectors integrated with single flux quantum readout circuits in a cryocooler,* Applied Physics Letters **99**, 111108 (2011).

[137] T. Ortlepp, M. Hofherr, L. Fritzsch, S. Engert, K. Ilin, D. Rall, H. Toepfer, H.-G. Meyer, and M. Siegel, *Demonstration of digital readout circuit for superconducting nanowire single photon detector,* Opt. Express **19**, 18593 (2011).

[138] H. Terai, T. Yamashita, S. Miki, K. Makise, and Z. Wang, *Low-jitter single flux quantum signal readout from superconducting single photon detector,* Optics Express **20**, 20115 (2012).

[139] S. Miki, S. Miyajima, M. Yabuno, T. Yamashita, T. Yamamoto, N. Imoto, R. Ikuta, R. A. Kirkwood, R. H. Hadfield, and H. Terai, *Superconducting coincidence photon detector with short timing jitter,* Applied Physics Letters **112**, 262601 (2018).

[140] M. Yabuno, S. Miyajima, S. Miki, and H. Terai, *Scalable implementation of a superconducting nanowire single-photon detector array with a superconducting digital signal processor,* Optics Express **28**, 12047 (2020).

2

[141] N. Takeuchi, F. China, S. Miki, S. Miyajima, M. Yabuno, N. Yoshikawa, and H. Terai, *Scalable readout interface for superconducting nanowire single-photon detectors using aqfp and rsfq logic families,* Opt. Express **28**, 15824 (2020).

[142] S. Doerner, A. Kuzmin, S. Wuensch, I. Charaev, F. Boes, T. Zwick, and M. Siegel, *Frequency-multiplexed bias and readout of a 16-pixel superconducting nanowire single-photon detector array,* Applied Physics Letters **111**, 032603 (2017).

[143] A. Gaggero, F. Martini, F. Mattioli, F. Chiarello, R. Cernansky, A. Politi, and R. Leoni, *Amplitude-multiplexed readout of single photon detectors based on superconducting nanowires,* Optica **6**, 823 (2019).

[144] J. Tiedau, T. Schapeler, V. Anant, H. Fedder, C. Silberhorn, and T. J. Bartley, *Single-channel electronic readout of a multipixel superconducting nanowire single photon detector,* Opt. Express **28**, 5528 (2020).

[145] Y. P. Korneeva, D. Y. Vodolazov, A. V. Semenov, I. N. Florya, N. Simonov, E. Baeva, A. A. Korneev, G. N. Goltsman, and T. M. Klapwijk, *Optical single-photon detection in micrometer-scale nbn bridges,* Phys. Rev. Applied **9**, 064037 (2018).

[146] D. Vodolazov, I. Florya, N. Manova, E. Smirnov, A. Korneev, M. Mikhailov, G. Goltsman, and T. Klapwijk, *Single photon detection in micron scale nbn and a-mosi superconducting strips,* EPJ Web of Conferences **190**, 04010 (2018).

[147] I. Charaev, Y. Morimoto, A. Dane, A. Agarwal, M. Colangelo, and K. K. Berggren, *Large-area microwire mosi single-photon detectors at 1550nm wavelength,* Applied Physics Letters **116**, 242603 (2020).

[148] S. S. Ustavschikov, M. Y. Levichev, I. Y. Pashenkin, A. M. Klushin, and D. Y. Vodolazov, *Approaching depairing current in dirty thin superconducting strip covered by low resistive normal metal,* Superconductor Science and Technology **34**, 015004 (2020).

[149] J. Chiles, S. M. Buckley, A. Lita, V. B. Verma, J. Allmaras, B. Korzh, M. D. Shaw, J. M. Shainline, R. P. Mirin, and S. W. Nam, *Superconducting microwire detectors based on wsi with single-photon sensitivity in the near-infrared,* Applied Physics Letters **116**, 242602 (2020).

[150] D. Vodolazov, N. Manova, Y. Korneeva, and A. Korneev, *Timing jitter in nbn superconducting microstrip single-photon detector,* Phys. Rev. Applied **14**, 044041 (2020).

[151] A. Boaron, G. Boso, D. Rusca, C. Vulliez, C. Autebert, M. Caloz, M. Perrenoud, G. Gras, F. Bussières, M.-J. Li, D. Nolan, A. Martin, and H. Zbinden, *Secure quantum key distribution over 421 km of optical fiber,* Phys. Rev. Lett. **121**, 190502 (2018).

[152] Y. Yu, F. Ma, X.-Y. Luo, B. Jing, P.-F. Sun, R.-Z. Fang, C.-W. Yang, H. Liu, M.-Y. Zheng, X.-P. Xie, W.-J. Zhang, L.-X. You, Z. Wang, T.-Y. Chen, Q. Zhang, X.-H. Bao, and J.-W. Pan, *Entanglement of two quantum memories via fibres over dozens of kilometres,* Nature **578**, 240 (2020).

[153] J.-P. Chen, C. Zhang, Y. Liu, C. Jiang, W. Zhang, X.-L. Hu, J.-Y. Guan, Z.-W. Yu, H. Xu, J. Lin, M.-J. Li, H. Chen, H. Li, L. You, Z. Wang, X.-B. Wang, Q. Zhang, and J.-W. Pan, *Sending-or-not-sending with independent lasers: Secure twin-field quantum key distribution over 509 km,* Phys. Rev. Lett. **124**, 070501 (2020).

[154] L. K. Shalm, E. Meyer-Scott, B. G. Christensen, P. Bierhorst, M. A. Wayne, M. J. Stevens, T. Gerrits, S. Glancy, D. R. Hamel, M. S. Allman, K. J. Coakley, S. D. Dyer, C. Hodge, A. E. Lita, V. B. Verma, C. Lambrocco, E. Tortorici, A. L. Migdall, Y. Zhang, D. R. Kumor, W. H. Farr, F. Marsili, M. D. Shaw, J. A. Stern, C. Abellán, W. Amaya, V. Pruneri, T. Jennewein, M. W. Mitchell, P. G. Kwiat, J. C. Bienfang, R. P. Mirin, E. Knill, and S. W. Nam, *Strong loophole-free test of local realism,* Phys. Rev. Lett. **115**, 250402 (2015).

[155] S. L. Todaro, V. B. Verma, K. C. McCormick, D. T. C. Allcock, R. P. Mirin, D. J. Wineland, S. W. Nam, A. C. Wilson, D. Leibfried, and D. H. Slichter, *State readout of a trapped ion qubit using a trap-integrated superconducting photon detector,* Phys. Rev. Lett. **126**, 010501 (2021).

[156] S. Khasminskaya, F. Pyatkov, K. Słowik, S. Ferrari, O. Kahl, V. Kovalyuk, P. Rath, A. Vetter, F. Hennrich, M. M. Kappes, G. Gol'tsman, A. Korneev, C. Rockstuhl, R. Krupke, and W. H. P. Pernice, *Fully integrated quantum photonic circuit with an electrically driven light source,* Nature Photonics **10**, 727 (2016).

[157] L. Elsinger, R. Gourgues, I. E. Zadeh, J. Maes, A. Guardiani, G. Bulgarini, S. F. Pereira, S. N. Dorenbos, V. Zwiller, Z. Hens, and D. Van Thourhout, *Integration of colloidal pbs/cds quantum dots with plasmonic antennas and superconducting detectors on a silicon nitride photonic platform,* Nano Letters **19**, 5452 (2019).

[158] C. Schuck, X. Guo, L. Fan, X. Ma, M. Poot, and H. X. Tang, *Quantum interference in heterogeneous superconducting-photonic circuits on a silicon chip,* Nature Communications **7**, 10352 (2016).

[159] F. Beutel, H. Gehring, M. A. Wolff, C. Schuck, and W. Pernice, *Detector-integrated on-chip qkd receiver for ghz clock rates,* npj Quantum Information **7**, 40 (2021).

[160] C. Schuck, W. H. P. Pernice, O. Minaeva, M. Li, G. Gol'tsman, A. V. Sergienko, and H. X. Tang, *Matrix of integrated superconducting single-photon detectors with high timing resolution,* IEEE Transactions on Applied Superconductivity **23**, 2201007 (2013).

2

2

[161] F. Najafi, J. Mower, N. C. Harris, F. Bellei, A. Dane, C. Lee, X. Hu, P. Kharel, F. Marsili, S. Assefa, K. K. Berggren, and D. Englund, *On-chip detection of non-classical light by scalable integration of single-photon detectors,* Nature Communications **6**, 5873 (2015).

[162] J. Li, R. A. Kirkwood, L. J. Baker, D. Bosworth, K. Erotokritou, A. Banerjee, R. M. Heath, C. M. Natarajan, Z. H. Barber, M. Sorel, and R. H. Hadfield, *Nano-optical single-photon response mapping of waveguide integrated molybdenum silicide (mosi) superconducting nanowires,* Opt. Express **24**, 13931 (2016).

[163] A. Vetter, S. Ferrari, P. Rath, R. Alaee, O. Kahl, V. Kovalyuk, S. Diewald, G. N. Goltsman, A. Korneev, C. Rockstuhl, and W. H. P. Pernice, *Cavity-enhanced and ultrafast superconducting single-photon detectors,* Nano Letters **16**, 7085 (2016).

[164] S. Buckley, J. Chiles, A. N. McCaughan, G. Moody, K. L. Silverman, M. J. Stevens, R. P. Mirin, S. W. Nam, and J. M. Shainline, *All-silicon light-emitting diodes waveguide-integrated with superconducting single-photon detectors,* Applied Physics Letters **111**, 141101 (2017).

[165] M. K. Akhlaghi, E. Schelew, and J. F. Young, *Waveguide integrated superconducting single-photon detectors implemented as near-perfect absorbers of coherent radiation,* Nature Communications **6**, 8233 (2015).

[166] J. Münzberg, A. Vetter, F. Beutel, W. Hartmann, S. Ferrari, W. H. P. Pernice, and C. Rockstuhl, *Superconducting nanowire single-photon detector implemented in a 2d photonic crystal cavity,* Optica **5**, 658 (2018).

[167] P. Cavalier, J.-C. Villegier, P. Feautrier, C. Constancias, and A. Morand, *Light interference detection on-chip by integrated SNSPD counters,* AIP Advances **1**, 042120 (2011).

[168] C. Schuck, W. H. P. Pernice, and H. X. Tang, *Nbtin superconducting nanowire detectors for visible and telecom wavelengths single photon counting on si3n4 photonic circuits,* Applied Physics Letters **102**, 051101 (2013).

[169] C. Schuck, W. H. P. Pernice, and H. X. Tang, *Waveguide integrated low noise NbTiN nanowire single-photon detectors with milli-Hz dark count rate,* Scientific Reports **3**, 1893 (2013).

[170] A. D. Beyer, R. M. Briggs, F. Marsili, J. D. Cohen, S. M. Meenehan, O. J. Painter, and M. D. Shaw, *Waveguide-coupled superconducting nanowire single-photon detectors,* in *2015 Conference on Lasers and Electro-Optics (CLEO)* (2015) pp. 1–2.

[171] R. Gourgues, I. E. Zadeh, A. W. Elshaari, G. Bulgarini, J. W. N. Los, J. Zichi, D. Dalacu, P. J. Poole, S. N. Dorenbos, and V. Zwiller, *Controlled integration of selected detectors and emitters in photonic integrated circuits,* Opt. Express **27**, 3710 (2019).

[172] S. Steinhauer, L. Yang, S. Gyger, T. Lettner, C. Errando-Herranz, K. D. Jöns, M. A. Baghban, K. Gallo, J. Zichi, and V. Zwiller, *NbTiN thin films for superconducting photon detectors on photonic and two-dimensional materials,* Applied Physics Letters **116**, 171101 (2020).

[173] G. Reithmaier, M. Kaniber, F. Flassig, S. Lichtmannecker, K. Müller, A. Andrejew, J. Vučković, R. Gross, and J. J. Finley, *On-chip generation, routing, and detection of resonance fluorescence,* Nano Letters **15**, 5208 (2015).

[174] G. E. Digeronimo, M. Petruzzella, S. Birindelli, R. Gaudio, S. Fattah Poor, F. W. Van Otten, and A. Fiore, *Integration of single-photon sources and detectors on gaas,* Photonics **3** (2016), 10.3390/photonics3040055.

[175] M. Kaniber, F. Flassig, G. Reithmaier, R. Gross, and J. J. Finley, *Integrated superconducting detectors on semiconductors for quantum optics applications,* Applied Physics B **122**, 115 (2016).

[176] D. Zhu, H. Choi, T. Lu, Q. Zhao, A. Dane, F. Najafi, D. R. Englund, and K. K. Berggren, *Superconducting nanowire single-photon detector on aluminum nitride,* in *2016 Conference on Lasers and Electro-Optics (CLEO)* (2016) pp. 1–2.

[177] M. G. Tanner, L. S. E. Alvarez, W. Jiang, R. J. Warburton, Z. H. Barber, and R. H. Hadfield, *A superconducting nanowire single photon detector on lithium niobate,* Nanotechnology **23**, 505201 (2012).

[178] J. P. Höpker, M. Bartnick, E. Meyer-Scott, F. Thiele, S. Krapick, N. Montaut, M. Santandrea, H. Herrmann, S. Lengeling, R. Ricken, V. Quiring, T. Meier, A. Lita, V. Verma, T. Gerrits, S. W. Nam, C. Silberhorn, and T. J. Bartley, *Towards integrated superconducting detectors on lithium niobate waveguides,* in *Quantum Photonic Devices*, Vol. 10358, edited by C. Soci, M. Agio, and K. Srinivasan, International Society for Optics and Photonics (SPIE, 2017) pp. 21 − 27.

[179] M. A. Wolff, S. Vogel, L. Splitthoff, and C. Schuck, *Superconducting nanowire single-photon detectors integrated with tantalum pentoxide waveguides,* Scientific Reports **10**, 17170 (2020).

[180] H. Atikian, S. Meesala, M. Burek, Y.-I. Sohn, J. Israelian, A. Patri, N. Clarke, A. Sipahigil, R. Evans, D. Sukachev, R. Westervelt, M. Lukin, and M. Loncar, *Novel fabrication of diamond nanophotonics coupled to single-photon detectors,* SPIE Newsroom (2017), 10.1117/2.1201611.006765.

[181] O. Kahl, S. Ferrari, P. Rath, A. Vetter, C. Nebel, and W. H. P. Pernice, *High efficiency on-chip single-photon detection for diamond nanophotonic circuits,* Journal of Lightwave Technology **34**, 249 (2016).

[182] S. Ferrari, C. Schuck, and W. Pernice, *Waveguide-integrated superconducting nanowire single-photon detectors,* Nanophotonics **7**, 1725 (01 Nov. 2018).

2

2

[183] J. Zhu, Y. Chen, L. Zhang, X. Jia, Z. Feng, G. Wu, X. Yan, J. Zhai, Y. Wu, Q. Chen, X. Zhou, Z. Wang, C. Zhang, L. Kang, J. Chen, and P. Wu, *Demonstration of measuring sea fog with an snspd-based lidar system,* Scientific Reports **7**, 15113 (2017).

[184] A. McCarthy, N. J. Krichel, N. R. Gemmell, X. Ren, M. G. Tanner, S. N. Dorenbos, V. Zwiller, R. H. Hadfield, and G. S. Buller, *Kilometer-range, high resolution depth imaging via 1560 nm wavelength single-photon detection,* Opt. Express **21**, 8904 (2013).

[185] A. Casaburi, M. Ejrnaes, N. Zen, M. Ohkubo, S. Pagano, and R. Cristiano, *Thicker, more efficient superconducting strip-line detectors for high throughput macromolecules analysis,* Applied Physics Letters **98**, 023702 (2011).

[186] M. Marksteiner, A. Divochiy, M. Sclafani, P. Haslinger, H. Ulbricht, A. Korneev, A. Semenov, G. Gol'tsman, and M. Arndt, *A superconducting NbN detector for neutral nanoparticles,* Nanotechnology **20**, 455501 (2009).

[187] M. Sclafani, M. Marksteiner, F. M. Keir, A. Divochiy, A. Korneev, A. Semenov, G. Gol'tsman, and M. Arndt, *Sensitivity of a superconducting nanowire detector for single ions at low energy,* Nanotechnology **23**, 065501 (2012).

[188] R. Cristiano, M. Ejrnaes, A. Casaburi, N. Zen, and M. Ohkubo, *Superconducting nano-strip particle detectors,* Superconductor Science and Technology **28**, 124004 (2015).

[189] J. A. Moon, R. Mahon, M. D. Duncan, and J. Reintjes, *Resolution limits for imaging through turbid media with diffuse light,* Opt. Lett. **18**, 1591 (1993).

[190] D. Tamborini, V. Anant, B. A. Korzh, M. D. Shaw, S. A. Carp, and M. A. Franceschini, *Superconducting nanowire single-photon detectors for diffuse correlation spectroscopy,* in *Biophotonics Congress: Optics in the Life Sciences Congress 2019 (BODA,BRAIN,NTM,OMA,OMP)* (Optical Society of America, 2019) p. BW1A.5.

[191] P. Eraerds, M. Legre, J. Zhang, H. Zbinden, and N. Gisin, *Photon counting otdr : Advantages and limitations,* Journal of Lightwave Technology **28** (2010), 10.1109/JLT.2009.2039635.

[192] Q. Zhao, L. Xia, C. Wan, J. Hu, T. Jia, M. Gu, L. Zhang, L. Kang, J. Chen, X. Zhang, and P. Wu, *Long-haul and high-resolution optical time domain reflectometry using superconducting nanowire single-photon detectors,* Scientific Reports **5**, 10441 (2015).

[193] M. G. Tanner, S. D. Dyer, B. Baek, R. H. Hadfield, and S. Woo Nam, *High-resolution single-mode fiber-optic distributed raman sensor for absolute temperature measurement using superconducting nanowire single-photon detectors,* Applied Physics Letters **99**, 201110 (2011).

[194] S. D. Dyer, M. G. Tanner, B. Baek, R. H. Hadfield, and S. W. Nam, *Analysis of a distributed fiber-optic temperature sensor using single-photon detectors,* Opt. Express **20**, 3456 (2012).

[195] E. Toomey, K. Segall, and K. K. Berggren, *Design of a power efficient artificial neuron using superconducting nanowires,* Frontiers in Neuroscience **13**, 933 (2019).

[196] E. Toomey, K. Segall, M. Castellani, M. Colangelo, N. Lynch, and K. K. Berggren, *Superconducting nanowire spiking element for neural networks,* Nano Letters **20**, 8059 (2020).

[197] J. M. Shainline, S. M. Buckley, R. P. Mirin, and S. W. Nam, *Superconducting optoelectronic circuits for neuromorphic computing,* Phys. Rev. Applied **7**, 034013 (2017).

[198] A. N. McCaughan, V. B. Verma, S. M. Buckley, J. P. Allmaras, A. G. Kozorezov, A. N. Tait, S. W. Nam, and J. M. Shainline, *A superconducting thermal switch with ultrahigh impedance for interfacing superconductors to semiconductors,* Nature Electronics **2**, 451 (2019).

[199] D. Silver, J. Schrittwieser, K. Simonyan, I. Antonoglou, A. Huang, A. Guez, T. Hubert, L. Baker, M. Lai, A. Bolton, Y. Chen, T. Lillicrap, F. Hui, L. Sifre, G. van den Driessche, T. Graepel, and D. Hassabis, *Mastering the game of go without human knowledge,* Nature **550**, 354 (2017).

[200] B. S. Robinson, A. J. Kerman, E. A. Dauler, R. J. Barron, D. O. Caplan, M. L. Stevens, J. J. Carney, S. A. Hamilton, J. K. Yang, and K. K. Berggren, *781 mbit/s photon-counting optical communications using a superconducting nanowire detector,* Opt. Lett. **31**, 444 (2006).

[201] A. Biswas, M. Srinivasan, S. Piazzolla, and D. Hoppe, *Deep space optical communications,* in *Free-Space Laser Communication and Atmospheric Propagation XXX*, Vol. 10524, edited by H. Hemmati and D. M. Boroson, International Society for Optics and Photonics (SPIE, 2018) pp. 242 − 252.

[202] M. E. Grein, A. J. Kerman, E. A. Dauler, O. Shatrovoy, R. J. Molnar, D. Rosenberg, J. Yoon, C. E. DeVoe, D. V. Murphy, B. S. Robinson, and D. M. Boroson, *Design of a ground-based optical receiver for the lunar laser communications demonstration,* in *2011 International Conference on Space Optical Systems and Applications (ICSOS)* (2011) pp. 78–82.

[203] D. G. Messerschmitt, P. Lubin, and I. Morrison, *Challenges in scientific data communication from low-mass interstellar probes,* The Astrophysical Journal Supplement Series **249**, 36 (2020).

[204] B. S. Robinson, D. M. Boroson, D. A. Burianek, and D. V. Murphy, *Overview of the lunar laser communications demonstration,* in *Free-Space Laser Communication Technologies XXIII*, Vol. 7923, edited by H. Hemmati, International Society for Optics and Photonics (SPIE, 2011) pp. 9 − 12.

2

[205] R. HANBURY BROWN, R. C. JENNISON, and M. K. D. GUPTA, *Apparent angular sizes of discrete radio sources: Observations at jodrell bank, manchester,* Nature **170**, 1061 (1952).

[206] F. Marsili, V. B. Verma, M. J. Stevens, J. A. Stern, M. D. Shaw, A. J. Miller, D. Schwarzer, A. Wodtke, R. P. Mirin, and S. W. Nam, *Mid-infrared single-photon detection with tungsten silicide superconducting nanowires,* in *CLEO: 2013* (Optical Society of America, 2013) p. CTu1H.1.

[207] Q. Chen, R. Ge, L. Zhang, F. Li, B. Zhang, Y. Dai, Y. Fei, X. Wang, X. Jia, Q. Zhao, X. Tu, L. Kang, J. Chen, and P. Wu, *Mid-infrared single photon detector with superconductor $mo_{80}si_{20}$ nanowire,* (2020), arXiv:2011.06699 .

[208] L. Chen, D. Schwarzer, V. B. Verma, M. J. Stevens, F. Marsili, R. P. Mirin, S. W. Nam, and A. M. Wodtke, *Mid-infrared laser-induced fluorescence with nanosecond time resolution using a superconducting nanowire single-photon detector: New technology for molecular science,* Accounts of Chemical Research **50**, 1400 (2017).

[209] L. Chen, D. Schwarzer, J. A. Lau, V. B. Verma, M. J. Stevens, F. Marsili, R. P. Mirin, S. W. Nam, and A. M. Wodtke, *Ultra-sensitive mid-infrared emission spectrometer with sub-ns temporal resolution,* Opt. Express **26**, 14859 (2018).

[210] E. E. Wollman, V. B. Verma, A. B. Walter, J. Chiles, B. Korzh, J. P. Allmaras, Y. Zhai, A. E. Lita, A. N. McCaughan, E. Schmidt, S. Frasca, R. P. Mirin, S.-W. Nam, and M. D. Shaw, *Recent advances in superconducting nanowire single-photon detector technology for exoplanet transit spectroscopy in the mid-infrared,* Journal of Astronomical Telescopes, Instruments, and Systems **7**, 1 (2021).

[211] D. R. Schaart, S. Ziegler, and H. Zaidi, *Achieving 10 ps coincidence time resolution in tof-pet is an impossible dream,* Medical Physics **47**, 2721 (2020).

[212] P. Lecoq, C. Morel, J. O. Prior, D. Visvikis, S. Gundacker, E. Auffray, P. Križan, R. M. Turtos, D. Thers, E. Charbon, J. Varela, C. de La Taille, A. Rivetti, D. Breton, J.-F. Pratte, J. Nuyts, S. Surti, S. Vandenberghe, P. Marsden, K. Parodi, J. M. Benlloch, and M. Benoit, *Roadmap toward the 10 ps time-of-flight PET challenge,* Physics in Medicine & Biology **65**, 21RM01 (2020).

[213] P. Lecoq, *Pushing the limits in time-of-flight pet imaging,* IEEE Transactions on Radiation and Plasma Medical Sciences **1**, 473 (2017).

[214] N. R. Gemmell, A. McCarthy, B. Liu, M. G. Tanner, S. D. Dorenbos, V. Zwiller, M. S. Patterson, G. S. Buller, B. C. Wilson, and R. H. Hadfield, *Singlet oxygen luminescence detection with a fiber-coupled superconducting nanowire single-photon detector,* Optics express **21**, 5005 (2013).

[215] A. Lai, T. Itoh, and C. Caloz, *Composite right/left-handed transmission line metamaterials,* IEEE Microwave Magazine **5**, 34 (2004).

[216] M. Mirhosseini, E. Kim, V. S. Ferreira, M. Kalaee, A. Sipahigil, A. J. Keller, and O. Painter, *Superconducting metamaterials for waveguide quantum electrodynamics,* Nature Communications **9**, 3706 (2018).

[217] E. Smith, R. De Alba, N. Zhelev, R. Bennett, V. Adiga, H. Solanki, V. Singh, M. Deshmukh, and J. Parpia, *Compact, inexpensive coaxial terminations and wiring for low temperature rf applications,* Cryogenics **52**, 461 (2012).

[218] N. R. Gemmell, M. Hills, T. Bradshaw, T. Rawlings, B. Green, R. M. Heath, K. Tsimvrakidis, S. Dobrovolskiy, V. Zwiller, S. N. Dorenbos, M. Crook, and R. H. Hadfield, *A miniaturized 4 K platform for superconducting infrared photon counting detectors,* Superconductor Science and Technology **30**, 11LT01 (2017).

[219] E. Lomonte, M. A. Wolff, F. Beutel, S. Ferrari, C. Schuck, W. H. Pernice, and F. Lenzini, *Single-photon detection and cryogenic reconfigurability in lithium niobate nanophotonic circuits,* arXiv preprint arXiv:2103.10973 (2021).

2

3

Optimizing the stoichiometry of ultrathin NbTiN films for high-performance superconducting nanowire single-photon detectors

The requirements in quantum optics experiments for high single-photon detection efficiency, low timing jitter, low dark count rate and short dead time have been fulfilled with the development of superconducting nanowire single-photon detectors. Although they offer a detection efficiency above 90%, achieving a high time resolution in devices made of amorphous materials is a challenge, particularly at temperatures above 0.8 K. Devices made from niobium nitride and niobium titanium nitride allow us to reach the best timing jitter but, in turn, have stronger requirements in terms of film quality to achieve a high efficiency. Here we take advantage of the flexibility of reactive co-sputter deposition to tailor the composition of $Nb_xTi_{1-x}N$ superconducting films and show that a Nb fraction of x = 0.62 allows for the fabrication of detectors from films as thick as 9 nm and covering an active area of 20 μm, with a wide detection saturation plateau at telecom wavelengths and in particular at 1550 nm. This is a signature of an internal detection efficiency saturation, achieved while maintaining the high time resolution associated with NbTiN and operation at 2.5K. With our optimized recipe, we reliably fabricated detectors with high critical current densities reaching a saturation plateau at 1550 nm with 80% system detection efficiency and with a FWHM timing jitter as low as 19.5 ps.

3.1. Introduction

The invention [1] and active development of superconducting nanowire single photon detectors (SNSPDs) have offered in recent years a unique tool to study and harvest the physics of single photons, from fundamental quantum optics experiments to impactful applications. Characterization of single photon emitters such as quantum dots [2] or color centers [3], loophole-free Bell test measurements [4], laser ranging [5, 6], quantum-secure communication [7, 8], CMOS testing [9, 10] or biological imaging [11] all take advantage of the unique combination of sensitivity, broad wavelength range, negligible dark count rate, and excellent time resolution of SNSPDs. The demonstration of SNSPDs based on amorphous WSi achieving 93% system detection efficiency [12] opened the way for the fabrication of high-yield, high efficiency detectors. However, the operation at sub-Kelvin temperature of these detectors, combined with a typically high timing jitter [12, 13] limits their range of applications. On the other hand, NbN and NbTiN detectors have shown a combination of high efficiency above 90%, low jitter of 10 ps and below and low dark count rate, together with a maximum count rate of hundreds of MHz and with a typical operation temperature > 2 K [14–17] but the fabrication of detectors with a good internal detection saturation at 1550 nm in these materials remains a challenge, requiring high quality films, lithography and etching [18]. Overall, this limits the fabrication yield of high performance detectors. Here we take advantage of the extra degree of freedom offered by the co-sputtering deposition of NbTiN to tailor the Nb content during the film deposition on standard SiO_2/Si substrates. The critical temperature (Tc) of the films was measured, and we carried out X-Ray Photoelectron Spectroscopy (XPS) analysis to precisely measure the concentration of niobium, titanium, and nitrogen. In parallel, we deposited selected NbTiN recipes on 10 nm thin silicon nitride support films and characterized their crystalline structure and nanoscale morphology with transmission electron microscopy (TEM).

Finally, we patterned the films into SNSPDs, and measured the photon count rates of the detectors as a function of applied bias in a Gifford-McMahon cryostat operating at 2.5 K, showing that our optimized film composition allows for the fabrication of devices with a pronounced detection efficiency saturation at 1310 nm and 1550 nm. The improved recipe was then used to deposit a film on a Distributed Bragg Reflector (DBR) microcavity, and detectors were fabricated and fully packaged using a standard self-aligning method to carefully measure their system detection efficiency (SDE), dark count rate (DCR) and timing jitter.

3.2. Superconducting thin film deposition and characterization

The superconducting thin films were deposited by reactive magnetron co-sputtering from two separate targets of Nb and Ti, in an atmosphere of Ar and N_2, as depicted in figure 3.1(a), on dry thermally oxidized silicon wafers. We deposited another set of films on 10 nm-thick SiN TEM support films, for 4 different recipes spanning the range of compositions investigated. The substrates were placed on a sample holder that was rotated during the depositions to maximize the films homogeneity. The base pressure of the system was kept between 5×10^{-9} and 1×10^{-8} Torr before the deposition; a mixture of 100 sccm Ar and 10 sccm N_2 was introduced and the pressure was set to 28 mTorr in order to strike the plasmas with 50 W for each target. The pressure was lowered to 3 mTorr while the plasma powers were ramped up to their targeted values. For our main series of films from which detectors were fabricated, the Ti target was biased with 240 W RF, while the Nb target powers were set from 240 W DC down to 60 W DC, in 20 W steps. A substrate shutter and a rate monitor were used to precisely control the deposition time and to determine the deposited thickness. For each recipe, we first deposited a film with a thickness in the order of 50 nm measured with a stylus profilometer, which we used to calibrate the deposition rate of each recipe, to measure the film T_c of the material, and to carry out XPS measurements. Subsequently, we used the deposition rate calibration to grow films with a nominal thickness of 9 nm (± 5%), which were used to measure the thin film room temperature sheet resistance, the thin film Tc, and which were eventually used to pattern the SNSPDs.

For electrical characterization, at least two samples of each film were carefully diced into squares and placed into a custom-made four-point T_c measurement setup which consists of a closed-cycle cryostat built around a cold head with a nominal base temperature of 4.2 K. The samples were contacted with a linear four-pin probe with spring-loaded pins, while the temperature was ramped up and down at a rate of 0.1 K/min. We measured the room temperature sheet resistance and the T_c, defined as the temperature at which the resistivity of the film was half of that at 20 K.

In parallel, XPS measurements were performed to study the different compositions of the 50 nm films, using a PHI Quantera II Scanning ESCA microprobe with monochromatic Al Kα radiation and a spot size of 100 μm. The composition of the top surface, a native oxide layer as observed elsewhere [19], as well as the average
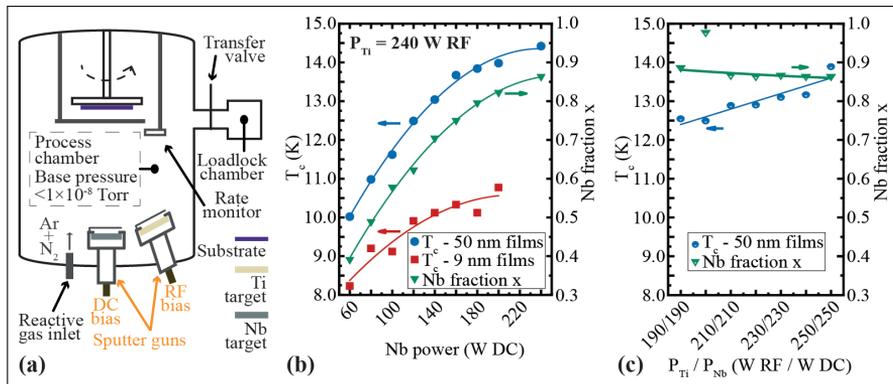
Figure 3.1: (a) Schematics of the sputtering chamber. (b) Critical temperature T_c and Nb fraction x in the alloy $Nb_xTi_{1-x}N$ vs. Nb sputtering power. The power applied to the Ti target was kept constant at 240 W RF for all film depositions. (c) Critical temperature Tc and Nb fraction x vs. sputtering power for a constant power ratio. The lines are a guide to the eye.

bulk composition of the superconducting layer were determined. For the latter, 1 kV Ar$^+$ sputter etched depth profiles with an area of 1x1 mm^2 were conducted, the thickness of 50 nm allowing for the etching without removing the underlying NbTiN layer and for comparing values close to bulk conditions. The sensitivity factors for determining the composition were obtained by reference measurements using time-of-flight elastic recoil detection analysis [20]. The XPS spectra reveal a composition of the superconducting layer without contaminant species and with a content of N of 50 ± 3%, which hints that our films can be considered as a mixture of stoichiometric NbN and TiN [21] where the proportions of Nb and Ti depend on the sputtering parameters. In figure 3.1(b) we compile the results from the T_c and the XPS measurements and show that we can precisely control the composition of the films in terms of Nb fraction x in the alloy $Nb_xTi_{1-x}N$ with a value ranging widely from 0.39 to 0.86. We confirm that films with a higher Nb content yield a higher Tc, varying from 10.02 K to 14.42 K for 50 nm films. To decouple the effect of the total sputtering power on the film growth and on the Tc of the material, we deposited another series of films, keeping the power ratio on both targets constant from P_{Ti} = P_{Nb} = 190 W, up to P_{Ti} = P_{Nb} = 250 W. We observed a much lower impact of the total power density on the T_c and a negligible impact on the Nb fraction x (figure 3.1(c)). We attribute the slight shift of the T_c from 12.5 K to 13.5 K to a change in the film density of our material, which is confirmed by the observation of lower deposition rates for higher sputtering power. We conclude that the effects we report in this article are mainly due to a change in the chemical composition of the material.

We controlled the thickness of the films by measuring lift-off steps with an atomic force microscope (AFM), as shown in figure 3.2(a). The roughness of a selection of films was extracted from the AFM measurements, and we observed root mean square (Rq) roughness values between 0.7 and 0.9 nm. Furthermore we used TEM
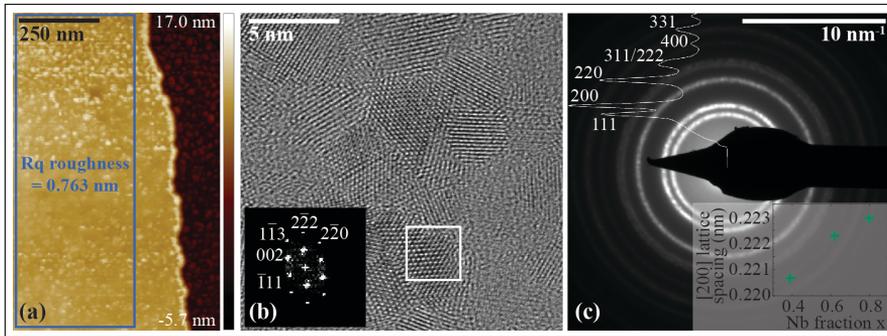
Figure 3.2: Characterization of films with an Nb fraction x = 0.62. (a) AFM map showing the thickness measurement step, and the Rq roughness value of 0.763 nm extracted from the region of interest. (b) HRTEM micrograph of NbTiN deposited on a SiN support film. Inset: Fourier transform of a single grain (indicated by the white square on the micrograph) imaged along the [110] zone axis. (c) Selected area electron diffraction of the film. Inset: the extracted [200] lattice spacing scaled with Nb fraction x for different samples.

to study the crystalline structure and nanoscale morphology of NbTiN obtained with three different recipes (Nb powers of 60 W, 120 W and 180 W; constant Ti power of 240 W RF). The instrument was operated at electron acceleration voltage of 300 kV and was equipped with an aberration corrector for the objective lens. The high resolution TEM (HRTEM) image presented in figure 3.2(b) was taken on the film with PNb = 120 W (Nb fraction x = 0.62) and reveals that our material is polycrystalline. The inset shows the Fourier transform of a single grain, which was indexed to the [110] zone axis of the face-centered cubic structure of NbTiN. For the three investigated samples, there was no sizeable change in the dimension and distribution of grains, which have on average a diameter of 4 to 5 nm, indicating that the growth mode of the different films was not affected when modifying the recipes. In figure 3.2(c) selected area electron diffraction results are presented, showing a ring pattern typical for polycrystalline films. As can be seen in the inset, the [200] lattice spacing (obtained by azimuthal integration using the PASAD plug-in [22] and Digital Micrograph software) was found to scale with the Nb fraction x, which is expected for the fully miscible ternary NbTiN alloy [19]. We note that the lattice parameters were extracted from films grown on SiN TEM support films with a thickness of 10 nm, which most probably does not correspond to the lattice parameters of films deposited on SiO$_2$/Si substrates due to different levels of microscopic strain [22]. To assess the influence of the substrate material in general, we directly compared the superconducting properties of two samples, one on SiN and one on SiO$_2$, deposited during the same sputtering run. We measured a difference in Tc of only 0.07 K for the recipe with PNb = 120 W, which indicates that the material growth modes on both substrates are similar. Hence, it is expected that the results presented here are relevant for a broader range of silicon photonics platforms, e.g. integrated circuits relying on SiN-based waveguides [23, 24].

3.3. Detectors

The binding energy of the Cooper pairs in the superconductor as described in the Bardeen-Cooper-Schrieffer theory [25] and in the Ginzburg-Landau description of the SNSPD model [26] dictates the Tc of the films of a fixed thickness. It influences the amount of quasi-particles that can be created upon absorption of a single photon of any given energy [27]; as a result, the Tc strongly affects the intrinsic detection efficiency of an SNSPD made from that material. Here we apply this concept and verify the correlation between the Tc of our material and the intrinsic detection efficiency of detectors made from eight different recipes and material compositions.
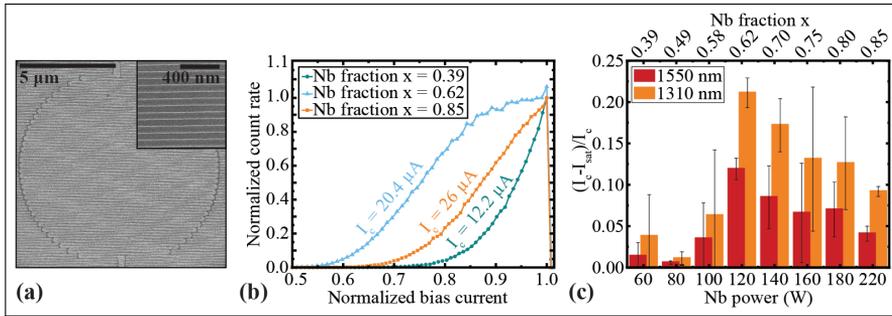

Figure 3.3: (a) SEM micrograph of the SNSPD structures patterned from the films. Inset: close-up view on the meander nanowire lines. (b) Examples of normalized count rate at 1550 nm vs normalized bias current of representative detectors from three different film recipes, all with a thickness of 9 nm. (c) Average relative saturation plateau $(I_c\text{-}I_{sat})/I_c$ for detectors made from films with different niobium sputtering powers. The power applied to the Ti target was kept constant at 240 W RF for all film depositions.

Figure 3.3 (a) depicts an SEM image of a meandering SNSPD patterned from one of the films, following the fabrication steps described by the authors elsewhere [14]. The meander covers a 10 μm of diameter area, with a 50% filling factor and a line width of 70 nm. A total of sixteen detectors were fabricated from each film, and six were tested at 2.5 K in a closed-cycle cryostat. The structures were flood-illuminated with continuous-wave lasers at two different wavelengths - 1310 nm and 1550 nm - and their response to light was characterized as a function of bias current.

In figure 3.3 (b) we show the normalized count rates of the detectors with the highest I_c from three different film recipes against the normalized bias current, and we observe different shapes of the photon count rate curves. For films with an Nb content of x = 0.39 and x = 0.85, the curves have an exponential shape up to the critical current, whereas for the film with x = 0.62 a saturation plateau appears at around 80% of the Ic. In figure 3.3 (c) we show the average of the relative saturation plateau width of the devices made from each deposition recipe, which we define as the difference between the critical current I_c and the saturation current Isat normalized to the critical current $(I_c\text{-}I_{sat})/I_c$, and where I_{sat} is the bias current value at which the count rate is equal to 90% of its maximum value. We observe an optimum of this plateau width for the recipe with x = 0.62 that can be explained

by the fact that for a higher Nb content the higher T_c implies a stronger binding of Cooper pairs in the material, reducing the internal detection efficiency. On the other hand, for lower Nb contents, we observe that the critical current is reduced, although it remains comparatively high for the operation temperature of 2.5K due to the relatively large thickness of the films. The non-saturated photon count rate in this composition regime could be linked to various composition-dependent material parameters and remains a topic for future studies. By reducing the Nb fraction in the alloy to 0.62 as measured by XPS, we can fabricate detectors with large cross-sections of 9 nm × 70 nm with a saturated detection efficiency at 2.5 K, a large critical current and a high yield with six working detectors out of six tested and with a narrow spread of performances, due to a lesser sensitivity to the substrate surface roughness. The parameters extracted from the films and detectors made for each recipe are summarized in Table 1.

3

Table 1. Summary of films and corresponding detectors parameters						
		Films			Detectors	
Nb fraction x	Nb power[1] W	Tc – 50 nm films K	RT sheet resistance Ω/□	Residual resistance ratio – 9 nm films	Max. J_c × 10⁹ A/m²	Average relative saturation plateau width at 1550 nm
0.86	240	14.42	No film	No film	No detector	No detector
0.85[2]	220	No film	480.25	3.80	20.79	0.04
0.82	200	13.98	445.40	0.91	No detector	No detector
0.80	180	13.84	598.54	0.79	16.83	0.07
0.75	160	13.67	539.13	0.80	14.52	0.07
0.70	140	13.04	595.02	0.81	15.79	0.09
0.62	120	12.49	320.56	0.41	16.98	0.12
0.58	100	11.62	550.83	0.26	12.46	0.04
0.49	80	10.98	608.39	0.88	9.68	0.01
0.39	60	10.02	658.35	0.92	9.76	0.01

[1]Ti sputter power constant at 240 W RF.
[2]From fit.

After selecting the optimal material recipe, we deposited a film with an Nb content x = 0.62 on a substrate consisting of a DBR micro-cavity designed to enhance light absorption at the surface for a wavelength of 1550 nm. We packaged detectors into fiber-coupled chips using a self-aligning technique [28], and tested them in a 2.5 K cryostat, allowing us to precisely measure the system detection efficiency and timing jitter. We kept the same filling factor and linewidth of the nanowire, and designed detectors with a 20 µm active area which is suitable for coupling not only with single mode fibers at 1550 nm but also with graded index multi-mode fibers, facilitating the signal coupling into the fiber for a broad range of optical instruments. The DCR only becomes noticeable at a bias current of around 98% of the Ic, with some background counts present at lower bias accounting for < 200 counts per second, which we attribute to a residual coupling of black-body radiation, as presented for one of the detectors in figure 3.4 (a). The use of fibers with DBR filtering on their end-facet as proposed elsewhere [29] is identified as a solution for reducing the background noise further. Using a diode laser operating at 1550 nm,

a calibrated power meter and a calibrated variable attenuator to set the input flux of photons to 80,800 /s, we measured the SDE of the devices to be up to 80%, as represented in figure 3.4 (a). We point out that due to the high critical current density (J_c) of the material, we also fabricated detectors from slightly thinner films, allowing to boost further the internal detection efficiency at the expense to a reduced critical current, although maintained high, and a reduced yield. With 30% of the detectors made from 9 nm thick films, system detection efficiencies of ~80% at 1550 nm and wide efficiency saturation starting between 0.8 and 0.9 Ic were achieved at 2.5 K. We attribute this remarkable fabrication yield for polycrystalline materials to the use of rather thick films, which are less sensitive to the substrate roughness. To measure the time jitter of the detector, we used a pulsed laser at 1550 nm, a calibrated variable attenuator and a 4 GHz, 40 GSample/s oscilloscope with a combined timing jitter of < 2 ps, and we measured the histogram of the time delay of the coincidence counts between the laser synchronization signal and the SNSPD pulses, as shown in figure 3.4 (b). The SNSPD was biased at 95% of its I_c using a low temperature bias tee and the pulses were amplified using a cryo-compatible HEMT amplifier, both operated at 40 K, and the fitted system timing jitter was measured to be as low as 19.5 ps (FWHM).
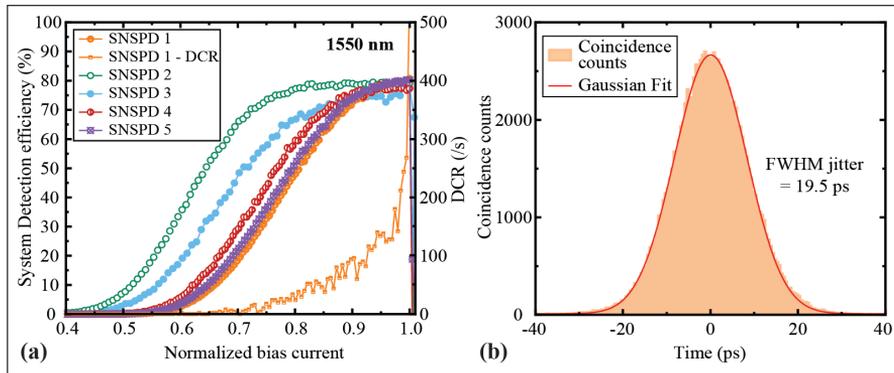

Figure 3.4: (a) Measurement at 2.5 K of the System Detection Efficiency at 1550 nm of five detectors and the Dark Count Rate (DCR) of one of the detectors vs. bias current for 20 μm active area devices made on DBR substrates from a 9 nm thick film. (b) Coincidence histogram of the SNSPD on DBR wafer with the laser synchronization signal, revealing a FWHM timing jitter of 19.5 ps.

3.4. Conclusion

In summary, we have shown tailored composition and superconducting properties of $Nb_xTi_{1-x}N$ thin films by controlling the power applied to separate targets in a reactive co-sputtering deposition system. We verified that the influence of the applied powers on the T_c and on the saturation capabilities of the detectors were mainly due to a change in the chemical composition of the ternary alloy. We fabricated devices from 9 nm thick films covering an active area of 20 μm with saturated detection efficiency at 1550 nm at 2.5 K, before moving on to realize fully packaged

devices on DBR substrates with 80% SDE at 1550 nm, a timing jitter of 19.5 ps, and a fabrication yield of 30%. Finally, the minimal impact on the film properties when deposited on SiN suggests the possibility to use this room temperature optimized recipe for the production of on-chip detectors integrated in temperature sensitive photonic circuits [30].

References

[1] G. Gol'tsman, O. Okunev, G. Chulkova, A. Lipatov, A. Semenov, K. Smirnov, B. Voronov, A. Dzardanov, C. Williams, and R. Sobolewski, *Picosecond superconducting single-photon optical detector,* Applied physics letters **79**, 705 (2001).

[2] L. Schweickert, K. D. Jöns, K. D. Zeuner, S. F. Covre da Silva, H. Huang, T. Lettner, M. Reindl, J. Zichi, R. Trotta, A. Rastelli, *et al.*, *On-demand generation of background-free single photons from a solid-state source,* Applied Physics Letters **112**, 093106 (2018).

[3] G. A. Steudle, S. Schietinger, D. Höckel, S. N. Dorenbos, I. E. Zadeh, V. Zwiller, and O. Benson, *Measuring the quantum nature of light with a single source and a single detector,* Physical Review A **86**, 053814 (2012).

[4] L. K. Shalm, E. Meyer-Scott, B. G. Christensen, P. Bierhorst, M. A. Wayne, M. J. Stevens, T. Gerrits, S. Glancy, D. R. Hamel, M. S. Allman, *et al.*, *Strong loophole-free test of local realism,* Physical review letters **115**, 250402 (2015).

[5] A. McCarthy, N. J. Krichel, N. R. Gemmell, X. Ren, M. G. Tanner, S. N. Dorenbos, V. Zwiller, R. H. Hadfield, and G. S. Buller, *Kilometer-range, high resolution depth imaging via 1560 nm wavelength single-photon detection,* Optics express **21**, 8904 (2013).

[6] J. Zhu, Y. Chen, L. Zhang, X. Jia, Z. Feng, G. Wu, X. Yan, J. Zhai, Y. Wu, Q. Chen, *et al.*, *Demonstration of measuring sea fog with an snspd-based lidar system,* Scientific reports **7**, 1 (2017).

[7] H. Takesue, S. W. Nam, Q. Zhang, R. H. Hadfield, T. Honjo, K. Tamaki, and Y. Yamamoto, *Quantum key distribution over a 40-db channel loss using superconducting single-photon detectors,* Nature photonics **1**, 343 (2007).

[8] H.-L. Yin, T.-Y. Chen, Z.-W. Yu, H. Liu, L.-X. You, Y.-H. Zhou, S.-J. Chen, Y. Mao, M.-Q. Huang, W.-J. Zhang, *et al.*, *Measurement-device-independent quantum key distribution over a 404 km optical fiber,* Physical review letters **117**, 190501 (2016).

[9] F. Stellari, A. Tosi, F. Zappa, and S. Cova, *Cmos circuit analysis with luminescence measurements and simulations,* in *32nd European Solid-State Device Research Conference* (Citeseer, 2002) pp. 495–498.

3

[10] M. Mc Manus, J. Kash, S. Steen, S. Polonsky, J. Tsang, D. Knebel, and W. Huott, *Pica: Backside failure analysis of cmos circuits using picosecond imaging circuit analysis,* Microelectronics Reliability **40**, 1353 (2000).

[11] N. R. Gemmell, A. McCarthy, B. Liu, M. G. Tanner, S. D. Dorenbos, V. Zwiller, M. S. Patterson, G. S. Buller, B. C. Wilson, and R. H. Hadfield, *Singlet oxygen luminescence detection with a fiber-coupled superconducting nanowire single-photon detector,* Optics express **21**, 5005 (2013).

[12] F. Marsili, V. B. Verma, J. A. Stern, S. Harrington, A. E. Lita, T. Gerrits, I. Vayshenker, B. Baek, M. D. Shaw, R. P. Mirin, *et al.*, *Detecting single infrared photons with 93% system efficiency,* Nature Photonics **7**, 210 (2013).

[13] V. B. Verma, B. Korzh, F. Bussieres, R. D. Horansky, A. E. Lita, F. Marsili, M. Shaw, H. Zbinden, R. Mirin, and S. Nam, *High-efficiency wsi supercon-ducting nanowire single-photon detectors operating at 2.5 k,* Applied Physics Letters **105**, 122601 (2014).

[14] I. Esmaeil Zadeh, J. W. Los, R. B. Gourgues, V. Steinmetz, G. Bulgarini, S. M. Dobrovolskiy, V. Zwiller, and S. N. Dorenbos, *Single-photon detectors com-bining high efficiency, high detection rates, and ultra-high timing resolution,* Apl Photonics **2**, 111301 (2017).

[15] B. Korzh, Q.-Y. Zhao, J. P. Allmaras, S. Frasca, T. M. Autry, E. A. Bersin, A. D. Beyer, R. M. Briggs, B. Bumble, M. Colangelo, *et al.*, *Demonstration of sub-3 ps temporal resolution with a superconducting nanowire single-photon detector,* Nature Photonics **14**, 250 (2020).

[16] W. Zhang, L. You, H. Li, J. Huang, C. Lv, L. Zhang, X. Liu, J. Wu, Z. Wang, and X. Xie, *Nbn superconducting nanowire single photon detector with effi-ciency over 90% at 1550 nm wavelength operational at compact cryocooler temperature,* Science China Physics, Mechanics & Astronomy **60**, 1 (2017).

[17] I. E. Zadeh, J. W. Los, R. Gourgues, G. Bulgarini, S. M. Dobrovolskiy, V. Zwiller, and S. N. Dorenbos, *A single-photon detector with high efficiency and sub-10ps time resolution,* arXiv preprint arXiv:1801.06574 (2018).

[18] F. Marsili, F. Bellei, F. Najafi, A. E. Dane, E. A. Dauler, R. J. Molnar, and K. K. Berggren, *Efficient single photon detection from 500 nm to 5 μm wavelength,* Nano letters **12**, 4799 (2012).

[19] L. Zhang, W. Peng, L. You, and Z. Wang, *Superconducting properties and chemical composition of nbtin thin films with different thickness,* Applied Physics Letters **107**, 122603 (2015).

[20] B. Schmidt and K. Wetzig, *Ion beams in materials processing and analysis,* (2012).

3

[21] H. Myoren, T. Shimizu, T. Iizuka, and S. Takada, *Properties of nbtin thin films prepared by reactive dc magnetron sputtering,* IEEE transactions on applied superconductivity **11**, 3828 (2001).

[22] K. Makise, H. Terai, M. Takeda, Y. Uzawa, and Z. Wang, *Characterization of nbtin thin films deposited on various substrates,* IEEE transactions on applied superconductivity **21**, 139 (2010).

[23] R. Gourgues, I. E. Zadeh, A. W. Elshaari, G. Bulgarini, J. W. Los, J. Zichi, D. Dalacu, P. J. Poole, S. N. Dorenbos, and V. Zwiller, *Controlled integration of selected detectors and emitters in photonic integrated circuits,* Optics express **27**, 3710 (2019).

[24] C. Schuck, W. H. Pernice, and H. X. Tang, *Waveguide integrated low noise nbtin nanowire single-photon detectors with milli-hz dark count rate,* Scientific reports **3**, 1 (2013).

[25] J. Bardeen, L. N. Cooper, and J. R. Schrieffer, *Microscopic theory of superconductivity,* Physical Review **106**, 162 (1957).

[26] A. Zotova and D. Y. Vodolazov, *Intrinsic detection efficiency of superconducting nanowire single photon detector in the modified hot spot model,* Superconductor Science and Technology **27**, 125001 (2014).

[27] J. Renema, R. Gaudio, Q. Wang, Z. Zhou, A. Gaggero, F. Mattioli, R. Leoni, D. Sahin, M. De Dood, A. Fiore, *et al.*, *Experimental test of theories of the detection mechanism in a nanowire superconducting single photon detector,* Physical review letters **112**, 117604 (2014).

[28] A. J. Miller, A. E. Lita, B. Calkins, I. Vayshenker, S. M. Gruber, and S. W. Nam, *Compact cryogenic self-aligning fiber-to-detector coupling with losses below one percent,* Optics express **19**, 9102 (2011).

[29] W. Zhang, X. Yang, H. Li, L. You, C. Lv, L. Zhang, C. Zhang, X. Liu, Z. Wang, and X. Xie, *Fiber-coupled superconducting nanowire single-photon detectors integrated with a bandpass filter on the fiber end-face,* Superconductor Science and Technology **31**, 035012 (2018).

[30] S. Ferrari, C. Schuck, and W. Pernice, *Waveguide-integrated superconducting nanowire single-photon detectors,* Nanophotonics **7**, 1725 (2018).

3

4

Superconducting nanowire single photon detectors based on disordered NbRe films

Superconducting Nanowire Single Photon Detectors (SNSPDs) from $Nb_{0.15}Re_{0.85}$ granular nanowires are developed. The devices have a meander structure of wires $50 - 100$ nm wide and cover a circular detection area with a diameter of about 10 - 16 μm. The main figures of merit of the detectors are extracted from a flood illumination process at 2.8 K, featuring a saturated internal efficiency up to $\lambda = 1301$ nm, recovery times between about 8 and 19 ns and jitter of about 35 ps. These results confirm that $Nb_{0.15}Re_{0.85}$ is a promising candidate for the realization of fast SSPDs, as recently suggested.

4.1. Introduction

4

SNSPDs [1–3] are recognized as a mature platform for many applications as, for instance, quantum information technology [4], Light Detection And Ranging (LIDAR) [5], spectroscopy [6], as well as mass spectrometry [7]. SSPDs indeed fulfill the requirements of low dark counts rates (DCR) [8], high detection efficiency (DE) [9, 10], fast response time [11], and low timing jitter [12–14] in a rather wide spectral range [15, 16]. Despite these high operation standards, great efforts are constantly spent to both gain insight on the mechanism responsible of the detection process [17–19] and improve their performances. This last goal can be achieved by optimizing the properties of the materials-of-choice in this field [20, 21], by developing alternative device design [1, 22–24], and testing new superconductors [1, 25–27]. As far as the choice of the material is concerned, significant amount of work was recently devoted to the use of amorphous superconductors (for example WSi, MoGe, MoSi) [9, 10, 25] as alternative to the traditionally employed NbN [28] and NbTiN [12]. Amorphous materials are distinguished for their detection performance in the mid-infrared and for the robustness of their superconducting properties with respect to fabrication processing and surface roughness. However, as a consequence of their lower energy gap, they suffer from low time resolution, high dark counts, and low operation temperatures (< 1 K) [1]. It is clear that the figures of merit of the devices based on these two classes of materials (crystalline nitrides and amorphous superconductors) are deeply linked to their microscopic parameters [1]. Based on these considerations, granular NbRe films was recently proposed as a valuable alternative to combine the requests of a material with rather large values of critical temperature, T_c, and critical current, I_c, intermediate between NbN and other amorphous superconductors, along with a relatively robust fabrication procedure, large expected hot-spot dimensions, and very short estimated quasiparticles relaxation rates [29]. Here, the performances of nanowire single photon detectors with a meander design realized on 8-nm-thick NbRe films are reported and their main figures of merit are extracted. In particular, the dark count rate and internal detection efficiency at different wavelengths ($\lambda = 516 - 1550$ nm), the deadtime, and the jitter were evaluated. In addition, variable angle ellipsometric measurements of the optical properties for $\lambda = 450 - 1650$ nm were performed. All the results are discussed and compared with the present literature.

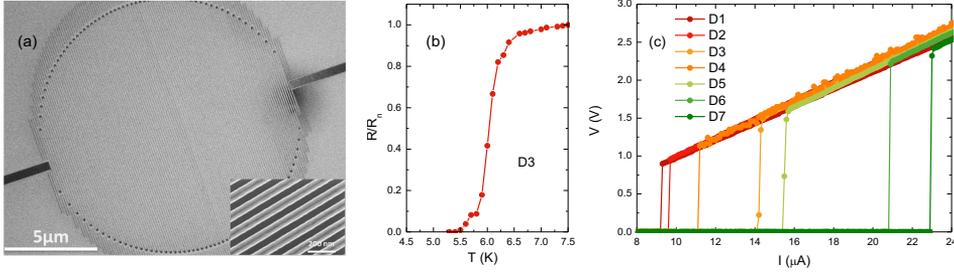## **4.2.** Film deposition, SNSPDs fabrication and Detector Statistics

Figure 4.1: (a) SEM image of a typical fabricated devices with $w = 70$ nm and $p = 140$ nm. Inset: zoomed image of the detector. (b) Normalized resistive transition, R/R_n of the detector D3. (c) $V(I)$ characteristics measured at $T = 2.8$ K on the detectors reported in Table 4.1.

NbRe films (composition $\mathrm{Nb_{0.15}Re_{0.85}}$) were deposited by DC magnetron sputtering in a UHV system at room temperature on oxidized 2" Si wafers from a target with the same composition. The base pressure was $P \approx 8 \times 10^{-9}$ mbar and the Ar pressure during the deposition was $P_\mathrm{Ar} = 4 \times 10^{-3}$ mbar. The thickness of the NbRe film is $d_\mathrm{NbRe} = 8$ nm, a value comparable with the superconducting coherence length estimated from upper critical field measurements, $\xi \sim 5$ nm [30]. At this reduced thickness, the films are expected to have a T_c well above the liquid helium temperature, a normal state resistivity of about $\rho_\mathrm{n} \approx 80$ $\mu\Omega$·cm, and a residual resistivity ratio, $RRR \approx 0.7$, where RRR is the ratio between the resistance at room temperature, R_RT, and at $T = 10$ K, R_n [30]. The samples were patterned by Electron Beam Lithography (EBL) using a 100 KV e-beam (Raith EBPG-5200) on ARP-6200 (thickness ≈ 100 nm). The patterns were transferred to NbRe layer by reactive ion etching with a $\mathrm{SF_6/O_2}$ chemistry (12.5/3.4 standard cubic centimeter per minute). The resulting meanders were capped by 12 nm of SiN deposited by plasma enhanced chemical vapor deposition, to prevent the film oxidation. To evaluate the NbRe performance, a selection of the fabricated detectors are characterized and presented here. In the following results on several devices, differing in the nanowire linewidth, pitch and covered area are reported. The devices' names and characteristics (linewidth w, pitch p, and radius r) are summarized in Table 4.1. In Fig. 4.1(a) a scanning electron microscope (SEM) image of a photon detector meander with $w = 70$ nm and $p = 140$ nm is reported. The inset is an enlarged image of the device, showing the well-defined nanowires. The devices were mounted on a flood illumination holder in a Gifford-McMahon closed cycle cryostat. All fabricated SSPDs were superconducting, as a confirmation of the robust properties of the films which consist of small oriented crystallites [30]. In panel (b) of Fig. 4.1 the normalized resistive transition of the detector D3 is reported. The value of the critical temperature, defined at the midpoint of the transition curve, $T_\mathrm{c} = 6.03$ K, is

name	w(nm)	p(nm)	$r(\mu m)$	t_{rise}(ps)	t_{fall}(ns)	J_c(A/m^2)
D1	50	100	5	500	14.4	2.3×10^{10}
D2	60	120	5	425	8.15	2.0×10^{10}
D3	70	120	5	495	13.3	2.5×10^{10}
D4	70	140	8	700	18.8	2.0×10^{10}
D5	80	160	4.5	393	9.3	2.4×10^{10}
D6	80	160	4.5	425	7.43	3.2×10^{10}
D7	100	200	6	800	7.64	3.6×10^{10}

Table 4.1: Summary of the characteristics of the detectors under study.

4

in agreement with published data on single unstructured films [30]. It is worth to underline that critical temperatures larger than 4.2 K simplifies the complexity of the refrigeration system of a future NbRe-based detector.

Another important parameter along with T_c, is the critical current, I_c. In earlier works, $V(I)$ characteristics were measured on micrometric strips either 15 or 5-nm-thick [29, 31]. Here, the devices are characterized by Voltage - Current [$V(I)$] measurements at $T = 2.8$ K, as shown in panel (c) of Fig. 4.1 for all the analyzed detectors. The values of the corresponding crital current density for the different samples are reported in Table 4.1. Here it can be noticed that, despite the fact that devices D3, D4 and D5, D6 are nominally identical, they differ for the critical current density value, J_c. This can be ascribed to the fact that they were fabricated on pieces obtained from different location on the wafer. It is useful to compare the results for J_c with value of the depairing current density at the same reduced temperature, $t = T/T_c$, estimated according to the expression for $(J_{dp}(t)/J_{dp}(0))$ vs t obtained in the framework of the theory of Kupriyanov and Lukichev [32]. Since from Ref. [29] it is $J_{dp}(0) \approx 2 \times 10^{11}$ A/m^2, it follows that $J_{dp}(2.8K) \approx 5.5 \times 10^{10}$ A/m^2, a value comparable with the measured value of J_c, also considering the approximation used when estimating $J_{dp}(0)$. In principle, this result should assure a good detection efficiency [1]. As far as the DE is concerned, the literature suggests that the polycrystalline structure with small crystallites and disorder-dominated transport properties typical of NbRe films [29, 30], should also promote high efficiency [9].

4.3. Single Photon Response of NbRe SNSPDs

In order to gain insight on the detection performance of the NbRe-based devices, the internal efficiency as a function of the bias current, I_b, was measured by flood illumination at different wavelengths in the range $\lambda = 516-1550$ nm, with the countrate of the devices kept around 100k events per second. The results, obtained at $T = 2.8$ K, are reported for a representative of samples in Fig. 4.2 (left scale), along with the dark counts rate (right scale). The internal quantum efficiency significantly saturates at lower wavelengths for all the devices, but decreases at lower photon energy. Interestingly, for $\lambda = 516 - 1060$ nm the saturation is reached for all the detectors at a value of J_b lower than the bias current at which the DCR starts to
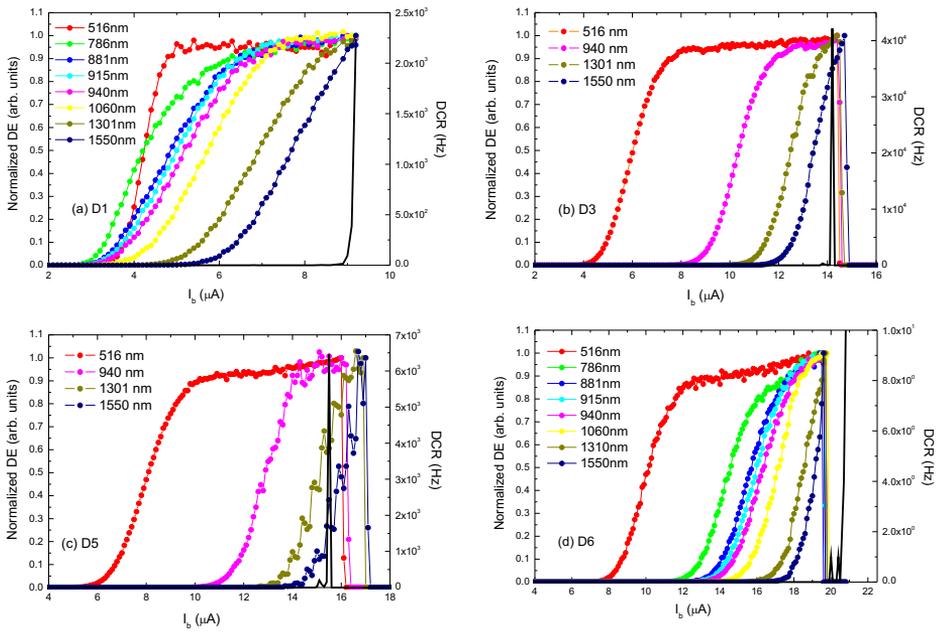
Figure 4.2: The normalized detection efficiency (dark count rates) as a function of the bias current measured at different wavelengths at $T = 2.8$ K is reported on the left (right) scale. Each panel corresponds to a different NbRe-based detector.

4

sensibly grow. These first results are encouraging, since no optimizations of the film properties were implemented.   The devices were also characterized in terms of time performance. In order to estimate the recovery time, the detectors were biased with a current I_b of about 95% of I_c, and illuminated by a a picosecond pulsed (5.2 ps) 1060 nm laser source. Single pulse and averaged pulse were recorded by a room temperature amplifier readout circuitry. Fig. 4.3 presents typical average voltage response as a function of time for a selection of detectors, obtained from the average of 100 pulse traces from a 4GHz bandwidth oscilloscope. In the inset, the average trace (line) is compared with a single shot pulse trace (points) for detector D5. Here the characteristic times for the rise and fall sides, evaluated as the 20% - 80% width of the rising edge and reduction of $1/e$ of the amplitude at the decaying side, respectively, are indicated. It results that the rise time spans from $t_{rise}^{D5} = 393$ ps of detector D5, to $t_{rise}^{D4} = 700$ ps and $t_{rise}^{D7} = 800$ ps of the wide area devices. The shortest fall time is $t_{fall}^{D5} = 9.3$ ns for detector D5, while t_{fall} is shorter than 20 ns for all the investigated devices. These values are competitive with those obtained for NbTiN-based SSPD [12] and for other high-performance materials investigated so far [1]. This result may be related to lower kinetic inductance comparing to other platforms. The characteristic times of all the analyzed devices are summarized in Table 4.1.   Fig. 4.4 shows the time jitter (points) measured on the detector D5
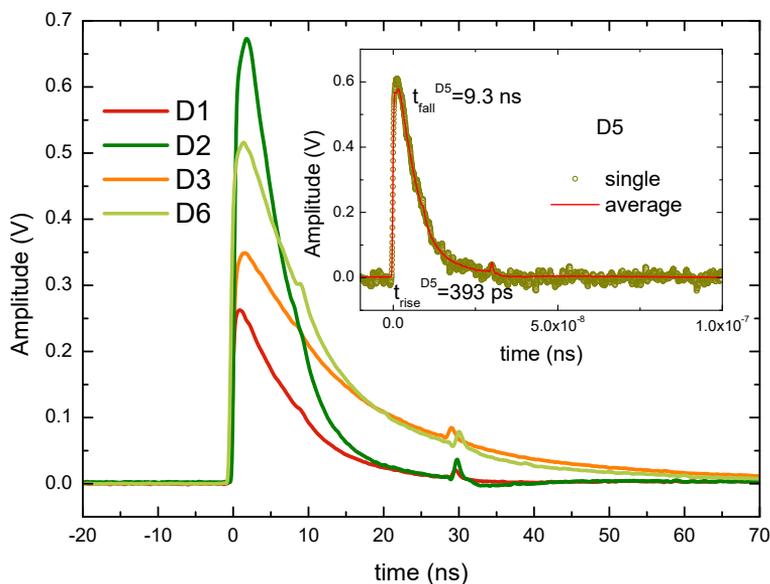

Figure 4.3: Average waveform transient for a representative of NbRe-based detectors measured at T = 2.8 K. Inset: detection pulses for device D5 at T = 2.8 K, the single pulse data (points) is superimposed on the averaged measurement (line). The characteristic times, t_{rise}^{D5} and t_{fall}^{D5}, are indicated.

biased with a current $I_b \approx 95\% \cdot I_c$ and illuminated by a 1030 nm ps pulsed laser. In order to enhance the signal to noise ratio a cryogenic amplifier was used. The data are slightly asymmetric probably due to small resistance variations in different sections of the nanowire, which can be ascribed to the film oxidation [14]. The points can be fitted by a Gaussian dependence (see line) and the timing jitter measurements evaluated as the full width half maximum (FWHM). It results a timing jitter of 35.1 ± 0.5 ps, a value comparable with respect to NbNTi at $T = 4.3$ K [15] which can be further improved by tuning the film properties, as well as optimizing the detector design and fabrication [1, 12].
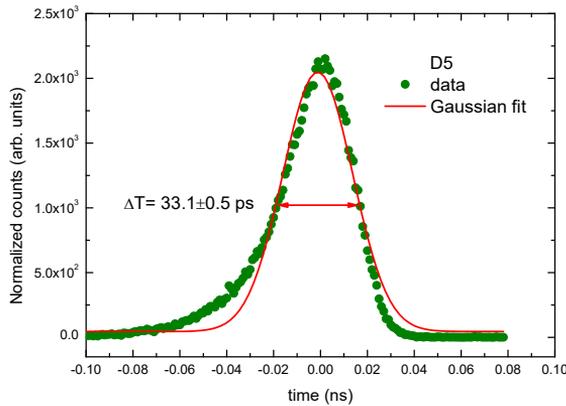

Figure 4.4: Timing jitter for the detector D5 recorder at $T = 3.3$ K. See text for details.

4.4. Optical Property of NbRe

Finally, NbRe optical absorption was evaluated by variable angle ellipsometry over the spectral range $\lambda = 450 - 1650$ nm. Ellipsometric spectra were acquired at angles of incidence of 55, 60, 65, and 70 degrees. In order to estimate the complex refractive index, the data were fitted by using transfer matrix simulations of the absorption for TE polarization. The simulated structure comprises the following layers, air/NbRe(8 nm)/SiO$_2$(230 nm)/Au reflector(150 nm)/Si substrate. The results concerning refractive index (n) and extinction (k) spectra as a function of λ are reported in Fig. 4.5. Both $n(\lambda)$ and $k(\lambda)$ present a quite a steep increase at longer wavelengths. At $\lambda = 1550$ nm $n = 6.22$ and $k = 5.90$. These values are higher than what reported for films of MoSi, NbN and NbTiN about 5-nm-thick, but also for NbN films of 12 nm [33]. The inset of Fig. 4.5 shows the simulated absorption as a function of λ for different values of the devices' filling factor, $ff = w/p$. Interestingly, in the infrared range the absorption is larger than 80% even for $ff = 0.2$, and at $\lambda = 1550$ nm the highest absorption as large as 99.97% is obtained for moderate $ff = 0.4$. This last result, along with the large values estimated for k,

suggests that it may be possible to realize devices with high absorption efficiency by using shorter meander with low ff, with the consequent effect of improving the time performance of the detector.   The main figures of merit of the inves-
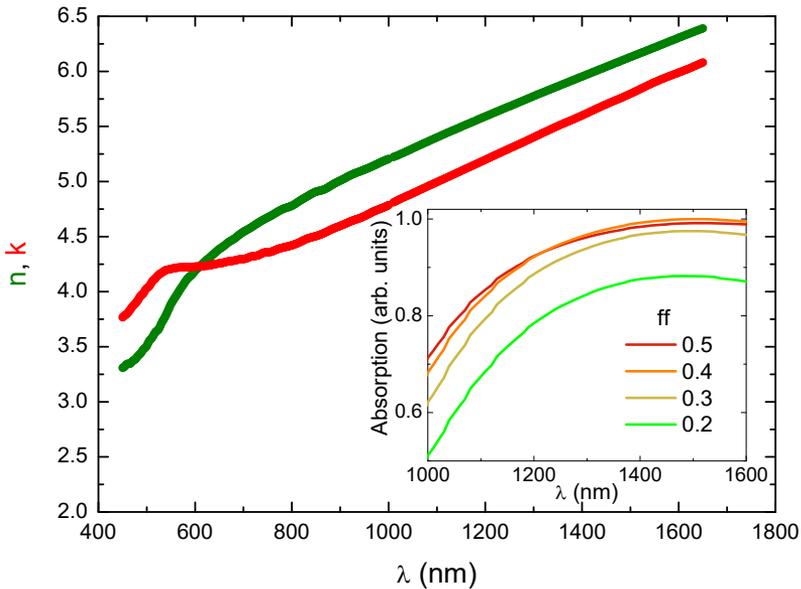

Figure 4.5: Wavelength dependence of refractive index (green line) and extinction coefficient (red line). Inset: wavelength dependence of the simulated absorption for different values of ff.

tigated devices confirm that NbRe is a promising material for the the realization of SSPD with high performances. The presented results are encouraging especially because this work represents a pilot experiment which was intended to probe the applicability of NbRe in the field of photon detection. In particular, it results that the performances in terms of time resolution are comparable with many of the already employed materials. For these reasons, further investigation of detectors based on this promising material will be subject of future works, with the aim to improve the performance of the devices as well as to shed a light on the detection mechanisms in this material. Concerning the first point, there is surely room for improvement in the material intrinsic parameters, as well as in the device fabrication. Film thickness and deposition conditions can be controlled to finely tune I_c, T_c, resistivity, and film microstructure, and, as a consequence, the detector performances. Moreover, it is desirable to perform further investigation to understand the detection mechanism involved in this material [17, 34], such as the study of vortex fluctuation and switching phenomena [35, 36].

4.5. Conclusion

In conclusion, the promising performance of NbRe-based SSPDs at an easily accessible cryogenic temperature was demonstrated. Due to both the reduced value of ξ and the granular film structure[30], the superconducting properties are robust with respect to the nano-patterning process. The devices show a clear saturated DE up to $\lambda = 1301$ nm at $T = 2.8$ K, with a time resolution, $\Delta T = 33.1$ ps, competitive with currently employed superconductors. In addition, at infrared wavelength, simulations return an extinction parameter exceeding 6, and an absorption more than 99% for $ff = 0.4$, which may indicate good performance also of shorter devices. This work paves the way for the optimization of future devices based on NbRe, in particular by tuning the film microscopical properties as well as geometry, along with the experimental set-up, NbRe-based devices may represent an alternative to Nitride based SSPDs as well as to amorphous materials because of their improved performances in terms of time resolution and the operating temperature higher than 4.2 K.

4

References

[1] I. Holzman and Y. Ivry, *Superconducting nanowires for single-photon detection: Progress, challenges, and opportunities,* Advanced Quantum Technologies **2**, 1800058 (2019).

[2] C. M. Natarajan, M. G. Tanner, and R. H. Hadfield, *Superconducting nanowire single-photon detectors: physics and applications,* Superconductor science and technology **25**, 063001 (2012).

[3] H. Zhang, L. Xiao, B. Luo, J. Guo, L. Zhang, and J. Xie, *The potential and challenges of time-resolved single-photon detection based on current-carrying superconducting nanowires,* Journal of Physics D: Applied Physics **53**, 013001 (2019).

[4] H. Takesue, S. W. Nam, Q. Zhang, R. H. Hadfield, T. Honjo, K. Tamaki, and Y. Yamamoto, *Quantum key distribution over a 40-db channel loss using superconducting single-photon detectors,* Nature photonics **1**, 343 (2007).

[5] A. McCarthy, N. J. Krichel, N. R. Gemmell, X. Ren, M. G. Tanner, S. N. Dorenbos, V. Zwiller, R. H. Hadfield, and G. S. Buller, *Kilometer-range, high resolution depth imaging via 1560 nm wavelength single-photon detection,* Optics express **21**, 8904 (2013).

[6] R. Cheng, C.-L. Zou, X. Guo, S. Wang, X. Han, and H. X. Tang, *Broadband on-chip single-photon spectrometer,* Nature communications **10**, 1 (2019).

[7] N. Zen, A. Casaburi, S. Shiki, K. Suzuki, M. Ejrnaes, R. Cristiano, and M. Ohkubo, *1 mm ultrafast superconducting stripline molecule detector,* Applied Physics Letters **95**, 172508 (2009).

[8] S. Dorenbos, E. Reiger, U. Perinetti, V. Zwiller, T. Zijlstra, and T. Klapwijk, *Low noise superconducting single photon detectors on silicon,* Applied Physics Letters **93**, 131101 (2008).

[9] F. Marsili, V. B. Verma, J. A. Stern, S. Harrington, A. E. Lita, T. Gerrits, I. Vayshenker, B. Baek, M. D. Shaw, R. P. Mirin, *et al.*, *Detecting single infrared photons with 93% system efficiency,* Nature Photonics **7**, 210 (2013).

[10] M. Caloz, M. Perrenoud, C. Autebert, B. Korzh, M. Weiss, C. Schönenberger, R. J. Warburton, H. Zbinden, and F. Bussières, *High-detection efficiency and low-timing jitter with amorphous superconducting nanowire single-photon detectors,* Applied Physics Letters **112**, 061103 (2018).

[11] A. Vetter, S. Ferrari, P. Rath, R. Alaee, O. Kahl, V. Kovalyuk, S. Diewald, G. N. Goltsman, A. Korneev, C. Rockstuhl, *et al.*, *Cavity-enhanced and ultrafast superconducting single-photon detectors,* Nano letters **16**, 7085 (2016).

[12] I. Esmaeil Zadeh, J. W. Los, R. B. Gourgues, V. Steinmetz, G. Bulgarini, S. M. Dobrovolskiy, V. Zwiller, and S. N. Dorenbos, *Single-photon detectors combining high efficiency, high detection rates, and ultra-high timing resolution,* APL Photonics **2**, 111301 (2017).

[13] B. Korzh, Q.-Y. Zhao, J. P. Allmaras, S. Frasca, T. M. Autry, E. A. Bersin, A. D. Beyer, R. M. Briggs, B. Bumble, M. Colangelo, *et al.*, *Demonstration of sub-3 ps temporal resolution with a superconducting nanowire single-photon detector,* Nature Photonics **14**, 250 (2020).

[14] I. Esmaeil Zadeh, J. W. Los, R. B. Gourgues, J. Chang, A. W. Elshaari, J. R. Zichi, Y. J. van Staaden, J. P. Swens, N. Kalhor, A. Guardiani, *et al.*, *Efficient single-photon detection with 7.7 ps time resolution for photon-correlation measurements,* ACS Photonics **7**, 1780 (2020).

[15] R. Gourgues, J. W. Los, J. Zichi, J. Chang, N. Kalhor, G. Bulgarini, S. N. Dorenbos, V. Zwiller, and I. E. Zadeh, *Superconducting nanowire single photon detectors operating at temperature from 4 to 7 K,* Optics express **27**, 24601 (2019).

[16] B. Baek, A. E. Lita, V. Verma, and S. W. Nam, *Superconducting aw x si 1-x nanowire single-photon detector with saturated internal quantum efficiency from visible to 1850 nm,* Applied Physics Letters **98**, 251105 (2011).

[17] A. Engel, J. Renema, K. Il'in, and A. Semenov, *Detection mechanism of superconducting nanowire single-photon detectors,* Superconductor Science and Technology **28**, 114003 (2015).

[18] J. Renema, R. Gaudio, Q. Wang, Z. Zhou, A. Gaggero, F. Mattioli, R. Leoni, D. Sahin, M. De Dood, A. Fiore, *et al.*, *Experimental test of theories of the detection mechanism in a nanowire superconducting single photon detector,* Physical review letters **112**, 117604 (2014).

[19] Y. P. Korneeva, N. Manova, I. Florya, M. Y. Mikhailov, O. Dobrovolskiy, A. Korneev, and D. Y. Vodolazov, *Different single-photon response of wide and narrow superconducting Mo$_x$Si$_{1-x}$ strips,* Physical Review Applied **13**, 024011 (2020).

[20] J. Zichi, J. Chang, S. Steinhauer, K. Von Fieandt, J. W. Los, G. Visser, N. Kalhor, T. Lettner, A. W. Elshaari, I. E. Zadeh, *et al.*, *Optimizing the stoichiometry of ultrathin nbtin films for high-performance superconducting nanowire single-photon detectors,* Optics express **27**, 26579 (2019).

[21] W. Zhang, Q. Jia, L. You, X. Ou, H. Huang, L. Zhang, H. Li, Z. Wang, and X. Xie, *Saturating intrinsic detection efficiency of superconducting nanowire single-photon detectors via defect engineering,* Physical Review Applied **12**, 044040 (2019).

[22] V. B. Verma, A. Lita, M. Stevens, R. Mirin, and S. Nam, *Athermal avalanche in bilayer superconducting nanowire single-photon detectors,* Applied Physics Letters **108**, 131108 (2016).

[23] S. Doerner, A. Kuzmin, S. Wuensch, I. Charaev, F. Boes, T. Zwick, and M. Siegel, *Frequency-multiplexed bias and readout of a 16-pixel superconducting nanowire single-photon detector array,* Applied Physics Letters **111**, 032603 (2017).

[24] F. Najafi, F. Marsili, V. B. Verma, Q. Zhao, M. D. Shaw, K. K. Berggren, and S. W. Nam, *Superconducting nanowire architectures for single photon detection,* in *Superconducting Devices in Quantum Optics* (Springer, 2016) pp. 3–30.

[25] V. B. Verma, A. E. Lita, M. R. Vissers, F. Marsili, D. P. Pappas, R. P. Mirin, and S. W. Nam, *Superconducting nanowire single photon detectors fabricated from an amorphous mo0. 75ge0. 25 thin film,* Applied Physics Letters **105**, 022602 (2014).

[26] R. Arpaia, M. Ejrnaes, L. Parlato, F. Tafuri, R. Cristiano, D. Golubev, R. Sobolewski, T. Bauch, F. Lombardi, and G. Pepe, *High-temperature superconducting nanowires for photon detection,* Physica C: Superconductivity and its Applications **509**, 16 (2015).

[27] O. Dobrovolskiy, D. Y. Vodolazov, F. Porrati, R. Sachser, V. Bevz, M. Y. Mikhailov, A. Chumak, and M. Huth, *Ultra-fast vortex motion in a direct-write nb-c superconductor,* Nature communications **11**, 1 (2020).

[28] C. Zhang, W. Zhang, J. Huang, L. You, H. Li, C. lv, T. Sugihara, M. Watanabe, H. Zhou, Z. Wang, *et al.*, *Nbn superconducting nanowire single-photon detector with an active area of 300 μm-in-diameter,* AIP Advances **9**, 075214 (2019).

[29] M. Caputo, C. Cirillo, and C. Attanasio, *Nbre as candidate material for fast single photon detection,* Applied Physics Letters **111**, 192601 (2017).

[30] C. Cirillo, G. Carapella, M. Salvato, R. Arpaia, M. Caputo, and C. Attanasio, *Superconducting properties of noncentrosymmetric nb 0.18 re 0.82 thin films probed by transport and tunneling experiments,* Physical Review B **94**, 104512 (2016).

[31] C. Cirillo, M. Caputo, L. Parlato, M. Ejrnaes, D. Salvoni, R. Cristiano, G. Pepe, and C. Attanasio, *Ultrathin superconducting nbre microstrips with hysteretic voltage-current characteristic,* Low Temperature Physics **46**, 379 (2020).

[32] M. Kupriyanov and V. Lukichev, *Temperature dependence of the critical de-pairing current in superconductors,* Sov. Phys.-Low Temp. Phys. **6**, 445 (1980).

[33] A. Banerjee, R. M. Heath, D. Morozov, D. Hemakumara, U. Nasti, I. Thayne, and R. H. Hadfield, *Optical properties of refractory metal based thin films,* Optical Materials Express **8**, 2072 (2018).

[34] D. Y. Vodolazov, *Single-photon detection by a dirty current-carrying supercon-ducting strip based on the kinetic-equation approach,* Physical Review Applied **7**, 034014 (2017).

[35] U. Nasti, L. Parlato, M. Ejrnaes, R. Cristiano, T. Taino, H. Myoren, R. Sobolewski, and G. Pepe, *Thermal fluctuations in superconduc-tor/ferromagnet nanostripes,* Physical Review B **92**, 014501 (2015).

[36] A. Murphy, A. Semenov, A. Korneev, Y. Korneeva, G. Gol'tsman, and A. Bezryadin, *Three temperature regimes in superconducting photon detec-tors: quantum, thermal and multiple phase-slips as generators of dark counts,* Scientific reports **5**, 1 (2015).

4

5

Multimode fiber coupled superconducting nanowire single photon detectors with high detection efficiency and time resolution

In the past decade superconducting nanowire single photon detectors (SNSPDs) have gradually become an indispensable part of any demanding quantum optics experiment. Until now, most SNSPDs are coupled to single-mode fibers. SNSPDs coupled to multimode fibers have shown promising efficiencies but are yet to achieve high time resolution. For a number of applications ranging from quantum nanophotonics to bio-optics, high efficiency and high time-resolution are desired at the same time. In this chapter, we demonstrate the role of polarization on the efficiency of multi-mode fiber coupled detectors and fabricated high performance 20, 25 and 50 μm diameter detectors targeted for visible, near infrared, and telecom wavelengths. A custom-built setup was used to simulate realistic experiments with randomized modes in the fiber. We achieved over 80% system efficiency and <20 ps timing jitter for 20 μm SNSPDs. Also, we realized 70% system efficiency and <20 ps timing jitter for 50 μm SNSPDs. The high efficiency multimode fiber coupled SNSPDs with unparalleled time resolution will benefit various of quantum optics experiments and applications in the future.

5

5.1. Introduction

Generating and detecting light at the single photon level has enabled a wide range of scientific breakthroughs in several fields, such as quantum optics, bio-imaging and astronomy. High performance single-photon sources have been realized in several platforms such as nonlinear crystals [1], color centers [2], atoms [3], molecules [4], and quantum dots (QDs) [5]. Collecting light from most of these single-photon emitters, however, is a challenge. For example, QDs have emerged as excellent sources of single photons with outstanding single-photon purity [6] and promising candidates for high throughput generation of entangled photons [7, 8]. Currently, most high performance QDs are realized on III-V semiconductor platforms. Due to the nature of their emission and also high refractive index of these materials, extracting photons and coupling them to single-mode fibers has been a major challenge. Many groups have explored processing of III-V quantum dots to enhance the coupling to optical fibers [9–11]. However, coupling photons from QDs to single mode fiber, which has a low numerical aperture (NA) and a small core diameter, imposes demanding constraints on the laboratory setup. Multimode fibers, on the other hand, offer larger core diameters as well as higher NA, and provide several optical modes which significantly relaxes the task of optical coupling. In the field of tissue imaging, photons rapidly get scattered. After a short distance in the tissue, in the order of 1 mm, the transmitted ballistic light is attenuated by about 10 orders of magnitude [12]. Therefore most collected photons are scattered and diffused ones. These photons cannot be easily collected and supported by single mode fibers thus large core, high NA and many modes are necessary. Similarly, in remote laser ranging applications, for example SNSPD-based lidar system, multimode fibers are preferably chosen since they offer larger active area and easier coupling to telescope compared with single mode fiber. However, the SNSPDs used in the lidar system are smaller than the core size of multimode fiber [13]. Thus large size SNSPDs coupled to multimode fiber with simultaneously high efficiency and high time resolution will benefit remote laser ranging applications.

Once light is coupled to fibers, SNSPDs are outstanding single-photon detectors because of their combined performances of high detection efficiency, high time resolution and low dark count rate[14]. Attempts have been made to couple SNSPDs to 50 μm and 100 μm multimode fibers [15–17]. Also using lenses to focus the input beam, multimode fibers were coupled to smaller SNSPDs and SNSPD arrays [18–20], but the achieved time resolution of the larger detectors have been limited to 76-105 ps. Recent works [21, 22] suggested significant tradeoff between SNSPD's length and its time response due to the geometrical jitter. However, a number of experimental observations [14, 23–25] contradict this. Here, we also demonstrate a very high time resolution for large area (long) SNSPDs.

In this paper, we designed and fabricated SNSPDs for several wavelength bands spanning from visible to telecom. To investigate the role of polarization on the system detection efficiency, we carefully characterized detectors using both standard SM fibers with polarization control and MM fibers with randomized modes and polarization. We also studied the influence of fiber dispersion on the instrument response function (IRF) of the system. Specially, with our low timing jitter 50 μm diameter SNSPD we extracted the jitter introduced by geometrical factor. Compared to previous reports, the much lower timing jitter for large size SNSPDs in our work will benefit quantum optics experiments and applications in the future.

5.2. SNSPD fabrication and measurement setup

Similar to [14], we fabricated SNSPDs for the wavelength range of 500-1550 nm out of sputtered 9-11 nm thick films of NbTiN. Figure 5.1(a) shows a scanning electron microscopy image of two fabricated SNSPDS, where left and right images show SNSPDs with 20 and 50 μm in diameter, respectively. To achieve saturation of internal efficiency, we fabricated the detectors for visible and near infrared using 10-11 nm films and the telecom SNSPDs out of 9 nm films. The meander width for visible detectors was 100 nm and for near infrared and telecom it was fixed to 70 nm. The filling factor in all cases was 0.5. As shown in figure 5.1(b) and (c), two optical setups were built to measure the SDE of SNSPDs with SM and MM fibers. In figure 5.1(b), light from a laser diode is guided by SM fiber to a digital attenuator, polarization controller, and then coupled to another SM fiber which brings the light into the 2.4 K cryostat. The right of figure 5.1(b) shows the Gaussian mode of light inside the SM fiber. In order to evaluate the efficiency of multi-mode coupled devices for practical applications, as shown in figure 5.1(c), light from a laser diode is coupled to an optical U-shape bench containing neutral density (ND) filters for attenuating the light power and two diffusers with different grades for generating hybrid light modes. Another MM fiber is used at the other end of the U-bench to couple light into the 2.4 K cryostat. Inside the cryostat, the same type of MM fiber is used to couple light to SNSPDs. As a comparison, the picture on the right side of figure5.1(c) represents an image of the core of MM fiber at the output of the U-bench indicating hybrid modes in the 50 μm multimode fiber.
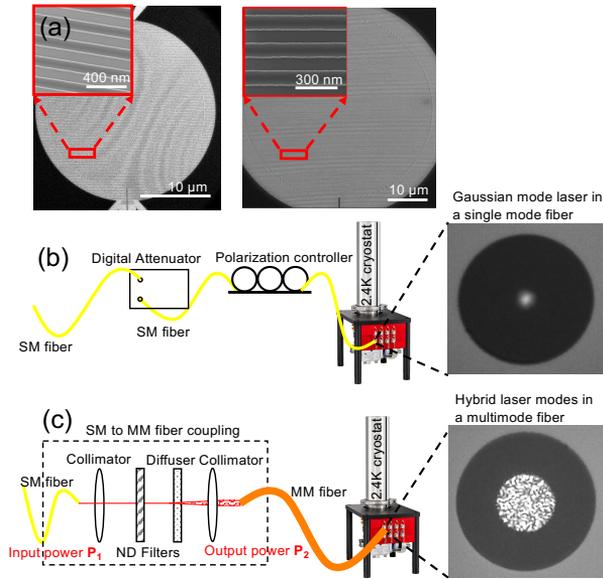
Figure 5.1: (a) Scanning electron microscopy images of a 20 μm diameter SNSPD (left) and 50 μm diameter SNSPD (right). System detection efficiency measurement with two different setups: (b) SM fiber setup and (c) MM fiber setup.

5.3. Simulation and system detection efficiency measurement

Figure 5.2 shows the FDTD simulation of three different optical cavities for enhancing the photon absorption in the meander. Since the absorption is dependent on the polarization of the vertically incident light [26], we simulated the maximum absorption (TE) and minimum absorption (TM) for Gaussian mode light. The average of TE and TM absorption, unpolarized (UP), is used to present the case where light is in hybrid mode. In figure 5.2(a), an aluminum mirror with a thin layer of SiO_2 (about 70 nm) is employed to enhance the absorption for a meander with 100 nm line-width and 200 nm pitch. One benefit of this cavity is that the peak absorption wavelength can be simply shifted by tuning the thickness of the SiO_2 layer or adding extra SiO_2 on top. In figure 5.2(a), the absorption wavelength center was set around 525 nm. At 516 nm, the absorption of TE mode reaches 89% while for the TM mode it is 86%. As a result, the averaged absorption of TE and TM remains at about 87.5%. For 900 nm and 1550 nm, we simulated detectors on a Distributed Bragg Reflector (DBR) cavity for a better agreement with our experimental samples. In both cases, the DBR comprised 6.5 periods of Nb_2O_5 and SiO_2 bilayers. The thickness of Nb_2O_5/SiO_2 was 155/99 nm for 900 nm and 268/173 nm for 1550 nm, respectively. For both cases, we set the meander to be 70 nm line-width and 140 nm pitch, which was the same in our fabrication process. In figure 5.2(b), the absorption of the TE mode approaches 92% while TM mode is

52% at 900 nm, and the averaged value is 72%. At 1550 nm the simulated TE and TM efficiency, shown in figure 5.2(c), are 92% and 22%, which yields an average of 57%. This significant difference in absorption for TE and TM is due to stronger polarization dependence at telecom wavelength comparing to VIS and NIR.

To characterize single mode SDE of our fabricated detectors, laser diodes with different wavelengths were used as photon source (continuous wave). The power of the laser was recorded by a calibrated power meter and was stabilized at 10 nW. After the power stabilization, an attenuation of BB was added by the digital attenuator and then the laser was coupled to the SNSPD. For SDE measurement with MM fiber, we recorded the laser power before (P_1) and after (P_2) the U-bench with a calibrated power meter. By adding different ND filters in the U-bench, we controlled the ratio of P_1/P_2 close to 50 dB. Then we set the power of the input laser also at 10 nW for efficiency measurements. In both cases, the total input photon number can be back calculated from the input laser power. A commercial SNSPD driver was used to control the bias current and read the count rate. In all SDE measurements we subtracted dark counts from the total photon counts, and this was negligible for single mode measurements and multimode measurements at visible and the near infrared. However, telecom detectors coupled to MM fiber detect a significant amount of fiber coupled blackbody radiation. We also removed another 3.6% to account for the end-facet reflection of the fiber where we measured the input power[14]. As shown in figure 5.3(a), at 516 nm the SDE of the 50 μm detector is 70% measured with both SM (red/cyan curve) and MM (purple curve) fiber. All detectors show well saturated internal efficiency. With SM fiber coupled to the SNSPD, there was negligible polarization dependence, which means the TE and TM modes are equally absorbed by the nanowiwe and therefore we also measured a similar efficiency with MM fiber coupled detectors. To avoid detector latching, we used a resistive bridge similar to [14]. We also fabricated 25 μm diameter SNSPDs (70 nm width/140 nm pitch) for visible wavelength range. Since this detector was significantly larger than the fiber, it offers more alignment tolerance and better absorption of cladding modes. An SDE about 80% was achieved for this type of detectors coupled to a 20 μm fiber (yellow curve in figure 5.3(a)). We also showed dark count rates of SNSPDs with both SM fiber, 25, and 50 μm multimode fiber in figure 5.3(a)). When SNSPDs reach saturated detection efficiency, the dark count rate is below 0.2 Hz for both single mode and multimode fiber coupling at 516 nm, however, for 878 nm, figure 5.3(b), and 1550 nm, figure 5.3(c), dark count rates are much higher when SNSPDs are coupled to multimode fibers. As shown in the inset of figure 5.3(c), when 1550 nm SNSPD is coupled to multimode fiber, the dark count rate is approximately 1000 times higher than the single mode fiber coupling. This is caused by black body radiation coupled to fiber modes and detected by efficient (compared to visible and NIR) telecom detector.

At 878 nm as shown in 5.3(b), TE and TM mode detection efficiency are signif-icantly different. For optimized polarization (TE), the SDE approached 80% while for TM polarization, SDE was only 40%. The polarization dependence ratio was a factor of 2, which is in close agreement with our simulations. With our multi-mode efficiency measurement setup, we coupled hybrid modes and fully illuminate

80

5. Multimode fiber coupled superconducting nanowire single photon detectors with high detection efficiency and time resolution

the SNSPD. We measured an SDE of 60% for MM fiber coupled detector at 878nm which is in perfect agreement with an average of TE and TM efficiency measured with SM fiber. Similarly, at 1550 nm the TE efficiency was 75% and TM was 20%. The measured polarization dependence was larger, a factor of 3.75 and thus the efficiency measured with a multi-mode fiber was only 50%. Polarization dependence can be improved by using index matching top dielectric layers [27, 28] at the cost of bandwidth or employing fractal structures detectors [29].
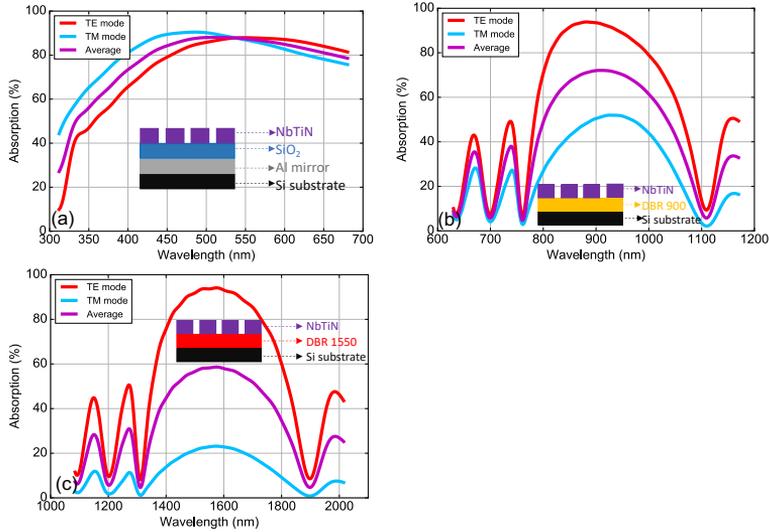

Figure 5.2: Simulated reflectivity of (a) Aluminum/SiO_2 cavity for visible wavelength (b) DBR for 900 nm and (c) DBR for 1550 nm wavelength.

5.4. Jitter measurement and analysis

For SNSPDs, the instrument response function (IRF) usually has a Gaussian distribution and FWHM is commonly used as value of IRF of the system, also known as jitter. In this work, we used a 50 MHz picosecond pulsed laser (4.2 ps pulse width) at 1064 nm and attenuated it to have much less than 1 photon per pulse (on detector < 50-100 kHz count rate). The electrical reference signal was provided by a fast photo diode. An oscilloscope with 4 GHz bandwidth and 40 GHz sampling rate was used to record the SNSPD signal pulse and to measure the jitter. We triggered on the rising edge of the SNSPD pulse as the start signal, and triggered the same way on the synchronized electric reference signal as stop. By building the distribution of time delay between start and stop, we acquired the IRF histogram and extracted its FWHM as jitter. In each jitter measurement we recorded over 100 thousand data points.
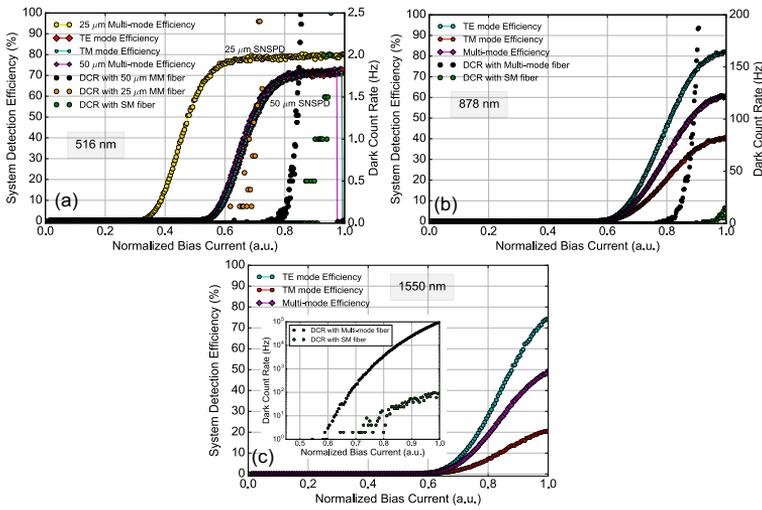
$$\sqrt{b^2 - a^2} = 11.5(ps). \tag{5.1}$$

Figure 5.3: (a) SDE of 25/50 μm diameter SNSPD at 516 nm (b) SDE of a 20 μm diameter SNSPD at 878 nm and (c) SDE of a 20 μm diameter SNSPD at 1550 nm.

5

This 11.5 ps consists geometrical jitter, and inhomogeneity induced jitter [30], however, the geometrical factor induced jitter is no more than 11.5 ps, which is two orders of magnitude lower than previous reported results [22, 31].(The total length of our 50 μm SNSPD is about 5 mm). The achieved jitter for both 20 and 50 μm SNSPDs in this work is the best reported time resolution for multimode fiber coupled SNSPDs so far and will offer opportunities for future quantum optics experiments with high time resolution requirements.

5.5. Conclusions

In this paper, we designed, fabricated, and characterized multimode fiber coupled SNSPDs for visible, near infrared, and telecom wavelength. For visible wavelength, polarization dependence was negligible thus both single-mode and multi-mode coupled SNSPDs showed >80% system detection efficiency. For near-infrared and telecom wavelengths, polarization dependence plays an important role and its ratio increases with wavelength. We reached 60% and 50% system detection efficiency with randomized mode illumination for 878 nm and 1550 nm, respectively. For jitter measurements, step-index multimode fibers introduce light dispersion thus the IRF showed multiple peaks. By using graded-index multimode fibers, this issue can be solved and together with cryogenic amplifier readout circuitry, the jitter of MM fiber coupled SNSPDs can be improved to sub-20 ps. Since our multimode fiber-coupled SNSPDs have high system detection efficiency and high timing resolution at the same time, they can improve the performance of existing experiments in quantum optics, life science and satellite based space communication in the future.
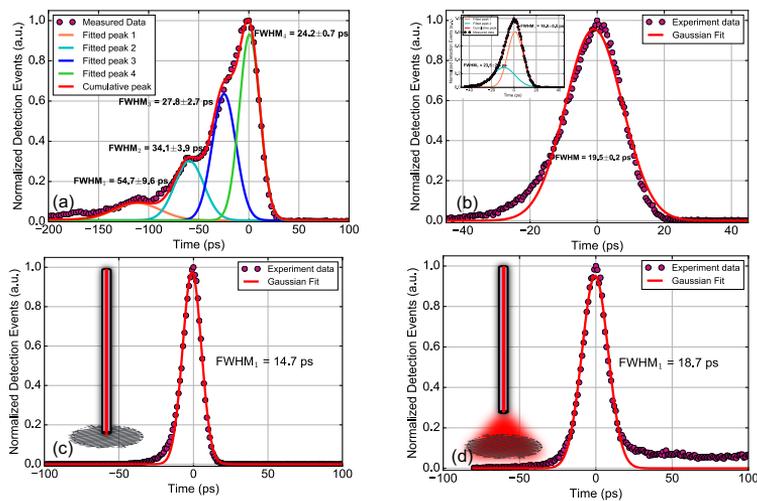
Figure 5.4: Jitter measurement of (a) 20 μm diameter SNSPD with step-index MM fiber/room-temperature amplifier (b) 20 μm diameter SNSPD with graded-index MM fiber/cryogenic amplifier (c) 50 μm diameter SNSPD with SM fiber plugged tightly/cryogenic amplifier and (d) 50 μm diameter SNSPD with SM fiber unplugged from detector/cryogenic amplifier.

References

[1] P. G. Kwiat, K. Mattle, H. Weinfurter, A. Zeilinger, A. V. Sergienko, and Y. Shih, *New high-intensity source of polarization-entangled photon pairs,* Phys. Rev. Lett. **75**, 4337 (1995).

[2] C. Kurtsiefer, S. Mayer, P. Zarda, and H. Weinfurter, *Stable solid-state source of single photons,* Phys. Rev. Lett. **85**, 290 (2000).

[3] M. Saffman and T. Walker, *Creating single-atom and single-photon sources from entangled atomic ensembles,* Physical Review A **66**, 065403 (2002).

[4] B. Lounis and W. E. Moerner, *Single photons on demand from a single molecule at room temperature,* Nature **407**, 491 (2000).

[5] M. E. Reimer, G. Bulgarini, N. Akopian, M. Hocevar, M. B. Bavinck, M. A. Verheijen, E. P. Bakkers, L. P. Kouwenhoven, and V. Zwiller, *Bright single-photon sources in bottom-up tailored nanowires,* Nature Communications **3**, 737 (2012).

[6] L. Schweickert, K. D. Jöns, K. D. Zeuner, S. F. Covre da Silva, H. Huang, T. Lettner, M. Reindl, J. Zichi, R. Trotta, A. Rastelli, and V. Zwiller, *On-demand generation of background-free single photons from a solid-state source,* Applied Physics Letters **112**, 093106 (2018), https://doi.org/10.1063/1.5020038 .

[7] N. Akopian, N. Lindner, E. Poem, Y. Berlatzky, J. Avron, D. Gershoni, B. Ger-

ardot, and P. Petroff, *Entangled photon pairs from semiconductor quantum dots,* Physical review letters **96**, 130501 (2006).

[8] Y. Chen, J. Zhang, M. Zopf, K. Jung, Y. Zhang, R. Keil, F. Ding, and O. G. Schmidt, *Wavelength-tunable entangled photons from silicon-integrated III-V quantum dots,* Nature Communications **7**, 10387 (2016).

[9] M. Pelton, C. Santori, J. Vučković, B. Zhang, G. S. Solomon, J. Plant, and Y. Yamamoto, *Efficient source of single photons: A single quantum dot in a micropost microcavity,* Phys. Rev. Lett. **89**, 233602 (2002).

[10] P. Schnauber, A. Thoma, C. V. Heine, A. Schlehahn, L. Gantz, M. Gschrey, R. Schmidt, C. Hopfmann, B. Wohlfeil, J.-H. Schulze, A. Strittmatter, T. Heindel, S. Rodt, U. Woggon, D. Gershoni, and S. Reitzenstein, *Bright single-photon sources based on anti-reflection coated deterministic quantum dot microlenses,* Technologies (2016), 10.3390/technologies4010001.

[11] X. Ding, Y. He, Z.-C. Duan, N. Gregersen, M.-C. Chen, S. Unsleber, S. Maier, C. Schneider, M. Kamp, S. Höfling, C.-Y. Lu, and J.-W. Pan, *On-demand single photons with high extraction efficiency and near-unity indistinguishability from a resonantly driven quantum dot in a micropillar,* Phys. Rev. Lett. **116**, 020401 (2016).

[12] J. A. Moon, R. Mahon, M. D. Duncan, and J. Reintjes, *Resolution limits for imaging through turbid media with diffuse light,* Opt. Lett. **18**, 1591 (1993).

[13] J. Zhu, Y. Chen, L. Zhang, X. Jia, Z. Feng, G. Wu, X. Yan, J. Zhai, Y. Wu, Q. Chen, and X. Zhou, *Demonstration of measuring sea fog with an SNSPD-based Lidar system,* Scientific reports **7**, 15113 (2017).

[14] I. Esmaeil Zadeh, J. W. Los, R. B. Gourgues, V. Steinmetz, G. Bulgarini, S. M. Dobrovolskiy, V. Zwiller, and S. N. Dorenbos, *Single-photon detectors combining high efficiency, high detection rates, and ultra-high timing resolution,* Appl. Photonics **2**, 111301 (2017).

[15] D. Liu, S. Miki, T. Yamashita, L. You, Z. Wang, and H. Terai, *Multimode fiber-coupled superconducting nanowire single-photon detector with 70% system efficiency at visible wavelength,* Opt.Expr. **22**, 21167 (2014).

[16] H. Li, L. Zhang, L. You, X. Yang, W. Zhang, X. Liu, S. Chen, Z. Wang, and X. Xie, *Large-sensitive-area superconducting nanowire single-photon detector at 850 nm with high detection efficiency,* Opt.Expr. **23**, 17301 (2015).

[17] C. Lv, H. Zhou, H. Li, L. You, X. Liu, Y. Wang, W. Zhang, S. Chen, Z. Wang, and X. Xie, *Large active area superconducting single-nanowire photon detector with a 100 μm diameter,* Superconductor Science and Technology **30**, 115018 (2017).

5

[18] L. Zhang, M. Gu, T. Jia, R. Xu, C. Wan, L. Kang, J. Chen, and P. Wu, *Multimode fiber coupled superconductor nanowire single-photon detector,* IEEE Photonics Journal **6**, 1 (2014).

[19] L. Zhang, C. Wan, M. Gu, R. Xu, S. Zhang, L. Kang, J. Chen, and P. Wu, *Dual-lens beam compression for optical coupling in superconducting nanowire single-photon detectors,* Science bulletin **60**, 1434 (2015).

[20] Q. Chen, B. Zhang, L. Zhang, R. Ge, R. Xu, Y. Wu, X. Tu, X. Jia, L. Kang, J. Chen, and P. Wu, *A 16-pixel nbn nanowire single photon detector coupled with 300 micrometer fiber,* arXiv preprint arXiv:1811.09779 (2018).

[21] N. Calandri, Q.-Y. Zhao, D. Zhu, A. Dane, and K. K. Berggren, *Superconducting nanowire detector jitter limited by detector geometry,* Applied Physics Letters **109**, 152601 (2016).

[22] M. Sidorova, A. Semenov, H.-W. Hübers, I. Charaev, A. Kuzmin, S. Doerner, and M. Siegel, *Physical mechanisms of timing jitter in photon detection by current-carrying superconducting nanowires,* Physical Review B **96**, 184504 (2017).

[23] J. Wu, L. You, S. Chen, H. Li, Y. He, C. Lv, Z. Wang, and X. Xie, *Improving the timing jitter of a superconducting nanowire single-photon detection system,* Applied optics **56**, 2195 (2017).

[24] I. E. Zadeh, J. W. Los, R. Gourgues, G. Bulgarini, S. M. Dobrovolskiy, V. Zwiller, and S. N. Dorenbos, *A single-photon detector with high efficiency and sub-10ps time resolution,* arXiv preprint arXiv:1801.06574 (2018).

[25] H. Wang, H. Li, L. You, P. Hu, X. Zhang, W. Yong, W. Zhang, X. Yang, L. Zhang, H. Zhou, and Z. Wang, *Large-area multispectral superconducting nanowire single-photon detector,* Applied optics **58**, 8148 (2019).

[26] S. N. Dorenbos, E. M. Reiger, N. Akopian, U. Perinetti, V. Zwiller, T. Zijlstra, and T. M. Klapwijk, *Superconducting single photon detectors with minimized polarization dependence,* Applied Physics Letters **93**, 161102 (2008), https://doi.org/10.1063/1.3003579 .

[27] A. Mukhtarova, L. Redaelli, D. Hazra, H. Machhadani, S. Lequien, M. Hofheinz, J.-L. Thomassin, F. Gustavo, J. Zichi, V. Zwiller, and E. Monroy, *Polarization-insensitive fiber-coupled superconducting-nanowire single photon detector using a high-index dielectric capping layer,* Opt. Expr. **26**, 17697 (2018).

[28] L. Redaelli, V. Zwiller, E. Monroy, and J. Gérard, *Design of polarization-insensitive superconducting single photon detectors with high-index dielectrics,* Superconductor Science and Technology **30**, 035005 (2017).

[29] X. Chi, K. Zou, C. Gu, J. Zichi, Y. Cheng, N. Hu, X. Lan, S. Chen, Z. Lin, V. Zwiller, and X. Hu, *Fractal superconducting nanowire single-photon detectors with reduced polarization sensitivity,* Opt. Lett. **43**, 5017 (2018).

5

[30] Y. Cheng, C. Gu, and X. Hu, *Inhomogeneity-induced timing jitter of super-conducting nanowire single-photon detectors,* Applied Physics Letters **111**, 062604 (2017), https://doi.org/10.1063/1.4985226 .

[31] N. Calandri, Q.-Y. Zhao, D. Zhu, A. Dane, and K. K. Berggren, *Superconducting nanowire detector jitter limited by detector geometry,* Applied Physics Letters **109**, 152601 (2016), https://doi.org/10.1063/1.4963158 .

5

6

Mid-infrared Single-photon Detection Using Superconducting NbTiN Nanowires with Sub-15 ps Time Resolution in a Gifford-McMahon Cryocooler

6. Mid-infrared Single-photon Detection Using Superconducting NbTiN
Nanowires with Sub-15 ps Time Resolution in a Gifford-McMahon
Cryocooler

88

Shortly after their inception [1], superconducting nanowire single-photon detectors (SNSPDs) became the leading quantum light detection technology [2]. With the capability of detecting single-photons with near-unity efficiency [3–5], high time resolution [6, 7], low dark count rate [8], and fast recovery time [9], SNSPDs outperform conventional single-photon detection techniques. However, detecting lower energy single-photons (<0.8 eV) with high efficiency and low timing jitter has remained a challenge. To achieve unity internal efficiency at mid-infrared wavelengths, previous works [10, 11] used amorphous superconducting materials with low energy gaps at the expense of reduced time resolution (close to a nanosecond [12]), and by operating them in complex mK dilution refrigerators. In this work, we provide an alternative approach with SNSPDs fabricated from 5-9.5 nm thick NbTiN superconducting films and devices operated in conventional Gifford-McMahon (GM) cryocoolers. By optimizing the superconducting film deposition process, film thickness and nanowire design, our fiber-coupled devices achieved > 70% system detection efficiency (SDE) at 2 µm and sub-15 ps timing jitter. Furthermore, detectors from the same batch demonstrated unity internal detection efficiency at 3 µm and 80% internal efficiency at 4 µm, paving the road for an efficient mid-infrared single-photon detection technology with unparalleled time resolution and without mK cooling requirements. We also systematically studied the dark count rates (DCRs) of our detectors coupled to different types of mid-infrared optical fibers and blackbody radiation filters. This offers insight into the trade-off between bandwidth and dark count rates for mid-infrared SNSPDs. To conclude, this paper significantly extends the working wavelength range for SNSPDs made from polycrystalline NbTiN to 1.5-4 µm, and we expect quantum optics experiments and applications in the mid-infrared range to benefit from this far-reaching technology.

6.1. Introduction

Detecting light at the single photon level has enabled novel scientific and industrial applications in recent decades [2]. Specifically, near- and mid-infrared detection are crucial for areas such as infrared fluorescence and spectroscopy [13–15], semiconductor and industrial production monitoring [16, 17], planetary soil studies [18], remote light detection and ranging [19] as well as two-photon entanglement and interference [20] experiments. However, since photon energy is inversely proportional to wavelength, detecting long wavelength photons is intrinsically more challenging than detecting shorter wavelength photons. Generally, Si-based detectors can be used for infrared detection but suffer from a low cut-off wavelength, typically around 1.1 µm [21], making them inefficient for long wavelength photon detection. Si:Sb based impurity band conduction detectors show mid-infrared light detection capability but not at the single-photon level [22]. Similarly, narrow-bandgap photoconductive semiconductors, like HgCdTe, InAs and InGaAs detectors suffer from low efficiency, large dark counts and poor time resolution [23]. In contrast, SNSPDs have high detection efficiency [3–5], high detection rates [24], low dark count rates (DCR) [8], unprecedented temporal resolution [6, 7] and thus outperform traditional infrared single-photon detectors.

In 2001, NbN-based SNSPDs were first demonstrated by detecting 810 nm single-

photons [1]. Subsequently, SNSPDs fabricated on different platforms were explored and developed [2]. Although high system detection efficiencies have been realized and reported for the UV [25], visible [26] and near-infrared/telecom [3–5, 27], detecting single-photons beyond 1550 nm with high efficiency and time resolution has remained a challenge [28]. Early works showed amorphous WSi based SNSPDs could be used for mid-infrared detection. However, these studies employed 4-6 nm thin superconducting films, resulting in low critical currents which is detrimental to the timing jitter. The reported temporal resolution was close to the nanosecond scale [12]. Also, these devices must be operated at sub-Kelvin temperatures, requiring complex dilution refrigerators. NbN-based SNSPDs with ultra-narrow line widths showed sensitivity up to 5 μm (saturated internal efficiency until 2.7 μm) [29]. A consequence of squeezing the nanowire width to around 30 nm makes fabrication challenging and degrades the detectors' time resolution with the reduced critical current.

Alternatively, our previous work [30] showed that by optimizing the stoichiometry of polycrystalline NbTiN film during reactive magnetron co-sputtering deposition, it is possible to make SNSPDs with strongly saturated efficiency plateaus in the near-infrared region at 2.8 K operating temperature, and also high performance at visible wavelengths up to 7 K [31]. Also, relatively thick NbTiN superconducting films were used [6, 32] to improve our detectors' optical absorption and critical current, therefore enhancing efficiency and time resolution. Building on our previous results, in this work we made SNSPDs from 5, 6.5, 7.5 and 9.5 nm thick NbTiN films with different nanowire designs. First, by characterizing our SNSPDs using flood illumination, we optimized the meander design in terms of internal detection efficiency. Encouraged by our initial characterization results, we fabricated fiber-coupled SNSPDs and achieved a system detection efficiency of >70% at 2 μm in Gifford-McMahon (GM) cryo-coolers (2.4-2.8 K). Broadband detectors were also demonstrated with >50% SDE over the entire 1550-2000 nm range with sub-15 ps timing jitter. Furthermore, devices made from 7.5 and 6.5 nm films showed unity internal detection efficiency at 3 μm and 80% internal efficiency at 4 μm. We also systematically studied the DCRs from the detector itself (intrinsic DCRs) and from black-body radiation delivered by different types of fibers as well as coated fibers as a technique to reduce the DCR. These results offer a comprehensive understanding of the origin of dark counts in mid-infrared SNSPD systems.

6.2. SNSPD Fabrication and Measurement Setup

Similar to [30], we deposited superconducting NbTiN films by a reactive magnetron co-sputtering deposition process. The stoichiometry of the films was controlled by adjusting the sputtering powers on the Ti and Nb targets. Film thickness was determined by a calibrated crystal microbalance and SNSPDs were fabricated as described in [6]. Our fabricated detectors were either tested under flood illumination (figure 6.1 (a)), or etched into a key-hole die shape and packaged using a standard ferrule and mating sleeves approach [33] (figure 6.1 (b)). This coupling method guarantees automatic alignment between detector and optical fibers for accurate system efficiency measurements. Both the flood illumination and fiber-

6. Mid-infrared Single-photon Detection Using Superconducting NbTiN
Nanowires with Sub-15 ps Time Resolution in a Gifford-McMahon
90   Cryocooler

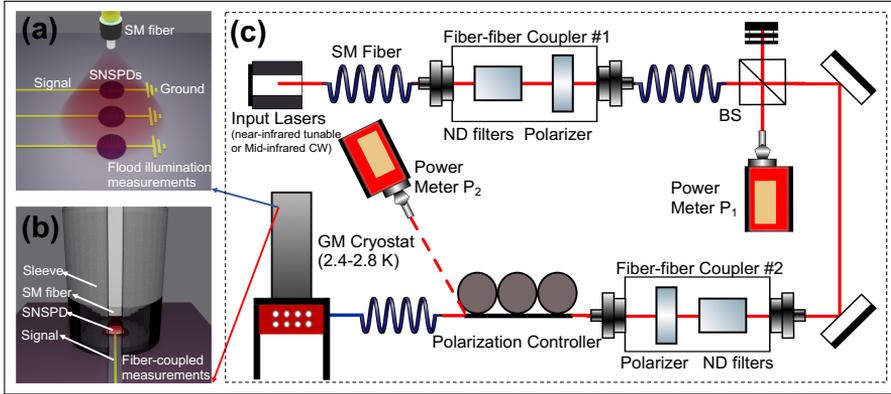coupled setup are shown in figure 6.1 (c).

Figure 6.1: Illustration of **(a)** detector flood illumination, **(b)** a fiber-coupled detector, and **(c)** schematic of the efficiency measurement set-up.

As shown in figure 6.1 (c), we employ a near-infrared tunable laser (JGR-TLS5, 1260-1650 nm) and mid-infrared CW lasers with different wavelengths (2000 and 2700 nm laser from Thorlabs, 3001 and 4013 nm laser from Nanoplus) as input photon sources. Single mode optical fibers are used to couple the light to the first fiber-to-fiber coupler (containing neutral density filters and a polarizer). A beam splitter is then used to create a reference arm with the majority of the power coupled to a calibrated power meter P_1. The signal beam with the lowest power is sent to the second fiber-to-fiber coupler, also containing a polarizer and neutral density filters. A polarization controller is used to tune the polarization state of the light after the second fiber-to-fiber coupler. After recording the light power intensity emerging from the polarization controller with power meter P_2, the light is guided to the system to carry out either flood illumination or fiber-coupled measurements. For flood illumination measurements, the input light is heavily attenuated to the single-photon regime. For fiber-coupled device measurements we use the following procedure: we first set the ratio P_1/P_2 to 50 dB by placing ND (neutral density) filters in both fiber-to-fiber couplers, and then add additional ND filters to the first coupler to reach P_1 = 10 nW. In this way, the input photon flux can be back calculated. For example, 10 nW with 50 dB attenuation at 2000 nm corresponds to an input photon flux of 1.006×10^6 photons per second. More measurement details can be found in our previous work [4].

6.3. Characterization of SNSPDs with Flood Illumination

In this work, SNSPDs with different nanowire widths (40/60/80 nm) and diameters (8/9/10 µm) were fabricated from 5-9.5 nm thick NbTiN films. For example, 60-120-r4 refers to a meandering nanowire design with 60 nm wide lines, a pitch of 120 nm, and 4 µm radius (see insert in figure 6.3 (b)).
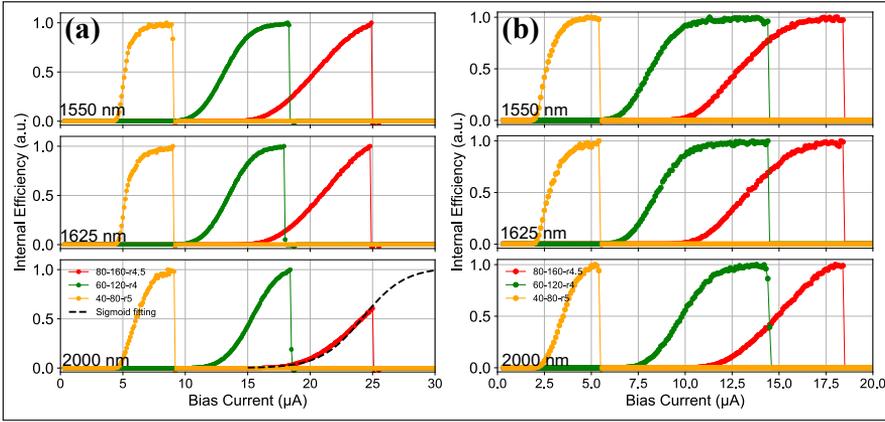
Figure 6.2: Internal efficiency measurements of SNSPDs fabricated from **(a)** 9.5 nm and **(b)** 7.5 nm thick NbTiN films.

As shown in figure 6.2 (a), at 1550 and 1625 nm, the 40 nm width device (yellow), 60 nm width device (green) and 80 nm width device (red) all showed saturated internal efficiencies. When the laser wavelength was increased to 2000 nm, the 40 and 60 nm wide nanowires (yellow and green) devices maintained saturated internal efficiencies, while the 80 nm wide nanowire device (red curve) does not reach unity internal efficiency. To obtain greater saturated internal efficiency, one possible solution is to make narrower lines. However, with narrower line width (<40 nm) the nanofabrication patterning, development, and etching, become more critical. This will, in general, affect the fabrication yield. Alternatively, we sputtered 7.5 nm thick NbTiN films and made detectors with the same designs and nanofabrication process. As shown in figure 6.2(b), by using 7.5 nm thick NbTiN film, all devices with line widths ranging from 40-80 nm showed unity internal efficiency at 2000 nm. Detailed performance of devices based on 9.5 and 7.5 nm films is summarized in table 6.1. A thinner film leads to lower critical currents (for the same meander design), timing jitter is thus higher because the output pulse has a lower signal to noise ratio [34]. The rise time (time interval for signal to go from 20%-80% of the pulse amplitude) of the devices on 7.5 nm NbTiN was longer than for the 9.5 nm devices and dead-time (width of pulse at level of 1/e of the amplitude) was also slightly longer, this can be explained by the fact that devices made with thinner films have higher kinetic inductance.

Meander Structure	I_c (µA) 9.5/7.5 nm	Rise-time (ps) 9.5/7.5 nm	Dead-time (ns) 9.5/7.5 nm	Jitter (ps) 9.5/7.5 nm
80-160-r4.5	25.0/18.4	350/375	9.3/10.6	30/44
60-120-r4	18.2/14	325/335	11.6/12.6	40/45
40-80-r5	8.40/6	400/425	38.4/49.2	93/97

Table 6.1: Flood illumination measurement results of 9.5 and 7.5 nm NbTiN based SNSPDs.

6. Mid-infrared Single-photon Detection Using Superconducting NbTiN
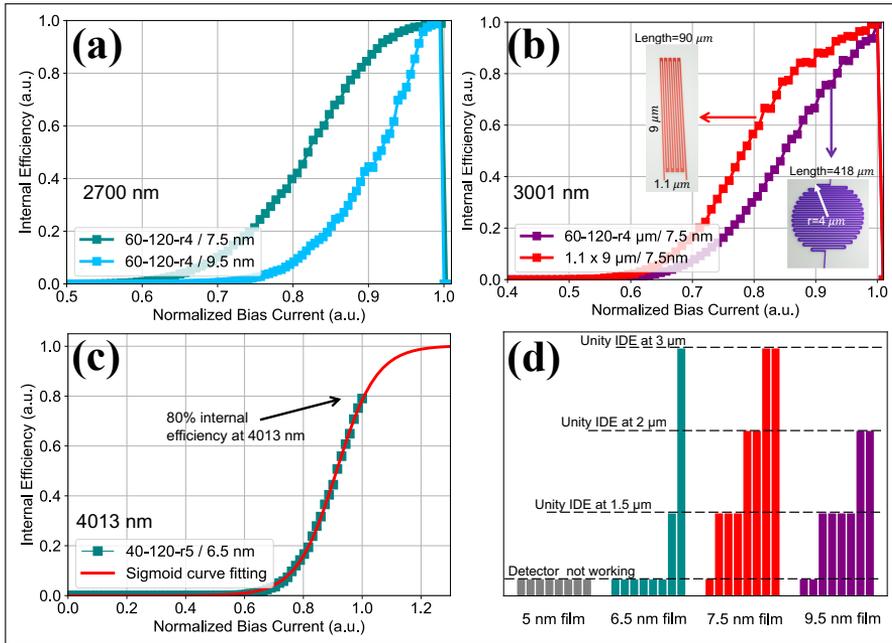Nanowires with Sub-15 ps Time Resolution in a Gifford-McMahon
Cryocooler
92

Figure 6.3: **(a)** Photon counting rate (PCR) curves at 2700 nm of 60-120-r4 detectors from 7.5 nm (green) and 9.5 nm (blue) film, **(b)** PCR curves at 3001 nm of 60-120-r4 detector/purple and 1.1×9 µm detector/red from 7.5 nm film, **(c)** PCR curves at 4013 nm of a 40-120-r5 detector from 6.5 nm film, and **(d)** statistics of device yield made from films with different thicknesses.

The above results show that saturated internal efficiency until 2000 nm can be obtained with detectors made from 9.5/7.5 nm thick films. In order to explore the internal saturation limit, we carried out longer wavelength flood illumination measurements at 2700 and 3001 nm for a number of selected detectors. Figure 6.3 (a) shows detectors with 60-120-r4 meander design from both 9.5/7.5 nm films at 2700 nm. Both detectors reach unity internal efficiency and detectors from 7.5 nm film (dark green curve) show stronger saturated internal efficiency than detectors from 9.5 nm film (light blue curve). This is because by reducing the thickness of the superconducting film, the superconducting energy gap is reduced with the same input photon power, it is easier to break the superconducting state and form a resistive region [35].

Previous measurements at 2700 nm indicate that detectors made from 7.5 nm films are still promising for detecting single photons beyond 2700 nm, we fabricated two types of SNSPDs from a 7.5 nm NbTiN film and measured their detection performances at 3001 nm. As shown in figure 6.3 (b), a 'large' meandering nanowire detector design of 60-120-r4 (purple), and a 'small' detector design with line-width 60 nm, filling factor 50%, 1.1×9 µm (red) were employed. Both detectors show saturated internal efficiency at 3001 nm and the smaller detector shows superior saturated internal efficiency over the larger one. According to a previous study [36], the performance of SNSPDs is influenced by the inhomogeneity of the super-

conducting film. Since the total length of the small detector ($\sim$ 90 μm) is more than 3 times shorter than the large ($\sim$ 418 μm), less inhomogeneity can be expected and better detection performance is observed. This shows that by reducing SNSPD's total length, better detection performance can be potentially achieved. In previous works [11], the best performing device was a single 10-μm-long line. As a consequence the active area is smaller, which can be increased by using different detector architectures, for example multi-pixel [37] or interleaved nanowire designs [38].

Finally, we evaluated detectors made from even thinner films (5 and 6.5 nm). In figure 6.3 (c), we demonstrate that a detector (40-120-r5) from 6.5 nm film achieves 80% internal efficiency at 4013 nm (determined using a sigmoid curve fitting). This represents the state-of-the-art mid-infrared polycrystalline material based SNSPDs. To get a better understanding of the film thickness on the detector performance, we created an overview in figure 6.3 (d). We present the statistics of 32 fabricated SNSPDs from 4 different films. It is clear that 5 and 6.5 nm films suffer from low yield. The detectors made from the 5 nm films do not work well, because of their low critical current (1-2 μA). The non-working detectors from the 6.5 nm film did not show unity internal efficiency at 1550 nm possibly caused by lower film homogeneity of the thin film [6]. In contrast, 7.5 and 9.5 nm films show higher yield but detectors from the 9.5 nm film start to show decreased internal efficiency in the mid-infrared compared to detectors from the 7.5 nm film. Here, we suggest two practical solutions to solve the trade-off between film thickness and performance for future mid-infrared SNSPDs study: Bias-assisted sputtering can be applied to improve the critical current of SNSPDs [39] and post-processing treatment (for example, helium ion irradiation [40]) can enhance the internal efficiency of SNSPDs made from thicker films.

6.4. Measurements of Fiber-coupled SNSPDs

For most quantum optics experiments and applications, a fiber-coupled detector/system is preferred because of mature fiber optics technology and instruments.

The previous section provides evidence that both 7.5 and 9.5 nm NbTiN superconducting films are suitable for making mid-infrared SNSPDs in terms of good yield and internal efficiency while a reduced thickness (5-6.5 nm) leads to fewer working devices. Thus, we fabricated fiber-coupled SNSPDs from 7.5 nm thick NbTiN film. Similar to [4], the NbTiN films were initially deposited on SiO_2 grown by thermal oxidation process and nanowire meanders were eventually located on top of a Au/SiO_2 membrane acting as optical cavity. After packaging and wire bonding, detectors were mounted in a closed-cycle cryocooler with a base temperature of 2.4-2.8 K and coupled to single mode fibers. Afterwards, lasers with different wavelengths were used for system detection efficiency (SDE) measurements as described in the previous section.

Figure 6.4 (a) shows the performance of detector #1 (60 nm line width) made from a 7.5 nm NbTiN film. The SDEs for 1300, 1550, 1625 and 2000 nm are 50%, 60%, 61%, and 63% respectively. The inset in figure 6.4 (a) shows detector #1's photon counting rate (PCR) curves at several wavelengths. Besides high SDE, high

6. Mid-infrared Single-photon Detection Using Superconducting NbTiN
Nanowires with Sub-15 ps Time Resolution in a Gifford-McMahon
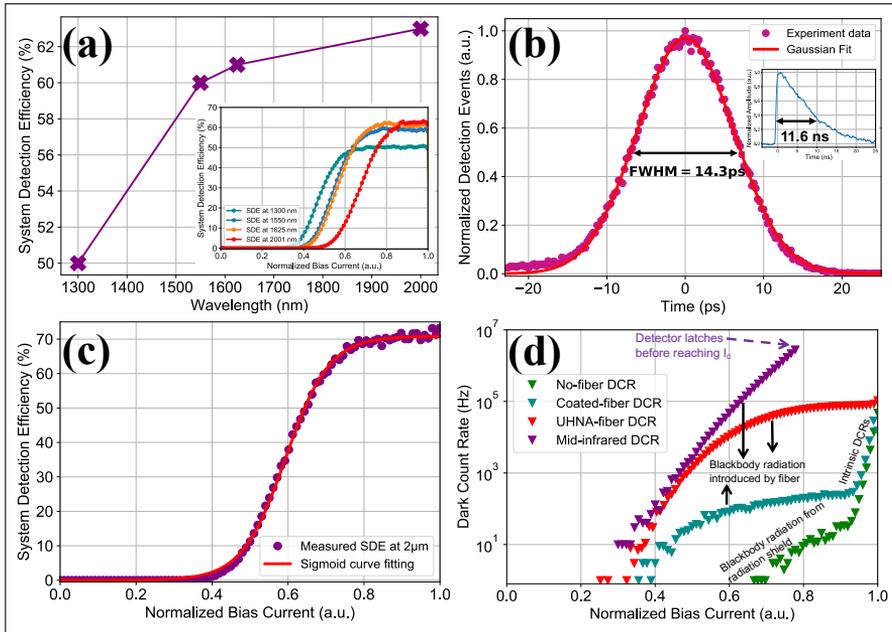94   Cryocooler

Figure 6.4: Fiber-coupled SNSPDs measurements of **(a)** SDE of detector #1 at 1310, 1625, 1550 and 2000 nm, **(b)** timing jitter of detector #1, **(c)** SDE of detector #2 at 2001 nm, and **(d)** DCRs of detector #2 under different conditions: no fiber (green), low-pass coated fiber (turquoise), UHNA fiber (red), and mid-IR fiber (purple) plugged in.

timing resolution is also highly desirable for many applications, for example, Li-DAR [19], fluorescence microscopy and spectroscopy [13, 14]. The Instrument Response Function (IRF) of detector #1 was characterized with a ps-pulsed laser (4.2 ps pulse-width at 1064 nm wavelength) and a fast oscilloscope (4 GHz bandwidth, 40 GHz sampling rate) as described in [4]. As shown in figure 6.4 (b), using a low-noise cryogenic amplifier operated at 40 K, the IRF of this device shows a Gaussian shaped histogram. After fitting, we obtain 14.3±0.1 ps timing jitter (full width at half maximum, FWHM). Compared to previous reported values for mid-infrared SNSPDs [12], we improved time resolution by nearly two orders of magnitude. The inset picture in figure 6.4 (b) shows the pulse trace of detector #1. It shows a dead-time of 11.6 ns, indicating good performance at high count rates [41]. Similarly, in figure 6.4 (c), we show the 2000 nm SDE measurement of detector #2, which is made from another 7.5 nm NbTiN film but has a slightly higher meander filling factor (approximately 10% higher). The benefit of a higher filling factor is an increased optical absorption, which means if the internal efficiency is saturated, a higher SDE can be achieved compared to a similar device with a lower filling factor. As can be seen, detector #2 shows well saturated internal efficiency (when $I_b \geqslant 0.8I_c$). After sigmoid fitting (to improve the efficiency estimation accuracy), we obtained a peak SDE over 70% at 2000 nm.

Besides achieving high system detection efficiency, high dark count rates of mid-

infrared SNSPDs are a major challenge. Previous work [19] showed that the DCRs of mid-infrared SNSPDs is typically in the order of 10^4 Hz without using additional filters. In figure 6.4 (d), we systematically studied the DCRs of detector #2 in four different schemes: DCR without any fiber connected to the detector (green curve), DCR with end-face coated SM2000 fiber (fiber operating wavelength 1.7-2.3 µm, cyan curve), DCR with ultra-high NA fiber without coating (fiber operating wavelength 1.5-2 µm, red curve) and DCR with mid-infrared ZrF_4 fiber without coating (fiber operating wavelength 2.3-4.1 µm, purple curve). As a result, at $I_b=0.8I_c$, the DCRs of detector #2 for the above mentioned four schemes are around the order of 10^1 Hz, 10^2 Hz, 10^5 Hz and 10^6 Hz, respectively. It is clear that the DCR of detector #2 when coupled to an end-face coated fiber is 3 orders of magnitude lower than coupled to ultra-high NA fiber without coating. By using this fiber end-facet coating (low-pass filter), the DCR of detector #2 is below 240 Hz when it reaches unity internal efficiency at 2000 nm. In contrast, when detector #2 is connected to mid-infrared ZrF_4 fiber for SDE measurements at 3-4 µm, the detector showed over 2.78 MHz DCR at 0.8 I_c bias and starts latching [42]. This prevents further SDE measurements of detector #2 at 3-4 µm. To solve this issue, low-pass filters should be employed before the detectors, either by using fiber end-face coating, or adding cold filtering stages inside the cryostat [43].

6.5. Discussion and Conclusion

In the past, amorphous materials were mainly used for mid-infrared single photon detection motivated by the intuition that their superconducting energy gap (0.59-0.61 meV for WSi [44]) is lower than polycrystalline material (2.46 meV for NbN [45]). This work pinpoints that NbTiN (polycrystalline) based SNSPDs can also achieve high mid-infrared single photon detection efficiency while maintaining unprecedented time resolution. Furthermore, given that the energy of a single photon even at 10 µm wavelength (123.9 meV) is still significantly larger than both materials' superconducting energy gap, other physical properties of the superconducting materials need to be investigated to enhance SNSPDs' mid-infrared detection response. Besides improving internal detection efficiency, reducing the dark count rates is another outstanding challenge for mid-infrared SNSPD systems. As shown in this work, only room temperature black body radiation delivered to the detector by ZrF_4 fiber has led to $>10^6$ Hz DCR. To overcome this issue, either extra cryogenic filters need to be added before the detectors or the entire experiment has to be performed at cryogenic temperatures.

In conclusion, we demonstrated SNSPDs made from magnetron co-sputtered NbTiN superconducting films (5-9.5 nm) with unity internal efficiency at 3 µm and 80% internal efficiency at 4013 nm when operated in closed-cycle Gifford-McMahon coolers (2.4-2.8 K). Our fiber coupled device achieves over 70% system detection efficiency at 2 µm and > 50% system detection efficiency from 1300 to 2000 nm with sub-15 ps time resolution. By employing an end-facet coated fiber, the dark count rate of mid-infrared SNSPDs was reduced by 3 orders of magnitude compared to uncoated single mode fibers. The DCR when coupled to mid-infrared ZrF_4 fiber is also studied, which offers valuable information for building mid-infrared fiber-

coupled SNSPDs systems in the future. To the best of our knowledge, the detectors presented in this work have the best system detection efficiency and temporal resolution among the mid-infrared SNSPDs reported so far, and NbTiN is a solid choice for making mid-infrared SNSPDs without mK dilution refrigerators.

References

[1] G. Gol'tsman, O. Okunev, G. Chulkova, A. Lipatov, A. Semenov, K. Smirnov, B. Voronov, A. Dzardanov, C. Williams, and R. Sobolewski, *Picosecond superconducting single-photon optical detector,* Applied Physics Letters **79**, 705 (2001).

[2] I. Esmaeil Zadeh, J. Chang, J. W. Los, S. Gyger, A. W. Elshaari, S. Steinhauer, S. N. Dorenbos, and V. Zwiller, *Superconducting nanowire single-photon detectors: A perspective on evolution, state-of-the-art, future developments, and applications,* Applied Physics Letters **118**, 190502 (2021).

[3] P. Hu, H. Li, L. You, H. Wang, Y. Xiao, J. Huang, X. Yang, W. Zhang, Z. Wang, and X. Xie, *Detecting single infrared photons toward optimal system detection efficiency,* Optics Express **28**, 36884 (2020).

[4] J. Chang, J. Los, J. Tenorio-Pearl, N. Noordzij, R. Gourgues, A. Guardiani, J. Zichi, S. Pereira, H. Urbach, V. Zwiller, *et al.*, *Detecting telecom single photons with 99.5- 2.07+ 0.5% system detection efficiency and high time resolution,* APL Photonics **6**, 036114 (2021).

[5] D. V. Reddy, R. R. Nerem, S. W. Nam, R. P. Mirin, and V. B. Verma, *Superconducting nanowire single-photon detectors with 98% system detection efficiency at 1550 nm,* Optica **7**, 1649 (2020).

[6] I. Esmaeil Zadeh, J. W. Los, R. B. Gourgues, J. Chang, A. W. Elshaari, J. R. Zichi, Y. J. Van Staaden, J. P. Swens, N. Kalhor, A. Guardiani, *et al.*, *Efficient single-photon detection with 7.7 ps time resolution for photon-correlation measurements,* ACS Photonics **7**, 1780 (2020).

[7] B. Korzh, Q.-Y. Zhao, J. P. Allmaras, S. Frasca, T. M. Autry, E. A. Bersin, A. D. Beyer, R. M. Briggs, B. Bumble, M. Colangelo, *et al.*, *Demonstration of sub-3 ps temporal resolution with a superconducting nanowire single-photon detector,* Nature Photonics **14**, 250 (2020).

[8] H. Shibata, K. Shimizu, H. Takesue, and Y. Tokura, *Ultimate low system dark-count rate for superconducting nanowire single-photon detector,* Optics Letters **40**, 3428 (2015).

[9] J. Münzberg, A. Vetter, F. Beutel, W. Hartmann, S. Ferrari, W. H. Pernice, and C. Rockstuhl, *Superconducting nanowire single-photon detector implemented in a 2D photonic crystal cavity,* Optica **5**, 658 (2018).

[10] Q. Chen, R. Ge, L. Zhang, F. Li, B. Zhang, Y. Dai, Y. Fei, X. Wang, X. Jia, Q. Zhao, *et al.*, *Mid-infrared single photon detector with superconductor $Mo_{80}Si_{20}$ nanowire,* arXiv preprint arXiv:2011.06699 (2020).

[11] V. Verma, B. Korzh, A. Walter, A. Lita, R. Briggs, M. Colangelo, Y. Zhai, E. Wollman, A. Beyer, J. Allmaras, *et al.*, *Single-photon detection in the mid-infrared up to 10 µm wavelength using tungsten silicide superconducting nanowire detectors,* APL Photonics **6**, 056101 (2021).

[12] L. Chen, D. Schwarzer, J. A. Lau, V. B. Verma, M. J. Stevens, F. Marsili, R. P. Mirin, S. W. Nam, and A. M. Wodtke, *Ultra-sensitive mid-infrared emission spectrometer with sub-ns temporal resolution,* Optics Express **26**, 14859 (2018).

[13] V. Verma, A. Lita, B. Korzh, E. Wollman, M. Shaw, R. Mirin, and S. Nam, *Towards single-photon spectroscopy in the mid-infrared using superconducting nanowire single-photon detectors,* in *Advanced Photon Counting Techniques XIII*, Vol. 10978 (International Society for Optics and Photonics, 2019) p. 109780N.

[14] L. Chen, D. Schwarzer, V. B. Verma, M. J. Stevens, F. Marsili, R. P. Mirin, S. W. Nam, and A. M. Wodtke, *Mid-infrared laser-induced fluorescence with nanosecond time resolution using a superconducting nanowire single-photon detector: New technology for molecular science,* Accounts of Chemical Research **50**, 1400 (2017).

[15] L. Elsinger, R. Gourgues, I. E. Zadeh, J. Maes, A. Guardiani, G. Bulgarini, S. F. Pereira, S. N. Dorenbos, V. Zwiller, Z. Hens, *et al.*, *Integration of colloidal pbs/cds quantum dots with plasmonic antennas and superconducting detectors on a silicon nitride photonic platform,* Nano Letters **19**, 5452 (2019).

[16] M. Manus, J. Kash, S. Steen, S. Polonsky, J. Tsang, D. Knebel, and W. Huott, *Pica: Backside failure analysis of cmos circuits using picosecond imaging circuit analysis,* Microelectronics Reliability **40**, 1353 (2000).

[17] U. Willer, M. Saraji, A. Khorsandi, P. Geiser, and W. Schade, *Near-and mid-infrared laser monitoring of industrial processes, environment and security applications,* Optics and Lasers in Engineering **44**, 699 (2006).

[18] A. Sprague, J. Emery, K. Donaldson, R. Russell, D. Lynch, and A. Mazuk, *Mercury: Mid-infrared (3–13.5 µm) observations show heterogeneous composition, presence of intermediate and basic soil types, and pyroxene,* Meteoritics & Planetary Science **37**, 1255 (2002).

[19] G. G. Taylor, D. Morozov, N. R. Gemmell, K. Erotokritou, S. Miki, H. Terai, and R. H. Hadfield, *Photon counting lidar at 2.3 µm wavelength with superconducting nanowires,* Optics Express **27**, 38147 (2019).

6

[20] S. Prabhakar, T. Shields, A. C. Dada, M. Ebrahim, G. G. Taylor, D. Morozov, K. Erotokritou, S. Miki, M. Yabuno, H. Terai, *et al.*, *Two-photon quantum interference and entanglement at 2.1 µm,* Science Advances **6**, eaay5195 (2020).

[21] C. L. Tan and H. Mohseni, *Emerging technologies for high performance infrared detectors,* Nanophotonics **7**, 169 (2018).

[22] J. E. Huffman, A. Crouse, B. Halleck, T. Downes, and T. L. Herter, *Si: Sb blocked impurity band detectors for infrared astronomy,* Journal of Applied Physics **72**, 273 (1992).

[23] A. Rogalski, *Next decade in infrared detectors,* in *Electro-Optical and Infrared Systems: Technology and Applications XIV*, Vol. 10433 (International Society for Optics and Photonics, 2017) p. 104330L.

[24] W. Zhang, J. Huang, C. Zhang, L. You, C. Lv, L. Zhang, H. Li, Z. Wang, and X. Xie, *A 16-pixel interleaved superconducting nanowire single-photon detector array with a maximum count rate exceeding 1.5 ghz,* IEEE Transactions on Applied Superconductivity **29**, 1 (2019).

[25] E. E. Wollman, V. B. Verma, A. D. Beyer, R. M. Briggs, B. Korzh, J. P. Allmaras, F. Marsili, A. E. Lita, R. Mirin, S. Nam, *et al.*, *Uv superconducting nanowire single-photon detectors with high efficiency, low noise, and 4 k operating temperature,* Optics Express **25**, 26792 (2017).

[26] J. Chang, I. E. Zadeh, J. W. Los, J. Zichi, A. Fognini, M. Gevers, S. Dorenbos, S. F. Pereira, P. Urbach, and V. Zwiller, *Multimode-fiber-coupled superconducting nanowire single-photon detectors with high detection efficiency and time resolution,* Applied Optics **58**, 9803 (2019).

[27] H. Le Jeannic, V. B. Verma, A. Cavaillès, F. Marsili, M. D. Shaw, K. Huang, O. Morin, S. W. Nam, and J. Laurat, *High-efficiency wsi superconducting nanowire single-photon detectors for quantum state engineering in the near infrared,* Optics Letters **41**, 5341 (2016).

[28] G. G. Taylor, D. Morozov, and R. H. Hadfield, *Mid-infrared photon counting with superconducting nanowires,* in *Quantum Optics and Photon Counting 2021*, Vol. 11771 (International Society for Optics and Photonics, 2021) p. 1177106.

[29] F. Marsili, F. Bellei, F. Najafi, A. E. Dane, E. A. Dauler, R. J. Molnar, and K. K. Berggren, *Efficient single photon detection from 500 nm to 5 µm wavelength,* Nano Letters **12**, 4799 (2012).

[30] J. Zichi, J. Chang, S. Steinhauer, K. Von Fieandt, J. W. Los, G. Visser, N. Kalhor, T. Lettner, A. W. Elshaari, I. E. Zadeh, *et al.*, *Optimizing the stoichiometry of ultrathin NbTiN films for high-performance superconducting nanowire single-photon detectors,* Optics Express **27**, 26579 (2019).

6

[31] R. Gourgues, J. W. Los, J. Zichi, J. Chang, N. Kalhor, G. Bulgarini, S. N. Dorenbos, V. Zwiller, and I. E. Zadeh, *Superconducting nanowire single photon detectors operating at temperature from 4 to 7 K,* Optics Express **27**, 24601 (2019).

[32] J. Chang, I. E. Zadeh, J. W. Los, J. Zichi, and V. Zwiller, *Superconducting nanowire single photon detector with high efficiency and time resolution for multimode fiber coupling,* in *CLEO: QELS_Fundamental Science* (Optical Society of America, 2019) pp. FF1A–2.

[33] A. J. Miller, A. E. Lita, B. Calkins, I. Vayshenker, S. M. Gruber, and S. W. Nam, *Compact cryogenic self-aligning fiber-to-detector coupling with losses below one percent,* Optics express **19**, 9102 (2011).

[34] L. You, X. Yang, Y. He, W. Zhang, D. Liu, W. Zhang, L. Zhang, L. Zhang, X. Liu, S. Chen, *et al.*, *Jitter analysis of a superconducting nanowire single photon detector,* AIP Advances **3**, 072135 (2013).

[35] M. Hofherr, D. Rall, K. Ilin, M. Siegel, A. Semenov, H.-W. Hübers, and N. Gippius, *Intrinsic detection efficiency of superconducting nanowire single-photon detectors with different thicknesses,* Journal of Applied Physics **108**, 014507 (2010).

[36] Y. Cheng, C. Gu, and X. Hu, *Inhomogeneity-induced timing jitter of superconducting nanowire single-photon detectors,* Applied Physics Letters **111**, 062604 (2017).

[37] E. E. Wollman, V. B. Verma, A. E. Lita, W. H. Farr, M. D. Shaw, R. P. Mirin, and S. W. Nam, *Kilopixel array of superconducting nanowire single-photon detectors,* Optics Express **27**, 35279 (2019).

[38] J. Huang, W. Zhang, L. You, C. Zhang, C. Lv, Y. Wang, X. Liu, H. Li, and Z. Wang, *High speed superconducting nanowire single-photon detector with nine interleaved nanowires,* Superconductor Science and Technology **31**, 074001 (2018).

[39] A. E. Dane, A. N. McCaughan, D. Zhu, Q. Zhao, C.-S. Kim, N. Calandri, A. Agarwal, F. Bellei, and K. K. Berggren, *Bias sputtered NbN and superconducting nanowire devices,* Applied Physics Letters **111**, 122601 (2017).

[40] W. Zhang, Q. Jia, L. You, X. Ou, H. Huang, L. Zhang, H. Li, Z. Wang, and X. Xie, *Saturating intrinsic detection efficiency of superconducting nanowire single-photon detectors via defect engineering,* Physical Review Applied **12**, 044040 (2019).

[41] I. Esmaeil Zadeh, J. W. Los, R. B. Gourgues, V. Steinmetz, G. Bulgarini, S. M. Dobrovolskiy, V. Zwiller, and S. N. Dorenbos, *Single-photon detectors combining high efficiency, high detection rates, and ultra-high timing resolution,* APL Photonics **2**, 111301 (2017).

6

[42] A. J. Annunziata, O. Quaranta, D. F. Santavicca, A. Casaburi, L. Frunzio, M. Ejr-
naes, M. J. Rooks, R. Cristiano, S. Pagano, A. Frydman, *et al.*, *Reset dynamics
and latching in niobium superconducting nanowire single-photon detectors,*
Journal of Applied Physics **108**, 084507 (2010).

[43] H. Shibata, K. Fukao, N. Kirigane, S. Karimoto, and H. Yamamoto, *Snspd with
ultimate low system dark count rate using various cold filters,* IEEE Transac-
tions on Applied Superconductivity **27**, 1 (2016).

[44] X. Zhang, A. Engel, Q. Wang, A. Schilling, A. Semenov, M. Sidorova, H.-W.
Hübers, I. Charaev, K. Ilin, and M. Siegel, *Characteristics of superconducting
tungsten silicide $W_x Si_{1-x}$ for single photon detection,* Physical Review B **94**,
174509 (2016).

[45] E. Antonova, D. Dzhuraev, G. Motulevich, and V. Sukhov, *Superconducting
energy gap in niobium nitride,* Zhurnal Ehksperimental'noj i Teoreticheskoj
Fiziki **80**, 2426 (1981).

6

7

Detecting telecom single photons with over 99% system detection efficiency and high time resolution

Single photon detectors are indispensable tools in optics, from fundamental measurements to quantum information processing. The ability of superconducting nanowire single photon detectors to detect single photons with unprecedented efficiency, short dead time and high time resolution over a large frequency range enabled major advances in quantum optics. However, combining near-unity system detection efficiency with high timing performance remains an outstanding challenge. In this work, we show novel superconducting nanowire single photon detectors fabricated on membranes with 99% system detection efficiency (SDE) at 1350 nm with 32 ps timing jitter (using room-temperature amplifier), and other detectors in the same batch showed 94-98% SDE at 1290-1500 nm with 15-26 ps timing jitter (using cryogenic amplifiers). The SiO_2/Au membrane enables broadband absorption in small SNSPDs, offering high detection efficiency in combination with high timing performance. With low noise cryogenic amplifiers operated in the same cryostat, our efficient detectors reach timing jitter in the range of 15-26 ps. We discuss the prime challenges in optical design, device fabrication as well as accurate and reliable detection efficiency measurements to achieve high performance single-photon detection. As a result, the fast developing fields of quantum information science, quantum metrology, infrared imaging and quantum networks will greatly benefit from this far-reaching quantum detection technology.

7.1. Introduction

A single photon stands for the quantum excitation of electromagnetic radiation. Driven by the explosive growth of quantum information science [1] and quantum computation technology [2] in the past few decades, technologies regarding to processing light at single photon level have been greatly explored and developed [3]. In the single photon detection end, avalanche photon diodes (APDs) are widely used due to its its wide detection spectrum range, tunable detection speed and non-cryogenic operation temperature [4]. Since APDs' response to infrared photons are typically lower comparing to visible photons, frequency upconversion detectors can solve this problem by upconverting telecom wavelength photons to visible wavelength [5] for easier detection. However, both APDs or frequency upconversion detectors have limited system detection efficiency, especially in the infrared region. As a comparison, superconducting nanowire single photon detectors (SNSPDs) emerged as a key enabling technology for quantum optics experiments and photonics applications over the last two decades [6–8]. Achieving unity system detection efficiency with SNSPDs has been a long-standing, promising yet challenging goal. It will largely benefit various of application, for example, in quantum key distribution (QKD) systems [9–11], single photon detectors with high efficiency are essential for receiving secured quantum keys over long distances. High efficiency detectors also allow closing loopholes and certify that a quantum communication scheme based on entanglement is secure [12]. Also, for experiments requiring coincidence measurements in multiple detectors, near-unity detection efficiency is required for each channel because the multi photon count rate depends on the efficiency product of detectors involved. For example, the 12-photon coincidence count rate [13] is about one per hour with 75% efficiency detectors. For the same

measurement, if 99.5% efficiency detectors could be used, the coincidence count rate would be increased to one per two minutes. Similarly, in Boson sampling, single photon detectors with high SDE are required in ambitious experiments aiming for quantum supremacy[14]. Besides near-unity system efficiency, high timing performance is crucial for applications where photon arrival time is required to be precisely recorded. For example, in high-dimensional QKD[15, 16], multiple bits per photon pair can be realized by encoding information in the photons' arrival times, high efficiency and time resolution are thus both required. Similarly, high timing performance is essential for improving depth resolution in light detection and ranging [17, 18], distinguishing signal from false counts in dark matter detection [19], enhancing the quality of quantum imaging systems [20, 21] as well as making photons with small energy difference indistinguishable for quantum erasure application [22]. More radically, the fast-expanding quantum technologies in recent years are based on quantum states that violate local realism, as shown in[23, 24], high performance SNSPDs have played important roles in experiments that successfully demonstrated loophole-free violation of Bell's inequalities.

With demands from emerging applications as well as the quest to understand SNSPDs' detection limits, efforts were made in the past years to improve SDE towards unity [25–30]. As summarized in table 7.1, different material platforms were developed to achieve the highest SDE. However, achieving unity efficiency simultaneously with ultrahigh time resolution remains a challenge. Here, using a 9 nm thick NbTiN superconducting film made from optimized magnetron co-sputtering deposition process [31] and membrane cavity, we demonstrate SNSPDs with over 99% SDE at 1350 nm (also over 98% SDE at 1425 nm, see Supplementary Material section S1 "List of measured devices") and above 94% efficiency in the wavelength range 1280-1500 nm. These detectors also achieved 15-26 ps timing jitter with cryogenic amplification readout circuitry and an electrical recovery time of about 33 ns (1/e recovery time). Additionally, we clarify explicitly SNSPDs' efficiency measurement pitfalls and requirements, which will be a solid reference for single photon applications and characterization of single photon detectors.

Table 7.1: Comparison of different high efficiency SNSPDs works

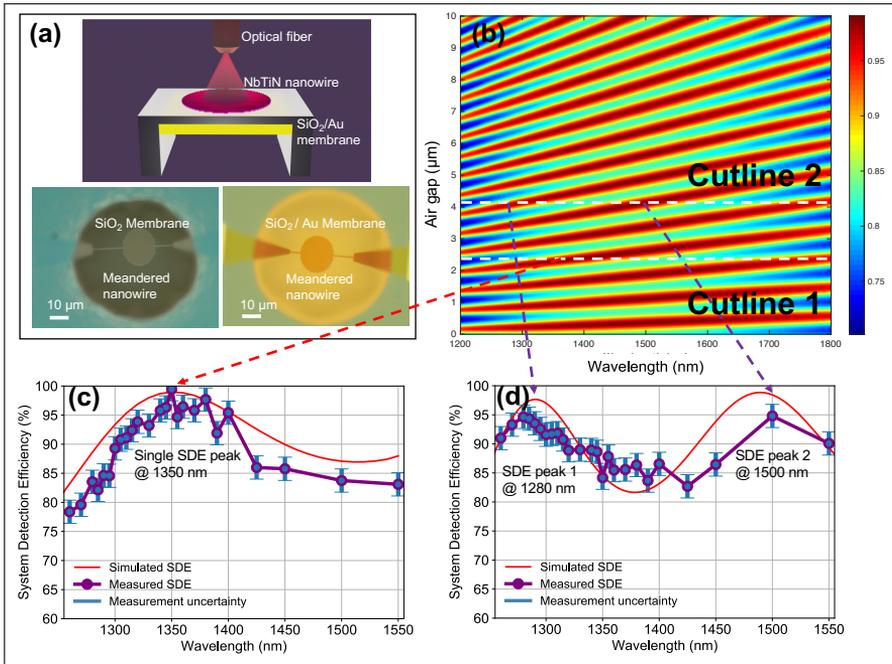| Material/Temperature	SDE/Jitter	Wavelength	Reference
WSi/120 mK	93%/150 ps	1550 nm	ref.[25]
NbN/1.8-2.1 K	90-92%/79 ps	1550 nm	ref.[26]
NbTiN/2.5 K	92%/14.8 ps	1310 nm	ref.[27]
MoSi/700 mK	95%/unknown	1520-1550 nm	ref.[28]
MoSi/700 mK	98%/unknown	1550 nm	ref.[30]
NbN/800 mK-2.1 K	95-98%/65.8-106 ps	1530-1630 nm	ref.[29]
NbTiN/2.5-2.8 K	94-99.5%/15.1 ps	1290-1500 nm	This work

Figure 7.1: (a) Top panel illustrates the device structure of meandered nanowire on SiO$_2$/Au membrane and bottom panel shows optical image of the meandered nanowire on SiO$_2$ membrane before/after (left/right) Au deposition. (b) Simulated optical absorption for a device with 0-10 μm air gap. Cutline 1 shows when the air gap is around 2.2 μm, only one SDE peak occurs around 1350 nm and cutline 2 shows that with an air gap of 4.1 μm, two SDE peaks are obtained. (c) Measurement and simulation of detector #1 with SDE over 99% at 1350 nm. (d) Measurement and simulation of detector #2 with dual peaks at 1280 nm and 1500nm, both exceeding 94% SDE.

7.2. Optical Simulation and Device Design

Typically, SNSPDs are meandering superconducting nanowires embedded in an optical cavity. An optimized optical cavity and meandered nanowire design are indispensable to achieve high system detection efficiency. Recently, works from two different groups showed Distributed Bragg Reflectors (DBR) integrated SNSPDs with ~98% SDE [29, 30]. In [29], SNSPDs made from twin-layer NbN nanowire on DBR (13 alternative SiO$_2$/Ta$_2$O$_5$ layers) showed 95% efficiency at 1550 nm (2.1 K) and 98% efficiency at 1590 nm (0.8 K). The sandwich structure (NbN/SiO$_2$/NbN, 6/3/6 nm) enabled simultaneous high optical absorption as well as saturated internal efficiency, thus high SDE was achieved. The other work [30] demonstrated SNSPDs made form 4.1 nm MoSi on DBR (13 layers of α-Si/SiO$_2$) with 98% SDE at 1550 nm (0.7 K). There, high SDE was achieved by employing amorphous MoSi with strong saturated internal efficiency, using optimized DBR, as well as adding fiber spacers. Since both works employed thick DBR cavity (a few μm), light divergence is high after bouncing several times inside the cavity stacks, thus bigger detectors (diameter 23-50 um) are needed for good optical absorption [30]. However, larger

SNSPDs leads to high kinetic inductance thus slower recovery, low yield and higher jitter. Especially for NbTiN based large detectors, the poly-crystalline materials nature [31] leads to degraded performance because of higher film inhomogeneity comparing to amorphous materials [32]. In order to overcome this challenge, our work employed thinner SiO_2/Au membrane cavity (~230/150 nm) and it has less beam divergence comparing to thick DBR stacks. As a result, we managed to fabricate smaller SNSPDs with high SDE (94-99.5%) and high time resolution (15-26 ps) simultaneously. Based on the above mentioned discussion, we made two different meandered nanowire designs: 50/120 nm and 70/140 nm (line-width/pitch). Both designs have a radius of 8 μm so that our device diameter is 30-70% smaller than recent reported high SDE works [29, 30]. The top panel in figure 7.1 (a) illustrates the NbTiN nanowire supported by SiO_2/Au membrane and bottom panel shows an optical microscope image of the meandered nanowire on SiO_2 membrane before (left) and after (right) deposition of Au reflector. This compact optical cavity design allows us to make smaller meandering nanowires without degrading the SDE. Also, a smaller device leads to lower kinetic inductance, translating into a faster detection signal rising edge and better timing performance. [33–36]. In addition, our NbTiN based detectors are operated in a 2.5-2.8 K Gifford-McMahon cryo-cooler, comparing to [29, 30], the cryostat in our work is simpler, less costly and more compact.

To achieve efficient optical fiber to detector coupling, we used the ferule-sleeve method described in [27]. The air gap between detector and fiber plays an important role in the total optical absorption. The air gap is defined by multiple sources: (i) fabrication residuals left around the device or dust on the fiber end surface,(ii) Au contacts around the detector, (iii) potential drift of fiber core during cooling/warming, leaving a gap between detector and fiber. In this work, Finite-difference time-domain (FDTD) simulations were carried out for a systematic study of the optical absorption. As shown in figure 7.1 (b), when the air gap is around 2.2 μm, only one efficiency peak can be observed along cutline 1. As a result, figure 7.1 (c) shows simulation and measurement results of detector #1 with >99% SDE at 1350 nm. With the increase of the air gap distance, more complex absorption situations are obtained. For example, along cutline 2, dual absorption peaks are expected. We point out that an air gap doesn't always reduce absorption. With proper control of the air gap, one could achieve maximum absorption at selected wavelengths. As a direct demonstration, figure 7.1 (d) shows simulation and measurments of detector #2 with two SDE peaks: at 1280 nm and at 1500 nm. Both SDEs exceed 94% similar to previously reported more complex cavities [37] and controlled design of such detectors would benefit applications where multiple wavelengths must be efficiently detected simultaneously.

7.3. Device Fabrication

Based on simulation results, device fabrication was carried out as described below. Initially, a 230 nm thick SiO_2 layer was grown by thermal oxidation on a commercial Si wafer. On top of the SiO_2, a NbTiN thin film was deposited by co-sputtering of Nb and Ti in a plasma of Ar and N_2 as described in [31]. The meandering

nanowire structure was then written by electron beam lithography with either HSQ (1st batch, negative) or ARP-6200.04 (2nd batch, positive) E-beam resist. After development, the nanowire pattern was transferred to the NbTiN layer by reactive ion etching with mixed gases of SF_6 and O_2. Afterwards, using deep reactive ion etching and metal evaporation, we fabricated a thin SiO_2 membrane with a Au mirror beneath the NbTiN nanowire as described in Supplementary Material section S2 "Device Fabrication". Finally, a deep Silicon etch step (Bosch etching) released the detectors.

Efficiency Measurement Setup
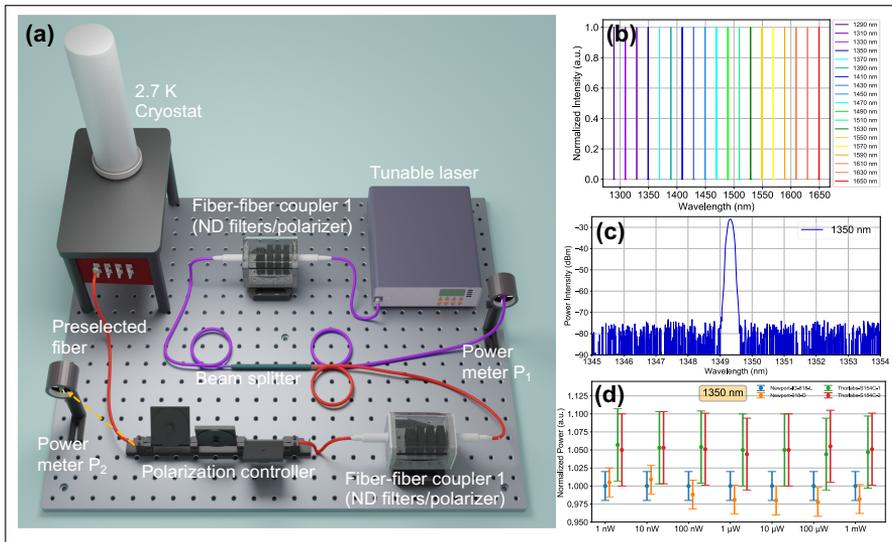
Figure 7.2: (a) System detection efficiency measurement setup. Emission from a tunable laser passes a bench containing neutral density (ND) filters and a polarizer, and goes through a 99-1 fiber-coupled beam splitter to split the signal towards power meter P_1 (99%) and power meter P_2 (1%). (b) Measured spectrum of the tunable laser at 1290-1650 nm. (c) Measured laser spectrum at 1350 nm shows a laser linewidth of < 1 nm. (d) Four different optical power meters' readings at 1350 nm with different error bars. All readings are normalized to the Newport IG-818-L power meter.

Prior to any measurement, the laser was turned on for > 1 hour for power stabilization. Every optical component including fibers were fixed to avoid influence from mechanical vibration and air turbulence. We used the following two-step procedure to carry out system efficiency measurements: (i) Building an accurate laser attenuator. Initially, the continuous-wave (CW) laser beam passes through the first fiber-to-fiber coupler (FBC-1550-FC, containing a polarizer) followed by a fiber-coupled beam splitter (with a splitting ratio of 99-1). The high power branch is recorded by an optical power meter P_1 while the low power branch is directed towards the second fiber-to-fiber coupler (containing neutral density filters and a polarizer) and a polarization controller. Similarly, the power after the polarization

controller is recorded with an optical power meter P_2. By adjusting polarizers in both fiber-to-fiber couplers and choosing the proper neutral density filters, we set the power ratio P_1/P_2 to the desired values (50-60 dB). After the attenuation ratio was set, all components were kept fixed. (ii) Controlling precisely the input photon flux. We lowered the input power by adding extra neutral density filters before passing through the first polarizer to lower P_1 to 1-10 nW. We also rechecked the attenuation ratio multiple times before and after the measurements to assure nothing has been changed in the setup (see Supplementary Material section S6 "Efficiency measurement stability"). After this two-step procedure, different input photon fluxes can be set up, for example 10 nW with 50 dB attenuation corresponds to 679k photons per second at 1350 nm. It must be noted that, to avoid fiber-to-fiber coupling losses when connecting to the detection system, we preselected the fibers which have the best coupling match to the fibers inside our cryostat. Finally, the fiber at the output of the polarization controller was connected to the pre-selected fiber and then guide light into the system for measurements.

Our SDE was calculated as η_{SDE}=(1-R_{rfl})·(N_{count}/N_{total}), where N_{count} is the total registered count rate by our system and N_{total} is the total input photon number. R_{rfl} is added to avoid overestimation of the SDE and it represents the simulated and measured fiber-air interface reflection (see Supplementary Material section S8 "Fiber end-face reflection"). Since the total input photon flux was calculated by N_{total} = P · λ/(hc), where P is the measured optical power, h is plank constant, c is the speed of light in vacuum and λ is the used wavelength, we carefully evaluate our laser spectrum with an optical spectrum analyzer. In figure 7.2 (b), we show the measured spectrum of the tunable laser at variable wavelengths, from 1290 to 1650 nm. As a result, figure 7.2 (c) demonstrates that the laser has a linewidth of < 1 nm. The slight shift of the measured wavelength with the set value is mainly due to the optical spectrum analyzer's calibration, which has negligible influence on our SDE measurement. For input power measurement, accurate optical power meters are necessary. As shown in 7.2 (d), four different optical power meters' readings at 1350 nm are presented with their uncertainties. All readings are normalized to the Newport IG-818-L (used for our measurements) since it has 2% accuracy from 20 pW until 10 mW and a good linearity uncertainty of 0.5%.

7.4. Detection performance and Discussion

Prior to SDE measurements, we studied the relationship between SNSPDs detection reset kinetics and their efficiency recovery. We performed auto-correlation measurements between two subsequent detection events with the detectors illuminated by a CW laser similar to [38]. After collecting more than 50 thousand events, as shown on the top panel of figure 7.3 (a), we built a delay time histogram. Together with the SNSPD detection pulse shown at the bottom panel of 7.3 (a), we can see that within the first 25 ns, no subsequent pulse can be detected thus τ_1=25 ns can be defined as the minimum separation dead time. For most SNSPD related studies, 1/e dead time (time for pulse to decay from peak amplitude to 1/e of the amplitude) is often used to describe the device recovery property. It can be seen that our device's 1/e dead time is τ_2=33 ns. Furthermore, τ_3=51 ns represents
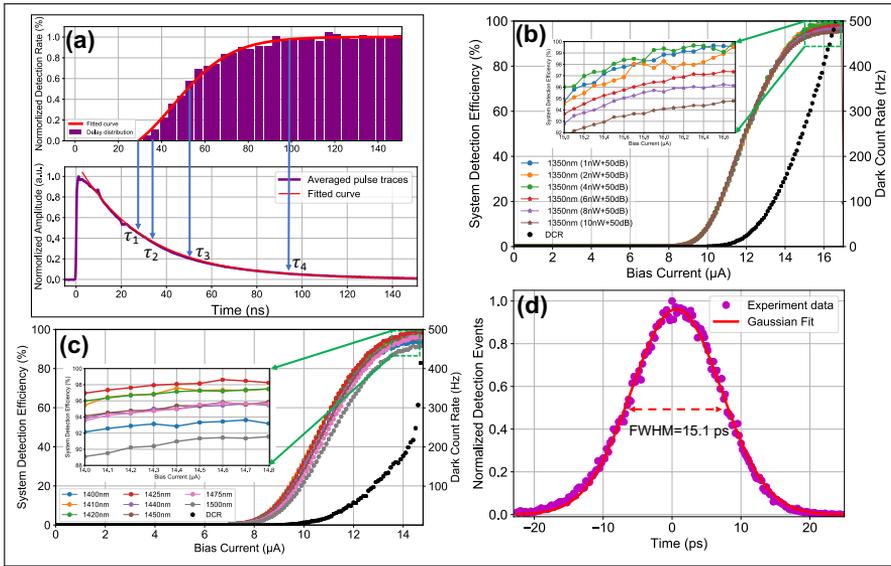
Figure 7.3: (a) The top inset shows the auto-correlation measurement of a detector indicating SDE recovery dynamics. The bottom inset shows an averaged pulse trace from the same detector. (b) SDE measurements of detector #1 at 1350 nm with different input photon fluxes. When input photon flux is below 4 nW plus 50 dB attenuation, the SDE of detector #2 reached >99%, which is also shown in the inserted picture. (c) SDE measurements of detector #3 at different wavelengths. The maximum SDE of detector #3 reached >98% at 1425 nm. (d) Jitter measurement from a detector with > 91% SDE with cryogenic amplifier. A Gaussian fit gives a FWHM jitter of 15.1 ps.

7

the time when the detector recovers 50% of the maximum efficiency, also known as -3dB efficiency dead time and τ_4=97 ns stands for full efficiency recovery time. These measurements indicate that input photon flux can influence SDE because if the photon flux is too high, photons arriving within the dead times of the detector can not be registered at the detectors' maximum efficiency, thus optimal input photon flux is necessary to achieve maximum detection efficiency. It must be noted that much higher photon fluxes can be achieved (with no loss of efficiency) if the source is pulsed (photons arriving with regular timings in between) [27].

We characterized 40 detectors in two separate fabrication rounds. As shown in figure 7.3 (b), detector #1 was the best detector from the first fabrication batch and was tested at 1350 nm with different input photon flux. Initially, the photon flux was set to 10 nW plus 50 dB attenuation ($\sim$ 679,000 photons/s), and device #1 showed SDE of 94-95%. With an input photon flux below 4 nW plus 50 dB attenuation ($\sim$ 271,600 photons/s), device #1 achieved saturated SDE of >99%. Similarly, detector #3 from the second fabrication batch was tested at different wavelengths and showed >98% SDE at 1425 nm as shown in figure 7.3 (c). It worth mentioning that as shown in figure 7.3 (b) and (c), the dark count rate (DCR) of our detector is in the order of (300-500) Hz. We believe this value can be further bring down to below (1-10) Hz by using cold filter [39] in the system or employing fiber with

end-face coatings [40]. For more examples, see Supplementary Material section S1 "List of measured devices".

Besides high SDE, time resolution is another crucial advantage of SNSPDs compared with other single photon detectors. The Instrument Response Function (IRF) of our detectors were characterized with a ps-pulse laser (1064 nm) and a fast oscilloscope (4 GHz bandwidth, 40 GHz sampling rate) as described in [27]. As shown in 7.3 (d), with a low-noise cryogenic amplifier mounted at 40 K stage in the same cryostat , the IRF of device #15 shows a Gaussian shape histogram, after fitting we obtain 15.1 ± 0.05 ps (full width at half maximum, FWHM) timing jitter. This detector was measured to have more than 91% SDE and the ultra low timing jitter was mainly achieved by fabricating relatively small detectors, which results in lower kinetic inductance and thus better jitter [34, 35]. For more statistics of jitter measurement, see Supplementary Material section S1.1 "Overview of tested detectors". In short we achieved 15.1-26 ps jitter with cryogenic amplifierd and 29-39 ps jitter with room-temperature amplifiers readout circuitry.

7.5. Conclusion

In conclusion, we demonstrated NbTiN based SNSPDs operated at 2.5-2.8 K with high performance: Our best detectors showed an SDE of $(99.5^{+0.5}_{-2.07})$% at 1350 nm (time jitter of 35ps, with room temperature amplifiers), and 98 ± 2.07% at 1425 nm (time jitter of 26ps with cryogenic amplifiers). Detectors from the same batch reached SDEs above 94% (in the wavelengths range of 1290-1500 nm), and sub-20ps (best detector 15ps) time jitter using cryogenic amplifiers. The ultrahigh efficiencies were achieved using the following methods: (i) optimized thick NbTiN superconducting film with saturated internal efficiency, (ii) optimized broadband membrane cavity coupled to small detectors, and (iii) accurate system efficiency measurements with a narrow linewidth tunable laser to precisely locate the high-efficiency peaks. Compared with previous reported high-efficiency SNSPDs [25, 28, 30], our work presents a platform with higher operation temperature (2.5-2.8 K, compatible with compact closed-cycle cryostats), short recovery time, and high timing resolution. At the same time, the system efficiency performance of our devices are inpar with recently reported NbN based SNSPDs [29] but using simpler fabrication (single-layer meander), higher operation temperature (no need for mK cooler), and better timing resolution. Our detectors can be further developed by considering the following aspects: (i) multiplexing detector and control individual pixels by cryo-CMOS electronics to realize imaging at the single photon level (ii) extending the detection spectrum in the mid-infrared by tailoring and optimizing NbTiN films and (iii) improving working temperature of the detectors with novel superconducting materials.

7.6. Methods

To achieve accurate SNSPD efficiency measurements, we addressed the following aspects separately.

Optical Simulation

To simulate the absorption of the optical stack, we used the commercially available FDTD Solutions software from Lumerical. The SNSPD was modeled as the cross-section of a single nanowire in an optical cavity. From top to bottom, the simulated stack structure was: optical fiber layer (SiO_2), airgap, NbTiN meander, 1/4 λ SiO_2 layer, and a 150 nm thick Au mirror. Also, in order to check the simulation reliability, we performed transfer matrix simulation to compare and double-check with our FDTD simulation. The negligible plasmonic loss in Au layer was also detailed explained in supplementary material, see Supplementary Material section S3 "Optical Simulation".

Laser Source

A tunable laser (JGR-TLS5) with attenuation was employed as a quasi single photon source. The laser covers the range 1260-1650 nm with a step size of 0.1 nm (FWHM). For more details on the laser, see Supplementary Material section S4 "Tunable laser source". Compared with previous work [27] which used photodiodes operated at a single wavelength, the tunable laser has two major advantages: First, its narrow spectrum (<1 nm) at a tuned frequency allows for precise measurements; Second, a laser with tunable wavelength enabled mapping system efficiency at different wavelengths. In this way we precisely determine peak efficiency and built the spectral response.

Optical Power Meters

A semiconductor-based optical power meter was the key reference for efficiency measurements. In this work, we used two different types of power meters: Thorlabs S154C (NIST traceable, $\pm$5% uncertainty), Newport 818-IG-L (NIST traceable, $\pm$2% uncertainty). However, for the measurement, one should not only take the power meter accuracy into consideration, but also consider sensor linearity, spectral range, power range, stability and all other related parameters.

Measurement Uncertainty Calculation

For system detection efficiency measurement uncertainty, we considered all possible uncertainties in our experiments and calculated the total measurement uncertainty with the root-mean-square (RMS) of the sum of the squared errors. The uncertainties in our measurements include the power meter measurement uncertainty (2%) and linearity uncertainty (0.5%), laser stability uncertainty (<0.1%) and optical attenuator uncertainty (<0.2%). For detailed measurement uncertainty calculations, see Supplementary Material section S6 "Efficiency measurement stability" and "Measurement uncertainty". In short, our efficiency measurement has a total uncertainty of $\pm$2.07% (RMS).

Fiber end-face reflection

When measuring laser power within the fiber with a power meter, the fiber end-facet was not in direct contact with the power meter's sensor. The existing fiber-to-air interface leads to a reflection up to a few percent back towards the light source. [27]. On the other hand, Physical Contact polished fiber to fiber connections have negligible back reflections (typically -30 to -40 dB). For all our efficiency measurements, we removed this back reflection contribution by multiplying a correction factor of (1-R_{rfl}). To determine the accura

Polarization Degree

Since our detectors were patterned along meandering shapes, light absorption can be significantly different based on the light polarization direction along the meander's direction [41]. Thus it is important to have a linearly polarized input light and fully control the polarization. In Supplementary Material section S9 "Polarization degree and control" we show detailed measurement of degree of linearity and polarization control.

Supplementary Materials

See Supplementary Material for complete details of list of measured devices (S1), device fabrication (S2), optical simulation (S3), tunable laser source (S4), optical power meters (S5), efficiency measurement stability (S6), measurement uncertainty (S7), fiber end-face reflection (S8), polarization degree and polarization control (S9) and electronics counting circuitry uncertainty (S10).

References

[1] C. Monroe, *Quantum information processing with atoms and photons,* Nature **416**, 238 (2002).

[2] L.-M. Duan and H. Kimble, *Scalable photonic quantum computation through cavity-assisted interactions,* Physical review letters **92**, 127902 (2004).

[3] M. D. Eisaman, J. Fan, A. Migdall, and S. V. Polyakov, *Invited review article: Single-photon sources and detectors,* Review of scientific instruments **82**, 071101 (2011).

[4] Y. Liang, Q. Fei, Z. Liu, K. Huang, and H. Zeng, *Low-noise ingaas/inp single-photon detector with widely tunable repetition rates,* Photonics Research **7**, A1 (2019).

[5] W. Kang, B. Li, Y. Liang, Q. Hao, M. Yan, K. Huang, and H. Zeng, *Coincidence-pumping upconversion detector based on passively synchronized fiber laser system,* IEEE Photonics Technology Letters **32**, 184 (2020).

[6] G. Gol'tsman, O. Okunev, G. Chulkova, A. Lipatov, A. Semenov, K. Smirnov, B. Voronov, A. Dzardanov, C. Williams, and R. Sobolewski, *Picosecond superconducting single-photon optical detector,* Applied physics letters **79**, 705 (2001).

[7] C. M. Natarajan, M. G. Tanner, and R. H. Hadfield, *Superconducting nanowire single-photon detectors: physics and applications,* Superconductor science and technology **25**, 063001 (2012).

[8] M. D. Eisaman, J. Fan, A. Migdall, and S. V. Polyakov, *Invited review article: Single-photon sources and detectors,* Review of scientific instruments **82**, 071101 (2011).

[9] Y.-L. Tang, H.-L. Yin, S.-J. Chen, Y. Liu, W.-J. Zhang, X. Jiang, L. Zhang, J. Wang, L.-X. You, J.-Y. Guan, *et al.*, *Measurement-device-independent quantum key distribution over 200 km,* Physical review letters **113**, 190501 (2014).

7

[10] J. Yin, Y. Cao, Y.-H. Li, J.-G. Ren, S.-K. Liao, L. Zhang, W.-Q. Cai, W.-Y. Liu, B. Li, H. Dai, *et al.*, *Satellite-to-ground entanglement-based quantum key distribution,* Physical review letters **119**, 200501 (2017).

[11] S.-K. Liao, W.-Q. Cai, W.-Y. Liu, L. Zhang, Y. Li, J.-G. Ren, J. Yin, Q. Shen, Y. Cao, Z.-P. Li, *et al.*, *Satellite-to-ground quantum key distribution,* Nature **549**, 43 (2017).

[12] S. Wengerowsky, S. K. Joshi, F. Steinlechner, J. R. Zichi, S. M. Dobrovolskiy, R. van der Molen, J. W. Los, V. Zwiller, M. A. Versteegh, A. Mura, *et al.*, *Entanglement distribution over a 96-km-long submarine optical fiber,* Proceedings of the National Academy of Sciences **116**, 6684 (2019).

[13] H.-S. Zhong, Y. Li, W. Li, L.-C. Peng, Z.-E. Su, Y. Hu, Y.-M. He, X. Ding, W. Zhang, H. Li, *et al.*, *12-photon entanglement and scalable scattershot boson sampling with optimal entangled-photon pairs from parametric down-conversion,* Physical review letters **121**, 250505 (2018).

[14] H. Wang, J. Qin, X. Ding, M.-C. Chen, S. Chen, X. You, Y.-M. He, X. Jiang, L. You, Z. Wang, *et al.*, *Boson sampling with 20 input photons and a 60-mode interferometer in a 1 0 14-dimensional hilbert space,* Physical review letters **123**, 250503 (2019).

[15] T. Zhong, H. Zhou, R. D. Horansky, C. Lee, V. B. Verma, A. E. Lita, A. Restelli, J. C. Bienfang, R. P. Mirin, T. Gerrits, *et al.*, *Photon-efficient quantum key distribution using time–energy entanglement with high-dimensional encoding,* New Journal of Physics **17**, 022002 (2015).

[16] N. T. Islam, C. C. W. Lim, C. Cahall, J. Kim, and D. J. Gauthier, *Provably secure and high-rate quantum key distribution with time-bin qudits,* Science advances **3**, e1701491 (2017).

[17] Z.-P. Li, X. Huang, P.-Y. Jiang, Y. Hong, C. Yu, Y. Cao, J. Zhang, F. Xu, and J.-W. Pan, *Super-resolution single-photon imaging at 8.2 kilometers,* Optics Express **28**, 4076 (2020).

[18] A. McCarthy, N. J. Krichel, N. R. Gemmell, X. Ren, M. G. Tanner, S. N. Dorenbos, V. Zwiller, R. H. Hadfield, and G. S. Buller, *Kilometer-range, high resolution depth imaging via 1560 nm wavelength single-photon detection,* Optics express **21**, 8904 (2013).

[19] Y. Hochberg, I. Charaev, S.-W. Nam, V. Verma, M. Colangelo, and K. K. Berggren, *Detecting sub-Gev dark matter with superconducting nanowires,* Physical review letters **123**, 151802 (2019).

[20] A. Pe'er, Y. Bromberg, B. Dayan, Y. Silberberg, and A. A. Friesem, *Broadband sum-frequency generation as an efficient two-photon detector for optical tomography,* Optics Express **15**, 8760 (2007).

7

[21] E. E. Wollman, V. B. Verma, A. E. Lita, W. H. Farr, M. D. Shaw, R. P. Mirin, and S. W. Nam, *Kilopixel array of superconducting nanowire single-photon detectors,* Optics express **27**, 35279 (2019).

[22] K. De Greve, L. Yu, P. L. McMahon, J. S. Pelc, C. M. Natarajan, N. Y. Kim, E. Abe, S. Maier, C. Schneider, M. Kamp, *et al.*, *Quantum-dot spin–photon entanglement via frequency downconversion to telecom wavelength,* Nature **491**, 421 (2012).

[23] L. K. Shalm, E. Meyer-Scott, B. G. Christensen, P. Bierhorst, M. A. Wayne, M. J. Stevens, T. Gerrits, S. Glancy, D. R. Hamel, M. S. Allman, *et al.*, *Strong loophole-free test of local realism,* Physical review letters **115**, 250402 (2015).

[24] M. Giustina, M. A. Versteegh, S. Wengerowsky, J. Handsteiner, A. Hochrainer, K. Phelan, F. Steinlechner, J. Kofler, J.-Å. Larsson, C. Abellán, *et al.*, *Significant-loophole-free test of bell's theorem with entangled photons,* Physical review letters **115**, 250401 (2015).

[25] F. Marsili, V. B. Verma, J. A. Stern, S. Harrington, A. E. Lita, T. Gerrits, I. Vayshenker, B. Baek, M. D. Shaw, R. P. Mirin, *et al.*, *Detecting single infrared photons with 93% system efficiency,* Nature Photonics **7**, 210 (2013).

[26] W. Zhang, L. You, H. Li, J. Huang, C. Lv, L. Zhang, X. Liu, J. Wu, Z. Wang, and X. Xie, *Nbn superconducting nanowire single photon detector with efficiency over 90% at 1550 nm wavelength operational at compact cryocooler temperature,* Science China Physics, Mechanics & Astronomy **60**, 120314 (2017).

[27] I. Esmaeil Zadeh, J. W. Los, R. B. Gourgues, V. Steinmetz, G. Bulgarini, S. M. Dobrovolskiy, V. Zwiller, and S. N. Dorenbos, *Single-photon detectors combining high efficiency, high detection rates, and ultra-high timing resolution,* Apl Photonics **2**, 111301 (2017).

[28] D. V. Reddy, R. R. Nerem, A. E. Lita, S. W. Nam, R. P. Mirin, and V. B. Verma, *Exceeding 95% system efficiency within the telecom c-band in superconducting nanowire single photon detectors,* in *CLEO: QELS_Fundamental Science* (Optical Society of America, 2019) pp. FF1A–3.

[29] P. Hu, H. Li, L. You, H. Wang, Y. Xiao, J. Huang, X. Yang, W. Zhang, Z. Wang, and X. Xie, *Detecting single infrared photons toward optimal system detection efficiency,* Optics Express **28**, 36884 (2020).

[30] D. V. Reddy, R. R. Nerem, S. W. Nam, R. P. Mirin, and V. B. Verma, *Superconducting nanowire single-photon detectors with 98% system detection efficiency at 1550 nm,* Optica **7**, 1649 (2020).

[31] J. Zichi, J. Chang, S. Steinhauer, K. Von Fieandt, J. W. Los, G. Visser, N. Kalhor, T. Lettner, A. W. Elshaari, I. E. Zadeh, *et al.*, *Optimizing the stoichiometry of ultrathin nbtin films for high-performance superconducting nanowire single-photon detectors,* Optics Express **27**, 26579 (2019).

7

[32] B. Baek, A. E. Lita, V. Verma, and S. W. Nam, *Superconducting aw x si 1-x nanowire single-photon detector with saturated internal quantum efficiency from visible to 1850 nm,* Applied Physics Letters **98**, 251105 (2011).

[33] S. Miki, M. Takeda, M. Fujiwara, M. Sasaki, A. Otomo, and Z. Wang, *Superconducting nbtin nanowire single photon detectors with low kinetic inductance,* Applied physics express **2**, 075002 (2009).

[34] J. K. Yang, A. J. Kerman, E. A. Dauler, V. Anant, K. M. Rosfjord, and K. K. Berggren, *Modeling the electrical and thermal response of superconducting nanowire single-photon detectors,* IEEE transactions on applied superconductivity **17**, 581 (2007).

[35] L. You, X. Yang, Y. He, W. Zhang, D. Liu, W. Zhang, L. Zhang, L. Zhang, X. Liu, S. Chen, *et al.,* *Jitter analysis of a superconducting nanowire single photon detector,* Aip Advances **3**, 072135 (2013).

[36] J. Chang, I. E. Zadeh, J. W. Los, J. Zichi, A. Fognini, M. Gevers, S. Dorenbos, S. F. Pereira, P. Urbach, and V. Zwiller, *Multimode-fiber-coupled superconducting nanowire single-photon detectors with high detection efficiency and time resolution,* Applied Optics **58**, 9803 (2019).

[37] H. Li, H. Wang, L. You, P. Hu, W. Shen, W. Zhang, X. Yang, L. Zhang, H. Zhou, Z. Wang, *et al.,* *Multispectral superconducting nanowire single photon detector,* Optics express **27**, 4727 (2019).

[38] S. Miki, M. Yabuno, T. Yamashita, and H. Terai, *Stable, high-performance operation of a fiber-coupled superconducting nanowire avalanche photon detector,* Optics express **25**, 6796 (2017).

[39] H. Shibata, K. Fukao, N. Kirigane, S. Karimoto, and H. Yamamoto, *Snspd with ultimate low system dark count rate using various cold filters,* IEEE Transactions on Applied Superconductivity **27**, 1 (2016).

[40] W. Zhang, X. Yang, H. Li, L. You, C. Lv, L. Zhang, C. Zhang, X. Liu, Z. Wang, and X. Xie, *Fiber-coupled superconducting nanowire single-photon detectors integrated with a bandpass filter on the fiber end-face,* Superconductor Science and Technology **31**, 035012 (2018).

[41] S. Dorenbos, E. Reiger, N. Akopian, U. Perinetti, V. Zwiller, T. Zijlstra, and T. Klapwijk, *Superconducting single photon detectors with minimized polarization dependence,* Applied Physics Letters **93**, 161102 (2008).

7

7.7. Supplementary

Contents:

S1 List of measured devices

S1.1 Overview of tested detectors

S1.2 Measurement reproducibility

S1.3 Detailed measurements of selected detectors

S2 Device Fabrication

S3 Optical Simulation

S3.1 Comparison of FDTD and transfer matrix simulation

S3.2 Material optical properties and Au reflector simulation

S4 Tunable laser source

S5 Optical power meters

S6 Efficiency measurement stability

S6.1 Optical attenuator stability

S6.2 Optical input power stability

S7 Measurement uncertainty

S8 Fiber end-face reflection

S8.1 Simulation of fiber end-face reflection

S8.2 Measurement of fiber end-face reflection

S9 Polarization degree and polarization control

S10 Electronics counting circuitry uncertainty

S11 References

S1 List of measured devices
S1.1 Overview of tested detectors

Detector No.	Wavelength (nm)	SDE (%)	Jitter[*] (ps)	SDE uncertainty
Table S1.1 Overview of all measured detectors				
1[a]	1350	99.5	31 (RT)	± 2.07%
2	1280/1500	94	29 (RT)	± 2.07%
3	1425	98	26 (cryo)	± 2.07%
4	1350	95	32 (RT)	± 2.07%
5	1310	94	39 (RT)	± 2.07%
6[b]	1550	83.3	18.7 (cyro)	± 5.9%
7	1550	80.5	24 (cyro)	± 5.9%
8	1550	83.3	35 (RT)	± 5.9%
9	1310	83.6		± 5.9%
10	1310	84		± 5.9%
11	1550	84		± 5.9%
12	1310	84.3		± 5.9%
13[c]	1392	93.6	35.3 (RT)	± 5.9%
14	1550	85	31 (RT)	± 5.9%
15	1278	91.3	15.1 (cryo)	± 5.9%
16	1550	89	17.3 (cryo)	± 5.9%
17	1392	85	19.1 (cryo)	± 5.9%
18	1550	82	19.5 (cryo)	± 5.9%
19	1550	82.5	19 (cryo)	± 5.9%
20	1310	85.4		± 5.9%
21	1310	87		± 5.9%
22	1310	85		± 5.9%
23	1550	90.1		± 5.9%
24	1510	91.4		± 5.9%
25	1301	91		± 5.9%
26	1301	90.5		± 5.9%
27	1301	85		± 5.9%
28	1425	93.5		± 5.9%
29	1310	89.7		± 5.9%
30	1310	85.6		± 5.9%
31	1310	87.2		± 5.9%
32	1550	80		± 5.9%
33-40	Low efficiency or broken detectors, not registered here.			

[*] Jitter with 'cyro' label means measured with a cryogenic amplifier and jitter with 'RT' label means measured with a room-temperature amplifier.
[a] Detectors labelled with red fonts have efficiency > 90%. They were fully tested at multiple wavelengths.
[b] Detectors labelled with black fonts have efficiency < 85%. However, they were only tested at a few wavelengths. At other wavelengths they may reach higher efficiencies.
[c] Detectors labelled with green fonts have efficiency > 85%. However, they were also only tested at a few certain wavelengths. At other wavelengths they may reach higher efficiencies.

S1.2 Measurement reproducibility

In order to show the measurement reproducibility, below in figure 1.1 we show SDE measurement of detector #1 on two different dates (19th-July-2020, blue and 15th-Aug-2020, yellow). As can be seen that there is negligible difference between these two measurements and both of them show >99% SDE at 1350nm. Please note that in between of these two dates, the detector was kept in vacuum but multiple cool-down and warm-up cycles were performed to check the system reliability.

Figure S1.1 SDE measurement of detector #1 on two different dates (19th-July-2020, blue and 15th-Aug-2020, orange).

7

S1.3 Detailed measurements of selected detectors

7
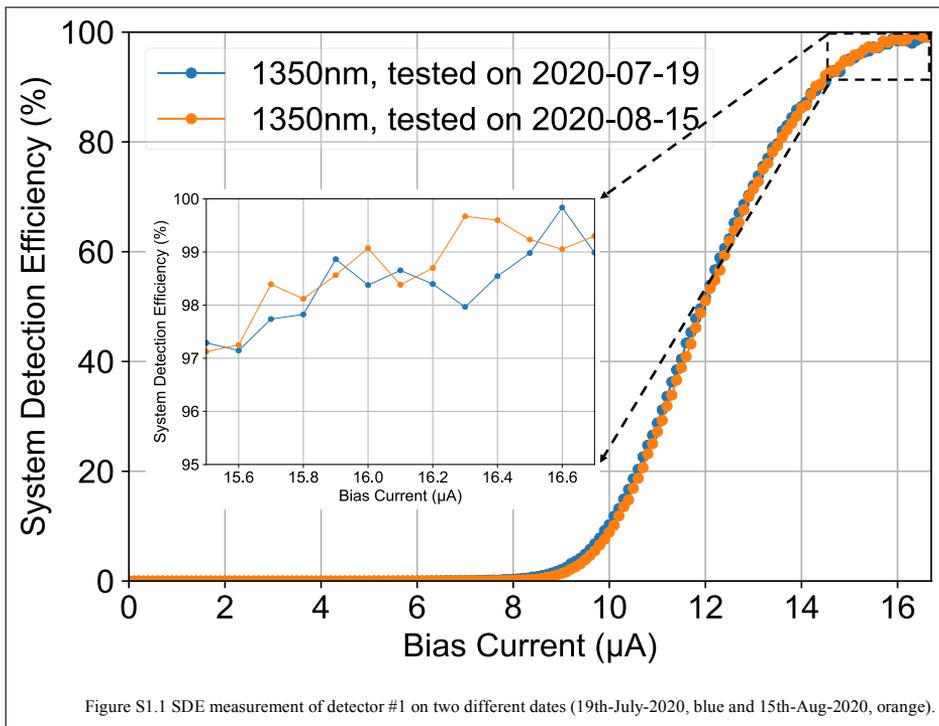
Table S1.2 Photocount rate curve and system efficiency measurement of selected detectors at different wavelengths.

Detector #1PCR curves

Detector #1 wavelength response curve

Detector #2 PCR curve

Detector #2 wavelength response curve

Detector #3 PCR curve

Detector #3 wavelength response curve

Detector #4 PCR curve

Detector #4 wavelength response curve

Detector #5 PCR curve

Detector #5 wavelength response curve
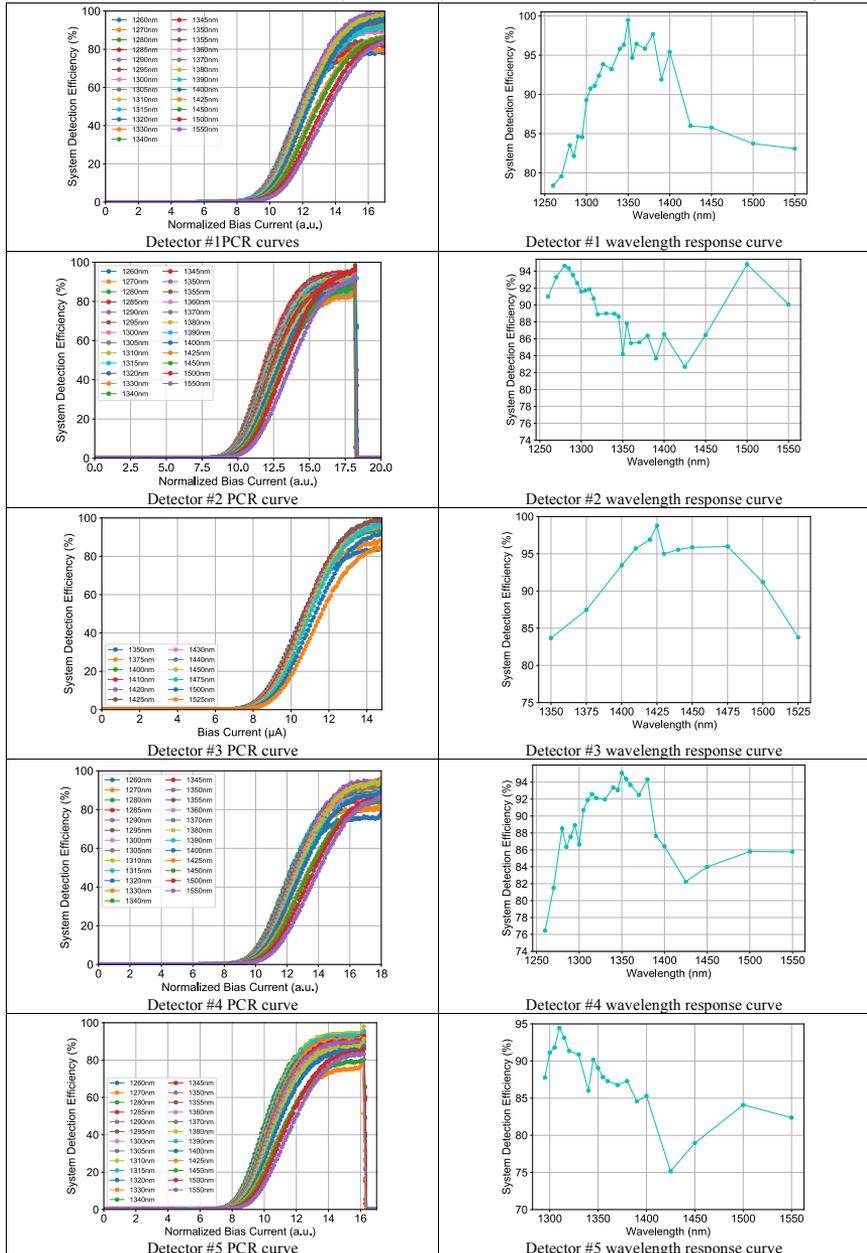
Note: the left column shows detectors' photocount rate (PCR) curve and right column shows detectors' efficiencies at different measured wavelengths. The system detection efficiencies have an uncertainty of ± 2.07%.

S2 Device Fabrication

We fabricated our detectors in the following order as shown in figure S2.1: Initially, a 230 nm thick SiO_2 layer was grown by thermal oxidation on a 4-inch Si wafer. On top of the SiO_2, a NbTiN thin film was deposited by magnetron co-sputtering (Nb and Ti) deposition in a mixture of Argon and Nitrogen [1]. After that, the contact pads were formed using optical lithography, metal evaporation (Cr/Au, 5/55nm) and lift-off. Meandered nanowire structure was defined by electron beam lithography with either HSQ (1st batch, negative resist) or ARP 6200.04 (2nd batch, positive resist) E-beam resist. After development, the nanowire patterns were transferred to the NbTiN layer by reactive ion etching in a mixture of SF_6 and O_2 chemistry. Afterwards, EUV optical lithography was employed to open windows with a photo-resist (S1813) at the back side of the wafer, aligning it to the active area of the devices on the front side. After making the opening, a selective deep reactive ion etching (a Bosch process) was used to remove $\sim$280 μm Si before stopping at the SiO_2 layer. Cr/Au (2-3nm/150nm) was then deposited to form the mirror under SiO_2 membrane. Finally, a second Bosch etching recipe was used to release each individual detector.

Figure S2.1 Device nanofabrication process
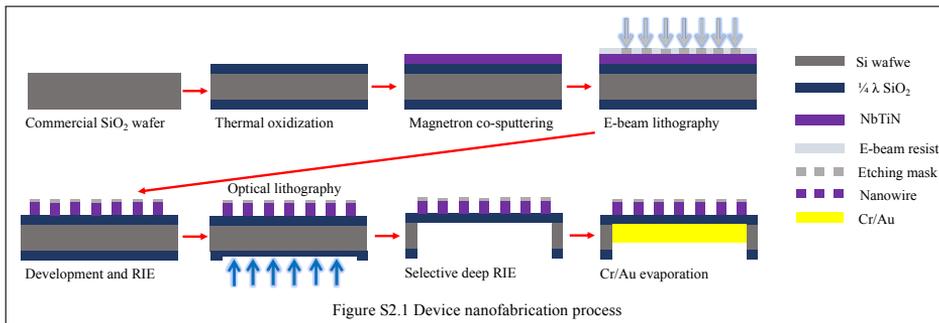
S3 Optical Simulation

We employed commercial software Lumerical for optical cavity simulation. To ensure accuracy, a mesh with a maximum mesh setting of 1/10 of the smallest feature size was applied around the meander. A power monitor was then placed over the meander layer to calculate light absorption. The absorption was then calculated as the net power flow into this monitor by normalizing to the total optical power.

S3.1 Comparison of FDTD and transfer matrix simulation and plasmonic loss in Au layer

For the optical constants, the following data was used. Since the thickness of Cr is much less than Au, and also Au diffuses into Cr layer, we take Au layer as reflector only in our simulation.

Fiber and ¼ λ layer:	SiO₂(Glass) – Palik.
Mirror:	Au (Gold) – CRC.
SNSPD meander:	NbTiN ellipsometry measurement of a film sputtered with a similar recipe.

In order to verify the reliability of our FDTD simulation, we performed extra transfer matrix simulation as described in [6] to compare and double check our FDTD simulation accuracy. As shown in figure 3.1 below, we show simulated absorption in the NbTiN layer with SiO2/Au membrane cavity at different air-gap. The FDTD simulation and transfer matrix simulation matched well with each other (difference«1%) and with proper airgap, absorption can reach 100% with both simulation methods. As a result, we would like to conclude that our simulations are concrete and solid. Another concern of the Au reflector is that there might be plasmonic loss in Au layer. We performed simulation to check this issue. As shown in figure 3.2, without NbTiN layer, indeed there is (1.2-1.6) % plasmonic loss, or absorption in Au layer with Au/Si structure, and absorption in Au is even higher (2.2-2.8 %) with SiO_2/Au/Si structure. But as shown in figure S3.1 above, as long as we add the thick NbTiN (9 nm) layer, the majority of the input light is absorbed by NbTiN layer. As a result, and absorption in Au is only a fraction of the "leftover light" after NbTiN's major absorption. With the existence of thick NbTiN layer, we can safely ignore the Au absorption issue.
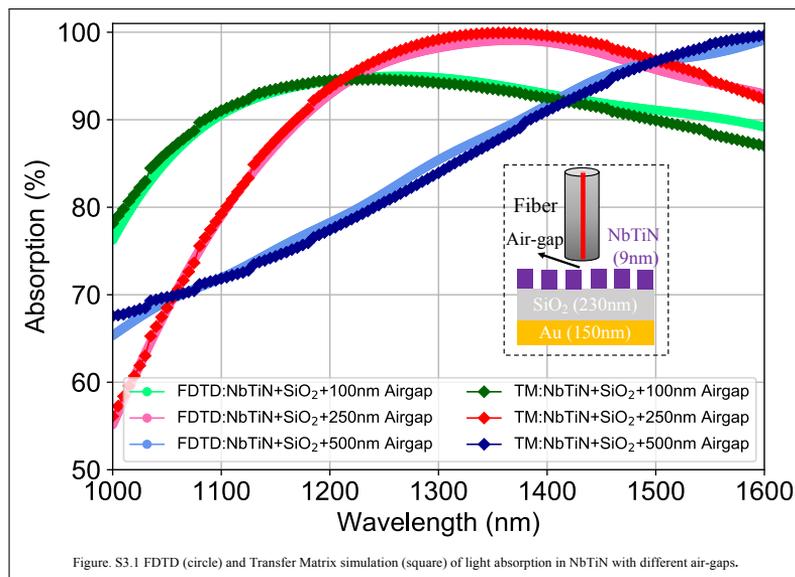
Figure. S3.1 FDTD (circle) and Transfer Matrix simulation (square) of light absorption in NbTiN with different air-gaps.

S3.2 Material optical properties and Au reflector simulation
The previous section S3.1 shows optical simulations based on commonly used 'CRC' Au data. However, in this work, our Au mirror was fabricated by thermal

Figure. S3.2 FDTD simulation of light absorption in Au layer with Au/SiO$_2$ (blue) and SiO$_2$/Au/Si (yellow) structure.
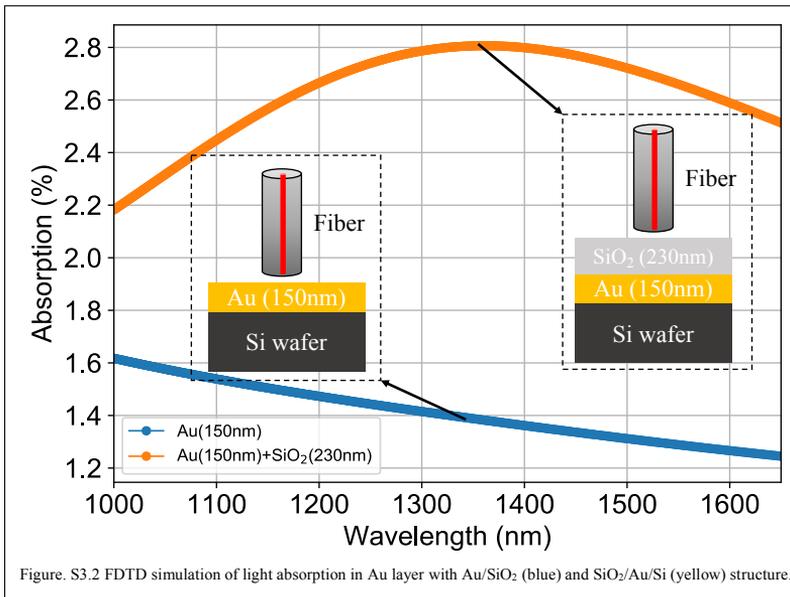
evaporation (Temescal FC2000) in Kavli Nanolab Delft. In order to better demonstrate the low plasmonic loss in Au, here we present extra data and simulations as follows. Figure S3.3 shows refractive index (n) and extinction coefficient (k) of our NbTiN from a similar sputtering recipe (left) and Au made in Kavli Nanolab Delft by thermal evaporation (right).

7

Fiber and ¼ λ layer:	SiO$_2$(Glass) – Palik.
Mirror:	Au (Gold) – Made by thermal evaporation (Temescal FC2000) in Kavli Nanolab Delft, and
	Au (Gold) – Commercially available gold mirror (from Thorlabs [8]).
SNSPD meander:	NbTiN ellipsometry measurement of a film sputtered with a similar recipe.

Figure S3.3 Refractive index (n) and extinction coefficient (k) of NbTiN (left) and Au made in Kavli Nanolab Delft (right).

Based on the n and k of NbTiN and Au (evaporated gold mentioned above, and commercial gold mirror from Thorlabs), we performed simulations to show that in the case of using evaporated Au, both air/Au (blue-dot curve) and SiO_2/Au (orange-dot curve) interfaces lead to absorption in Au within the range of (1.3-1.9) % at 1350nm, which means over (98.1-98.7) % of the light is reflected; On the other hand, when using commercial protected gold mirror (Thorlabs), air/Au (green-cross curve) and SiO_2/Au (red-cross curve) interfaces lead to absorption in Au within the range of (2.3-3.3) %, which means lower light reflection (96.7-97.7) %. This clearly shows that our evaporated gold has excellent light reflection performance thus it supports high system detection efficiency for the fabricated SNSPDs on top of it. These results are shown in figure S3.4. However, we would like to point out that for a complete optical cavity, air-gap and quarter-wavelength SiO_2 layer must also be considered. In figure S3.5, we present one specific simulation showing that with 2 μm airgap, 230 nm SiO_2 layer, as well as evaporated gold, more complex absorption scheme could be observed. Thus, for a real device, its system detection efficiency is really depending on the corresponding air-gap, SiO_2 thickness. The overall point is again that there's no fundamental limit on reaching >99% system detection efficiency by using our membrane optical cavity.

7
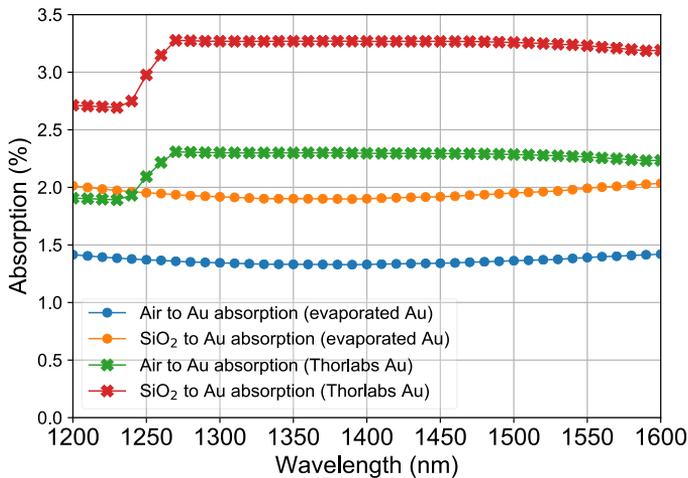
Figure S3.4 Light absorption in Au layer with air/Au interface (blue-dot for evaporated Au, green-cross for commercial Au) and SiO₂/Au interface (orange-dot for evaporated Au, red-cross for commercial Au).
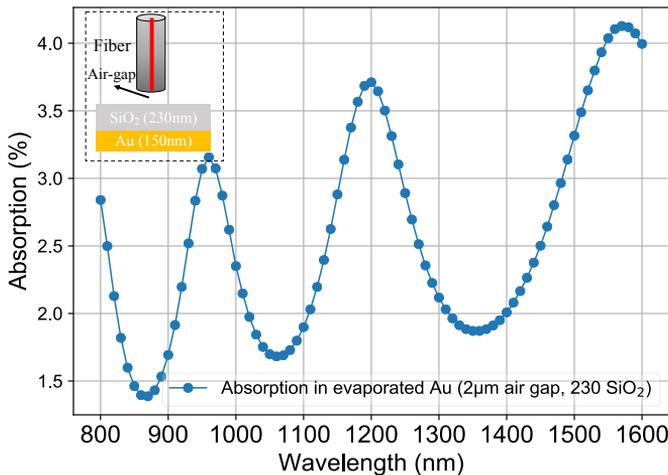
Figure S3.5 Light absorption in Au layer with evaporated gold, 2 μm air gap and 230 nm SiO₂ layer.

S4 Tunable laser source

In this work, we used a JGR-TLS5 tunable laser as light source for system efficiency measurements. As shown in the figure S4.1, we measured the laser spectrum with YOKOGAWA (AQ6374) optical spectrum analyzer. Figure S4.1. (a) shows the laser spectrum in the range of 1290-1650 nm; figure S4.1.(b) shows two measured wavelengths, 1340 and 1350 nm; and figure S4.1.(c) shows the laser spectrum at 1450 nm with FWHM linewidth of 0.1 nm. In table S4.2, detailed optical specifications of the laser are listed.

S5 Optical power meters

S4 Tunable laser source

In this work, we used a JGR-TLS5 tunable laser as light source for system efficiency measurements. As shown in the figure S4.1, we measured the laser spectrum with YOKOGAWA (AQ6374) optical spectrum analyzer. Figure S4.1. (a) shows the laser spectrum in the range of 1290-1650 nm; figure S4.1.(b) shows two measured wavelengths, 1340 and 1350 nm; and figure S4.1.(c) shows the laser spectrum at 1450 nm with FWHM linewidth of ~0.1 nm. In table S4.2, detailed optical specifications of the laser are listed.

Table S4.2 Optical specifications of the laser [2].

Parameter	Specification
Power stability	±0.01 dB
FWHM linewidth	0.1 nm
Side Mode Suppression Ratio @0.1nm BW	>60 dB
Wavelength stability	± 50 pm
Resolution	0.1 nm
Operation temperature	0-40 °C
Wavelength range	1260-1650 nm
Humidity	Maximum 95% RH (0 to 40 °C)
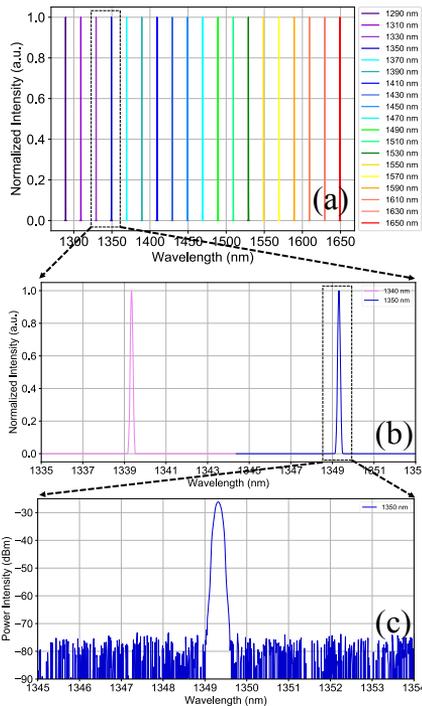
Figure S4.1. (a) Measured tunable laser spectrum at 1290-1650 nm, (b) measured laser spectrum at 1340 and 1350 nm, and (c) measured laser spectrum at 1350 nm.

Optical power meters can be used to measure CW laser power. In our work, we compared and measured the performance of three different types of semiconductor optical power meters. The details are shown in table S5.1. In our SDE measurement, we employed the Newport 818-IG-L (InGaAs) power meter for setting up the optical power attenuation ratio (for example, P_1/P_2=50dB, see figure S6.1) as well as measuring the optical power at the reference port (P1, see figure S6.1). The main reason for using Newport 818-IG-L power meter is because of high linearity (±0.5%), good accuracy (±2%) and of prime importance its high input dynamic range (20 pW-10 mW).

S6 Efficiency measurement stability

S6.1 Optical attenuator stability

Table S5.1 Performance of different types of semiconductor optical power meters.

Power meter Specification	Thorlabs S154C (InGaAs)	Newport 818-IG-L (InGaAs)	Newport 918D OD3R (Germanium)
Serial Number	190906316/ 190906317	N-12680	1659
Wavelength range	800-1700 nm	800-1650 nm	780-1800 nm
Optical power working range	100 pW-3 mW	20 pW-10 mW	5 nW-2 mW
Linearity	± 0.5%	± 0.5%	±2% @ 911-1700 nm
Measurement Uncertainty	± 5%	± 2%	± 2%

As shown in figure S6.1 (also described in the main text, see section 'Efficiency Measurement Setup'), the optical attenuator is built by setting up the power ratio P_1/P_2 = (50-60) dB. We measure the power P_1 and P_2 with Newport 818-IG-L power meter before and after SDE measurements as shown in table S6.2. As a result, the attenuation ratio before and after SDE is maintained at 50dB with an uncertainty of < 0.2%.

7
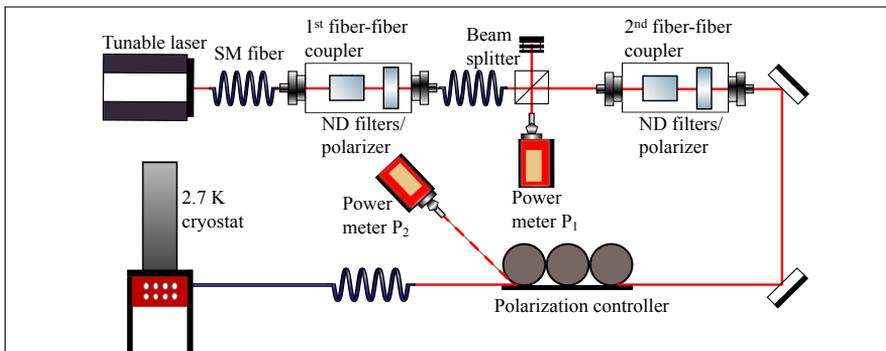
Figure S6.1 System detection efficiency measurement setup.

Table S6.2 Typical power meter readings before and after SDE measurement.

Powers meters Recorded values	Power meter P_1 (before SDE measurement)	Power meter P_2 (before SDE measurement)	Power meter P_1 (after SDE measurement)	Power meter P_2 (after SDE measurement)
Mean power	358.79 µW	3.59 nW	358.54 µW	3.59 nW
Attenuation ration	50 dB		50 dB	

S6.2 Optical input power stability

Since our SDE measurement setup has two ports: reference port (power meter P_1) and measurement port (power meter P_2), it allows us to monitor the input photon flux in real time during SDE measurement by reading power meter P_1. For example, after setting the attenuation ratio P_1/P_2=50 dB, we add neutral density filters in the first fiber-fiber coupler before the polarizer to make P_1=1 nW. Then we start SDE measurement and at the same time, we record the readings from power meter P_1 constantly. Table S6.3 and figure S6.4 show the reading from power meter P_1 during one of our SDE measurement and the input photon flux uncertainty is < 0.1%.

Table S6.3 Optical power P_1 reading during one SDE measurement						
Time	0-10 s	10-20 s	20-30 s	30-40s	40-50 s	50-60 s
Power P_1 (nW)	1.001	0.99961	1.0008	1.0006	0.99934	0.99955

Figure S6.4 Optical power P_1 reading during SDE measurement.
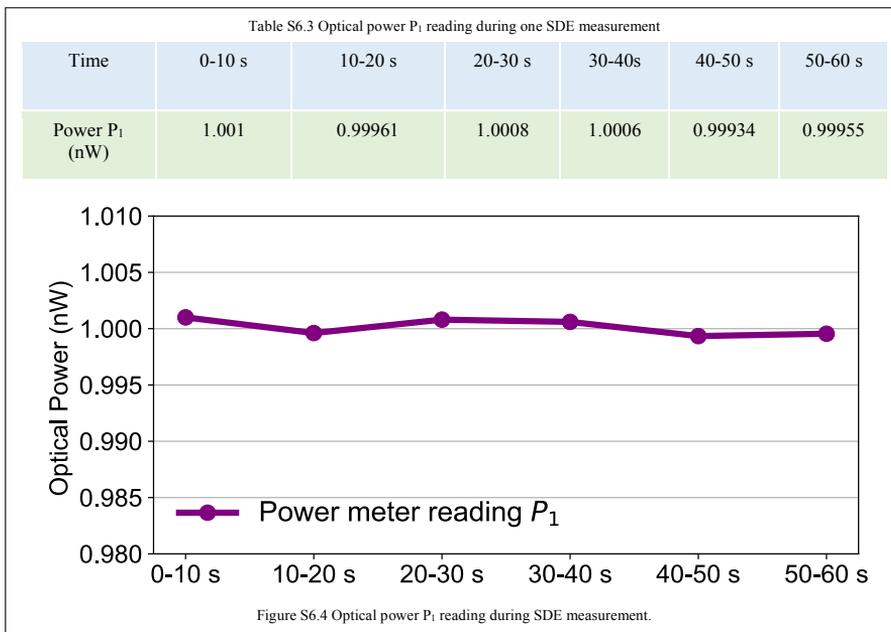
S7 Measurement uncertainty

For SDE measurement uncertainty, we considered all possible uncertainties in our experiments and then calculated the total measurement uncertainty with the root-mean-square (RMS) of the sum of the squared errors [3]. The uncertainties in our measurements include the power meter uncertainty (σ_1=2%) and its linearity uncertainty (σ_2=0.5%), laser stability uncertainty (σ_3<0.1%) and optical attenuator uncertainty (σ_4<0.2%). Our efficiency measurement has a total uncertainty of $\sqrt{\sigma_1^2 + \sigma_2^2 + \sigma_3^2 + \sigma_4^2} = 2.07\%$.

S8 Fiber end-face reflection S8.1 Simulation of fiber end-face reflection

As discussed in the main text (see section 'Fiber end-face reflection'), when measuring the laser power within the fiber with a power meter, the fiber end-facet is not in direct contact with the power meter's sensor. The existing fiber-to-air interface causes reflection, back towards the light source. On the other hand, physical contact polished fiber to fiber connections (when connecting the same fiber to the

system input fiber) have negligible back reflections (typically -30 to -40 dB). Thus, for all our efficiency measurements, we removed this back-reflection contribution by multiplying a correction factor of (1-Rrfl) [4]. Below we show FDTD simulation results of the fiber end-face reflection at different wavelengths. In short, we built the optical fiber structure (core radius 4.1 μm, refractive index 1.45625/cladding radius 62.5 μm, refractive index 1.45282) and then put a Gaussian mode source inside the fiber. A monitor was placed at the back side of the mode source and collected the reflected light from the fiber end-face and air interface. As shown in figure S8.1, the reflection Rrfl is in the range of 3.41-3.43% from 1300-1550 nm.

Figure S8.1 Simulated fiber end-face reflection at different wavelengths.
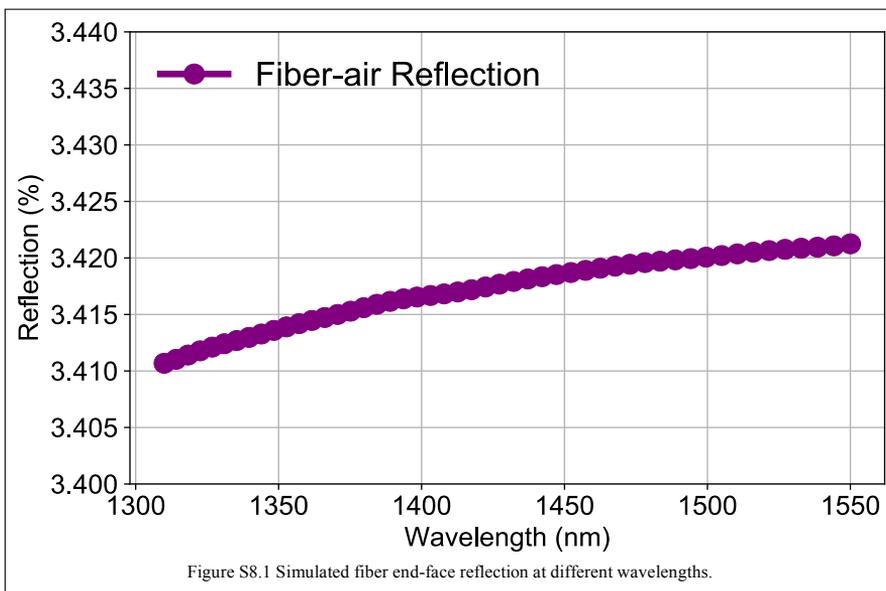
S8.2 Measurement of fiber end-face reflection

Besides FDTD simulation, we also experimentally measured the fiber end face reflection. Figure S8.2 shows how we experimentally acquire the value of Rrfl. Light from the tunable laser source pass through the free space fiber-fiber coupler (containing neutral density filter and polarizer) and goes to an optical circulator. Then light is directed to a polarization controller (PC) and at the end of the PC, the fiber is connected to either an optical reflector (connection 1), or an optical terminator (connection 2) or towards air (connection 3). The reflected light from the end of the PC is guided by the optical circulator to an optical power meter P1 and its power is recorded. The recorded reflection power from the above mentioned 3 different connections are recorded as P_{Ref}, P_{Ter} and P_{Air}. Based on these values, we acquired the fiber end face reflection value Rrfl = $(P_{Air}-P_{Ter})/P_{Ref}$. We acquired a R_{rfl} in the range of (3.4-3.6) % thus for our efficiency measurement, we considered a conservative correction factor of Rrfl = 3.6%.

S9 Polarization degree and polarization control

Since our detectors are patterned into meandering shapes, light absorption can

Figure 8.2 Fiber end-face reflection measurement.
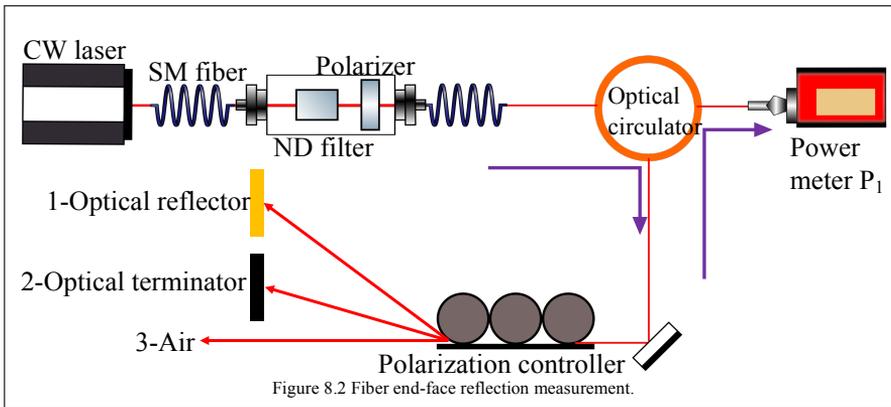
be significantly different based on the light polarization direction [5]. Thus, it is important to have a linearly polarized input light and fully control the polarization. In figure S9.1, we show the measurement of light polarization before connecting to the system for SDE measurement (set up is shown in figure S6.1) with a polarimeter (Thorlabs-PAX1000IR2/M). As shown from figure S9.1. (a) to S9.1. (f), by turning the polarization controller, we can fully control the polarization of the light. More importantly, in S9.1. (f) we show that the light has a degree of polarization of ∼100% (±0.09%), a degree of linear polarization of 99.97%. It indicates that the light is linearly polarized and its polarization can be fully controller by the polarization controller, which is important to reach near-unity SDE.

S10 Electronics counting circuitry uncertainty

As discussed before, N_{count} represents the count rate recorded by the commercial electronics driver (from Single Quantum) we used during the efficiency measurements. As presented below, we performed extra measurements to verify the accuracy of our electronics system. We created 10 MHz pulses signal by a Rohde & Schwarz signal generator (SMC100A) and the signal generator is synchronized to a Leobodbar GPS reference clock. Then the generated signal is sent to our commercial driver to record the count rate. Also, we double checked the count rate with a Rigol oscilloscope (DS2072A, it has built-in counter). As a result, the difference between our commercial driver's count rate with respect to both the signal generator and the oscilloscope were negligible (<0.01%). Also, according to the technical specification of the Rohde & Schwarz signal generator [7], its frequency error is below 10-7, thus we believe we can safely ignore the uncertainty caused by N_{count}.

Figure 9.1 (a)-(f) show fully control of light polarization and (g) shows that light for our SDE measurement is ~100% linearly polarized.

7

Figure 10.1 Verifying the accuracy of the electronics counting system.
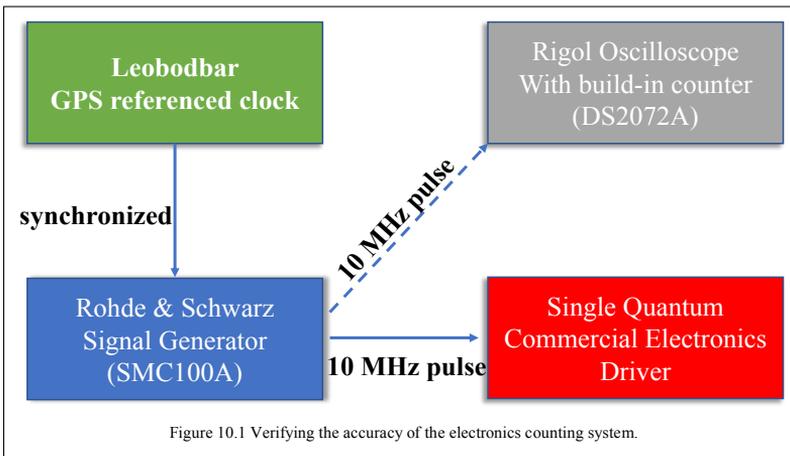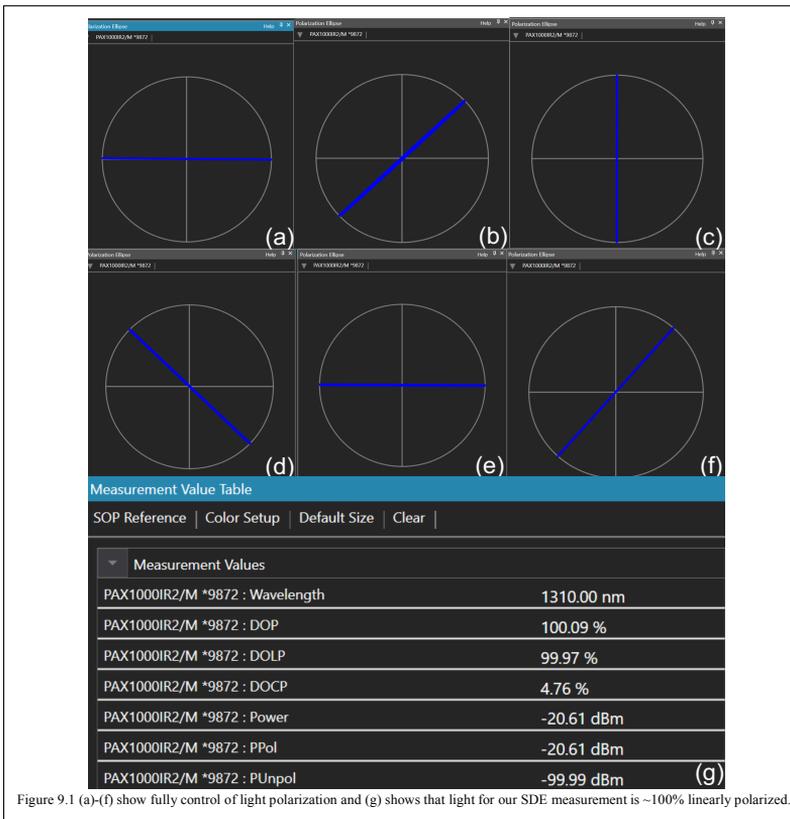
S11 References:

[1] Zichi, J. et al. Optimizing the stoichiometry of ultrathin NbTiN films for high-performance superconducting nanowire single-photon detectors. Opt. Express 27, 26579–26587 (2019).

[2] https://jgroptics.com/uploads/files/TLS5-Spec-Sheet-1020.pdf

[3] Marsili, F. et al. Detecting single infrared photons with 93% system efficiency. Nat. Photonics7, 210–214 (2013).

[4] Esmaeil Zadeh, I. et al. Single-photon detectors combining high efficiency, high detection rates, and ultra-high timing resolution. APL Photonics 2, 111301 (2017).

[5] Dorenbos, S. et al. Superconducting single photon detectors with minimized polarization dependence. Appl. Phys. Lett. 93, 233161102 (2008).

[6] Sunter, Kristen A., and Karl K. Berggren. "Optical modeling of superconducting nanowire single photon detectors using the transfer matrix method." Appl. Optics 57.17 (2018): 4872-4883

[7] https://cdn.rohde-schwarz.com

[8] https://www.thorlabs.com

7

8

Conclusion and future perspective

8.1. Conclusion of the thesis

Efficient and high time resolution single-photon detectors are an indispensable tool in a wide range of quantum information and quantum optics experiments. Tremendous efforts have been made in the past decades to have a deeper understanding of their operation mechanism and push their performance to a higher level. In this thesis, we started by optimizing and exploring novel superconducting films for making high-performance SNSPDs. Then, we fabricated multiple types of SNSPDs targeted for visible until mid-infrared wavelength based on the optimized films. Furthermore, We pushed SNSPDs' performance towards an "ideal" single-photon detector by realizing near-unity detection efficiency and sub-20 ps time resolution at the same time. The main achievements of this thesis can be concluded from the following three aspects:

(i) From the material aspect, we first tailor the composition and superconducting properties of $Nb_xTi_{1-x}N$ thin films by separately controlling the power applied to Nb/Ti targets during the reactive co-sputtering deposition process. We verify that the influence of the applied power on the T_c and on the internal detection efficiency of the detectors was mainly due to a change in the chemical composition of the ternary alloy. Our fiber-coupled devices fabricated from a 9-nm-thick film with DBR cavity achieve >80% SDE at 1550 nm, a timing jitter of 19.5 ps, and a fabrication yield of 30%. Besides, the minimal impact on the film properties when deposited on SiN substrate suggests the possibility to use the same room-temperature deposition recipe for integrating SNSPDs with temperature-sensitive photonic circuits. This work shows the internal efficiency of NbTiN based SNSPDs can be tuned and optimized by using the flexibility of the co-sputtering deposition process.

Though NbTiN based SNSPDs have demonstrated unprecedented time resolu-

tion when compared to amorphous superconducting materials (for example, WSi and MoSi), the poly-crystalline material nature makes NbTiN superconducting film suffers from degraded homogeneity, thus devices made from such materials suffer from low yield and more variation in their performance. As an alternative, for the first time, we reported SNSPDs made from NbRe, a novel superconducting film with a granular structure. The NbRe SNSPDs showed a clear saturated internal detection efficiency up to 1301 nm at 2.8 K with a time resolution of 33.1 ps, competitive with SNSPDs made from currently employed superconductors. Given that this is the first demonstration of NbRe based SNSPDs, there is still room for improvements, for example optimizing the film sputtering condition and employing better meandered nanowire designs. This work shows that NbRe-based devices are an alternative to Nitride-based SNSPDs in terms of better film uniformity, and to amorphous materials because of their improved time resolution and higher operating temperature.

(ii) We have significantly expanded NbTiN based SNSPDs' application scenarios by realizing two types of innovative SNSPDs: large-area multimode fiber-coupled SNSPDs, and mid-infrared SNSPDs. Conventionally, SNSPDs were coupled to single-mode fibers with a limited active area (5-10 μm diameter), in order to improve the photon collection efficiency for larger areas, we designed, fabricated, and characterized multimode fiber-coupled SNSPDs covering the wavelength range of (516-1550) nm. For visible wavelengths, we demonstrate multimode fiber-coupled SNSPDs with >80% system detection efficiency. However, for 878 nm and 1550 nm, we reach only 60% and 50% system detection efficiency because the polarization of incoming light is random. We also show that step-index multimode fibers introduce mode dispersion thus timing jitter histogram has multiple peaks. We solved this issue by using graded-index multimode fibers and together with cryogenic amplifier readout circuitry, the jitter of 50 μm diameter SNSPD reached sub-20 ps, which is exceptionally low comparing to previously published works. This work shows that large-size (20-50 μm diameter), multimode fiber-coupled SNSPDs can have high system detection efficiency and unprecedented timing resolution simultaneously.

Efficient mid-infrared photon detection is demanded for many emerging applications but very challenging because of decreased photon energy at longer wavelengths. Traditionally, small superconducting energy gap materials such as WSi and MoSi were used for mid-infrared detection. As a consequence, more costly and complex dilution fridges were needed to reach their working temperature (a few hundred mK). By using an optimized co-sputtering deposition recipe, our relatively thick (9.5 and 7.5 nm) NbTiN based SNSPDs reached saturated internal efficiency until 3 μm when operated in a 2.8K close-cycle Gifford-McMahon (GM) coolers. We demonstrate a fiber-coupled device with > 50% system detection efficiency from 1300-2000 nm with sub-15 ps time resolution. By employing end-facet coated fiber, the dark count rate (<100 Hz) was reduced by 3 orders of magnitude compared to the conventional single-mode fiber-coupled device (>10^4Hz). This work demonstrates that NbTiN based SNSPDs can efficiently detect mid-infrared single photons with sub-20 ps timing jitter. So far, this is the best-reported mid-infrared SNSPD from a poly-crystalline superconducting film. More importantly, it reveals the capability of NbTiN superconducting material for mid-infrared detecting without cooling

the detectors to mK temperature, which is the working temperature for most amorphous materials-based SNSPDs. As a result, we offer a solid candidate - NbTiN - for making future mid-infrared SNSPDs with high system detection efficiency and time resolution.

(iii) From a reliable and high-efficiency detection aspect, we demonstrate telecom wavelength SNSPD with exceeding 99.5% SDE at 1350 nm (time jitter of 35 ps, with room temperature amplifiers), and over 98% SDE at 1425 nm (time jitter of 26 ps with cryogenic amplifiers). Detectors from the same batch reach SDEs above 94% with peaks in the wavelength range of 1280-1500 nm and sub-20 ps (best detector 15 ps) time jitter using cryogenic amplifiers.

The near-unity efficiencies were achieved by using optimized thick NbTiN superconducting film with saturated internal efficiency, broadband membrane cavity coupled to small detectors (diameter of 16 μm), and accurate system efficiency measurements. Also, we show how to combine the SNSPD merits of near-unity efficiency, short recovery time, low dark count rate, and unprecedented timing resolution at the same time. We believe our near-unity efficiency SNSPDs will highly benefit scientific demonstrations and industrial applications where multiphoton correlation measurements are needed, for example, second-order photon correlation measurement and photonic implementation of Boson sampling.

Detectors shown in this thesis have already been used by our collaborators (researchers) for multiple quantum optics experiments, including stimulated emission depletion microscopy (STED), light range and detection (LiDAR) [1], quantum key distribution (QKD) [2], boson sampling, and bio-imaging in many countries, and besides scientific exploration, this thesis gives inspiration for commercial production of SNSPDs by offering optimized recipes for magnetron co-sputtering of NbTiN superconducting thin film, showing novel NbRe materials as a new SNSPDs candidate, and presenting accurate SNSPDs lab characterization methods.

8.2. Perspective on future SNSPDs

Considering the work presented in this thesis and recently published papers towards near-unity efficiency SNSPDs [3, 4], we would like to conclude that after nearly two decades of development since 2001 [5], SDEs of SNSPDs have drastically improved from below 1% to near-unity (> 98-99%). At the same time, the jitter of SNSPDs has been pushed down to < 10 ps [6, 7], which makes SNSPDs the currently best available technology for efficient single-photon detection in a wide electromagnetic spectrum range [8, 9] with unprecedented timing resolution. However, the performance of SNSPDs available nowadays is still not perfect. In the future, we foresee many challenges ahead of us to make better single-photon detectors.

(a) From improving SNSPDs' performance perspective, many challenges still exist. For example, as predicted in [10], when biasing current is close to its depairing current, SNSPDs' jitter can be as small as $\hbar/k_B T_c$ (k_B is the Boltzmann constant and T_c is the critical temperature, and for a device with 10 K critical temperature, the lowest jitter was predicted to be 0.8 ps). However, the best-reported timing jitter of an SNSPD so far is still far from this value [7]. Also, though detecting single photons with saturated internal efficiency up to 10 μm was shown [8, 11], it

came with the consequence of sacrificing the detection area (only 10-μm-long line). Given that the superconducting energy gap of superconductors for making SNSPDs is typically a few meV, longer wavelength (10-100 μm) single-photon detection is yet to be achieved.

It is worth mentioning that SNSPDs characterization becomes more challenging when it comes to long-wavelength ($> 2\mu$m) characterization or high accuracy characterization (<0.5% error bar). For example, most SNSPDs' system efficiency measurements rely on using semiconductor optical power meters as a reference and employ fainted lasers as quasi-single-photon sources. The former condition leads to limited measurement accuracy (typically 0.5-5%) and the latter inevitably introduces multi-photon detection events, whose influence on SNSPD's timing jitter and high count rate response has not been throughout studied.

(b) From practical applications' point of view, near-term challenges include: (i) How to make larger SNSPDs for applications where an active area of hundreds of micrometers or even a centimeter-scale is needed? This requires fabricating superconducting film with excellent uniformity and detection response as well the use of large SNSPDs arrays; (ii) How to fabricate and read out an SNSPD camera with thousands or millions of pixels? This requires new designs of multipixel SNSPDs as well as scalable read-out circuitry; (iii) How to improve the working temperature of SNSPDs so that more compact and inexpensive cryostat can be utilized? This requires high-temperature superconductor material with good detection performance; (iv) How to improve the yield of high-performance detectors to lower the commercial SNSPD systems' costs? This requires a better understanding of SNSPDs' detection mechanism, employing robust device design and fabrication recipe, and high-throughput SNSPDs characterization. If the above-mentioned aspects can be realized, SNSPDs will enable more ground-breaking quantum optics applications and experiments in the future.

8

References

[1] T. Staffas, *Live 3D imaging quantum LiDAR,* (2021).

[2] M. Pittaluga, M. Minder, M. Lucamarini, M. Sanzaro, R. I. Woodward, M.-J. Li, Z. Yuan, and A. J. Shields, *600-km repeater-like quantum communications with dual-band stabilization,* Nature Photonics , 1 (2021).

[3] P. Hu, H. Li, L. You, H. Wang, Y. Xiao, J. Huang, X. Yang, W. Zhang, Z. Wang, and X. Xie, *Detecting single infrared photons toward optimal system detection efficiency,* Optics Express **28**, 36884 (2020).

[4] D. V. Reddy, R. R. Nerem, S. W. Nam, R. P. Mirin, and V. B. Verma, *Superconducting nanowire single-photon detectors with 98% system detection efficiency at 1550 nm,* Optica **7**, 1649 (2020).

[5] G. Gol'tsman, O. Okunev, G. Chulkova, A. Lipatov, A. Semenov, K. Smirnov, B. Voronov, A. Dzardanov, C. Williams, and R. Sobolewski, *Picosecond superconducting single-photon optical detector,* Applied physics letters **79**, 705 (2001).

[6] I. Esmaeil Zadeh, J. W. Los, R. B. Gourgues, V. Steinmetz, G. Bulgarini, S. M. Dobrovolskiy, V. Zwiller, and S. N. Dorenbos, *Single-photon detectors combining high efficiency, high detection rates, and ultra-high timing resolution,* APL Photonics **2**, 111301 (2017).

[7] B. Korzh, Q.-Y. Zhao, J. P. Allmaras, S. Frasca, T. M. Autry, E. A. Bersin, A. D. Beyer, R. M. Briggs, B. Bumble, M. Colangelo, *et al.*, *Demonstration of sub-3 ps temporal resolution with a superconducting nanowire single-photon detector,* Nature Photonics **14**, 250 (2020).

[8] V. Verma, A. Lita, B. Korzh, E. Wollman, M. Shaw, R. Mirin, and S. Nam, *Towards single-photon spectroscopy in the mid-infrared using superconducting nanowire single-photon detectors,* in *Advanced Photon Counting Techniques XIII*, Vol. 10978 (International Society for Optics and Photonics, 2019) p. 109780N.

[9] K. Inderbitzin, A. Engel, A. Schilling, K. Il'in, and M. Siegel, *An ultra-fast superconducting Nb nanowire single-photon detector for soft x-rays,* Applied Physics Letters **101**, 162601 (2012).

[10] D. Y. Vodolazov, *Minimal timing jitter in superconducting nanowire single-photon detectors,* Physical Review Applied **11**, 014016 (2019).

[11] V. Verma, B. Korzh, A. Walter, A. Lita, R. Briggs, M. Colangelo, Y. Zhai, E. Wollman, A. Beyer, J. Allmaras, *et al.*, *Single-photon detection in the mid-infrared up to 10 micron wavelength using tungsten silicide superconducting nanowire detectors,* arXiv preprint arXiv:2012.09979 (2020).

8

Acknowledgements

Finally, it has come to the moment of writing acknowledge section, which means I'm very close to the finishing line of the long PhD study journey! At this very special moment, I'd like to express my sincere appreciations and thanks to all the people who have significantly helped me in the past years. Without your helps, I can barely imagine what my life would be like.

First, I'd like to thank my **parents**, my **parents in law**, my wife **Yun** and all my family members and relatives for their unconditional love. Your supports give me the strength to chase all dark clouds away, and I want to say I love you!

My PhD promoter, **Val**, also my lifelong friend, has enabled all the works in the past years. I still remember the first time I had Skype with you talking about joining your group in 2016; remember for many times you drove the boat to picked me up from the seaside for dinner at your home on Stockholm island; remember every time meeting, drinking and discussing with you in different places and the second day was always filled with hopes and motivations; remember you would reply to every of my email in a few minutes and tell me go for it! You're the greatest mentor I've ever seen, thanks Val!

My PhD promoter, **Paul**, as I always told others that you're not only a distinguished professor, but also a real gentleman. Without your help I could not come to TUDelft and started my PhD. You have significantly supported all my PhD activities and unconditionally signed all documents for me, thanks Paul!

My postdoc promoter, **Simon**, I feel lucky and excited to join your group for the coming years of research on optomechanics. You have sharp understanding of science and quantum technology, and I definitely believe we will make great works together in the coming years!

Professor **Lixing You** initiated my research in SNSPDs by helping me for my PhD scholarship application in 2016. Without your help, I may lose the opportunity to enter the SNSPD community. Also, you have profound version of SNSPDs' development: Your review paper a few years ago had predicted every possible progress in SNSPDs community so far! I still remember that you told me, 'welcome to the SNSPD family'. Now I can say we are family members!

Professor **Robert Hadfield**, it's my honor to have you in my PhD committee. You're the best SNSPD expert and quantum optics scientist I knew. I still remember that in 2018, we firstly met in Bad Honnef and discussed important scientific questions. Thanks for revising my thesis!

Professor **Blanter Yaroslav**, thanks for joining my PhD committee. It's nice to know you on both the first day of my PhD and meet you again on the first day of my postdoc. I never doubt that I can find all physics questions' answers and hints of solutions from your office. Since I have moved to next door to your office, I'm one step closer to physics!

Professor **Dennis Schaart**, a great physicist in high-energy physics, a great collaborator to work together and a great member to have in my defense committee. I hope we can still push research of positron emission tomography in the future together!

My dear friend, CEO of Single Quantum, Dr. **Sander** is the best CEO I've ever seen. Sander, you're a genius researcher and I never doubt that there are answers to every SNSPD question in your PhD thesis back in 2011. You have significantly supported all kinds of experiments in my PhD period and I enjoy every time drinking together with you (and Val)! I firmly believe my connection with SQ will never be disconnected.

I'd also like to take this opportunity to give my special thanks to three giants: professor **Teunis Klapwijk**, professor **Peiheng Wu** and professor **Qifeng Yu**. You're well-established scientists; I'm a young, inexperienced student, however, you replied every of my naive questions with great enthusiasms and pointed out promising directions for me when I feel lost. All of you are the light-towers in the sailing of my life, thanks!

Above are the 'bosses' who set up the solid platform to guarantee my smooth PhD study. On top of that, I learned all the fancy research ideas, hard-core lab skills, and positive life attitude from my best friends in TUDelft and Single Quantum:

Professor **Iman**, you have a mind of great ideas and have taught me numerous of lab-skills and research ideas. It's an enjoyable experience working together with you, and we were also very productive in the past years! We kept pushing the performance records of SNSPDs to higher levels until no one can easily make it better. I'm 100% sure we will keep making more exciting papers in the future, just do it!

My dear friend, **Niels Los**, you once told me that there must be thousands of 'Jins' competing with me in China. It might be true, but I doubt how many of them could be as lucky as me to have the help of 'Niels' during the PhD. You're a real encyclopedia of SNSPDs, and I gained great amount of skills from you in the past years. Also, I enjoyed every time our chatting about life, science, economics, and our ultimate list of stocks to buy. We still have so many unfinished plans, and let's realize them in the future!

My dear friend, **Andreas Fognini**, you are the earliest mentor in my PhD life. I still remember that you showed me how to use command line while I was struggling to start programming; You trained me to use solder station to make my first electronic amplifier and many more. I always wonder how many fancy ideas you have in your mind, and you are also a great friend in life. I wish you and your family all the best!

Of course, I'd like to thank everyone in the Optics Research Group. Every one of you have made my PhD life full of happiness and joys: Many thanks to dear **Silvania** for revising my paper with great patience every time, to professor **Jianrong Gao** and **Behnam** for teaching me THz detector knowledge, to **Yvonne**, **Roland** and **Thim** for all kinds of supports, to **Omar, Aurule, Yifeng, Xi Zheng, Min, Sven, Sergei, Yuri, Jeff, Wenye, Dmytro, Thomas and Malee** for making my life colorful and special thanks to my roommate **Alex** for all the physics discussions! I

wish one day you could finish learning the physics courses on the list!

My PhD would be ten times more difficult without the support of **Single Quantum**, and I gained great knowledge and industrial experience in the past years by working together with the outstanding people in SQ. Here, I'd like to thank **Jessie** first. Thought we were not directly working together in the lab, I knew that you always support me when I need help, and you always think for me when there is a change in work or life. Thanks, Jessie! Dear **Tim**, you supported me as much as Jessie did, and I really appreciate the friendship between us. You are not only a great manager, but also a gentleman with great wisdoms. I enjoy every time talking to you and learn life philosophy from you! Dear **Jason**, I cannot wait for the next travel back to China and meet you again, even sometimes in my dream, I have travelled back. Every time meeting you was full of fun, great food and free upgrade for fancy hotel rooms. You have greatly expanded SQ China business and wish you a bigger success in the coming future!

I'd also like to thank many more SQ colleagues: **Sergiy**, the real expert in nano fabrication and my mentor in the clean room. I enjoy a lot of the time going to clean room with you and travel to Stockholm together. We will still meet in the coming years I believe! **Rene**, my dear friend, you always count me on many activities, and I really appreciate that! You took me to the training in the seaside and invited me to your birthday parties, and I like those beautiful memories! Dr. **Ronan**, Dr. **Antonio**, my friend **Machail**, I like the days that we worked together in the labs and on the campus. You are not only my colleagues, my friends, but also my 'classmates'. Good luck to all your future careers! My dear friends in SQ nanofab team, I'd like to say that you guys can build anything if you want! I never doubt that besides SNSPDs, you can build quantum computers, integrated circuits, and all kinds of fancy devices. I learned great knowledge from every one of you, dear **Nima, Niels Noordzij, Gertjan and Oscar**, thanks! Also, every colleague in SQ, I'm standing on your shoulders and that's why I can do experiments faster than other students, thank you, dear **Mario, Monique, Gijs, Yves, Masoume, Federica, Mikayla, Jan, Annalisa, Jeroen, Peiyi, Henri, John, Monique, Eduard, Jelle, Alexis, Bea, Nicolai, Eddy, Gabriele, Victor and everyone**! (SQ is growing everyday so please forgive me if I miss anyone.)

In Stockholm, there are beautiful sceneries, delicious food and more importantly, good friends in KTH! The one who made the best NbTiN films in the world, **Julien and Stephan**. Without your films, we could almost do nothing in the lab. Also, I had good memories together with **Ali, Samuel, Thomas, Bruno, Klaus, Lucas, Katha, Marijn, and Michael** either in winter school in the Alps mountain, in Stockholm sea swimming next to Val's house or meeting in Delft. Good luck to every one of you!

During my PhD time, it was great to know excellent Chinese professor **Xiaolong Hu and Labao Zhang**. Professor Hu is a talented researcher and a good friend. I got many inspirations from you and personal suggestions in research direction. Professor Zhang is my alumnus from NWPU and also leading young researcher in SNSPDs, and I hope to meet you soon, maybe in Nanjing!

Very special thanks to four great teachers, friends and brothers (if I may) that

8

Curriculum Vitæ

Jin Chang

1990.9	Born in Zibo City, Shandong Province, China.

Education

2010–2014	BSc in Materials Physics Northwestern Polytechnical University (China)
2014–2016	MSc in Materials Physics National University of Defense University (China)
2017–2021	PhD. Physics Delft University of Technology (the Netherlands) *Thesis:* Detecting Single Photons with Superconducting Nanowires *Promotor:* Prof. H.P. Urbach & Prof. Val Zwiller

Awards

2014	Excellent Graduate, Northwestern Polytechnical University
2016	Outstanding Student, National University of Defense Technology

List of Publications

Journal Papers

10. Y. Gan, B. Mirzaei, J.R.G. Silva, **Chang, J.**, S. Cherednichenko, F. van der Tak, and J.R. Gao. Low noise MgB_2 hot electron bolometer mixer operated at 5.3 THz and at 20 K, in preparation, 2021.

9. **Chang, J.**, Johannes WN Los, Ronan Gourgues, Stephan Steinhauer, S. N. Dorenbos, Silvania F. Pereira, H. Paul Urbach, Val Zwiller, and Iman Esmaeil Zadeh Mid-infrared Single-photon Detection Using Superconducting NbTiN Nanowires with Sub-15 ps Time Resolution in a Gifford-McMahon Cryocooler. ArXiv:2107.06354 (2021).

8. I. Esmaeil Zadeh, **Chang, J.**, Johannes W. N. Los, Samuel Gyger, Ali W. Elshaari, Stephan Steinhauer, Sander N. Dorenbos, and Val Zwiller "Superconducting Nanowire Single-Photon Detectors: a perspective on evolution, state-of-the-art, future developments and applications", Appl. Phys. Lett. 118, 190502 (2021) (***Invited paper***)

7. **Chang, J.**, Los, J. W. N., Tenorio-Pearl, J. O., Noordzij, N., Gourgues, R., Guardiani, A., Zichi, J.R., Pereira, S.F., Urbach, H.P., Zwiller, V. and Dorenbos, S.N. and Esmaeil Zadeh, I. (2021). Detecting telecom single photons with 99.5− 2.07+ 0.5% system detection efficiency and high time resolution. APL Photonics, 6(3), 036114. (***Editor's Pick***)

6. Cirillo, C., **Chang, J.**, Caputo, M., Los, J.W.N., Dorenbos, S., Esmaeil Zadeh, I. and Attanasio, C., 2020. Superconducting nanowire single photon detectors based on disordered NbRe films. Appl. Phys. Lett. 117(17), p.172602.

5. Esmaeil Zadeh, I., Los, J.W., Gourgues, R.B., **Chang, J.**, Elshaari, A.W., Zichi, J.R., van Staaden, Y.J., Swens, J.P., Kalhor, N., Guardiani, A. and Meng, Y., 2020. Efficient single-photon detection with 7.7 ps time resolution for photon-correlation measurements. ACS Photonics, 7(7), pp.1780-1787.

4. **Chang, J.**, Zadeh, I.E., Los, J.W., Zichi, J., Fognini, A., Gevers, M., Dorenbos, S., Pereira, S.F., Urbach, P. and Zwiller, V., 2019. Multimode-fiber-coupled superconducting nanowire single-photon detectors with high detection efficiency and time resolution. Applied Optics, 58(36), pp.9803-9807. (***Editor's Pick***)

3. Zichi, J., **Chang, J.**, Steinhauer, S., Von Fieandt, K., Los, J.W., Visser, G., Kalhor, N., Lettner, T., Elshaari, A.W., Zadeh, I.E. and Zwiller, V., 2019. Optimizing the stoichiometry of ultrathin NbTiN films for high-performance superconducting nanowire single-photon detectors. Optics Express, 27(19), pp.26579-26587.

2. Gourgues, R., Los, J.W., Zichi, J., **Chang, J.**, Kalhor, N., Bulgarini, G., Dorenbos, S.N., Zwiller, V. and Zadeh, I.E., 2019. Superconducting nanowire single photon detectors operating at temperature from 4 to 7 K. Optics Express, 27(17), pp.24601-24609.

1. Jia, J., Bai, S., Xiong, D., Wang, J. and **Chang, J.**, 2019. Effect of tungsten based coating characteristics on microstructure and thermal conductivity of diamond/Cu composites prepared by pressueless infiltration. Ceramics International, 45(8), pp.10810-10818.

Conference Paper and Presentation

3. Steinhauer, S., Gyger, S., Elshaari, A.W., Zichi, J., Zadeh, I.E., **Chang, J.**, Los, J.W., Kalhor, N., Dorenbos, S. and Zwiller, V., 2020. Superconducting Nanowire Devices for Light Detection at the Single-Photon Level. Multidisciplinary Digital Publishing Institute Proceedings, 56(1), p.4.

2. **Chang, J.**, Zadeh, I.E., Los, J.W., Zichi, J. and Zwiller, V., 2019, May. Large diameter superconducting nanowire single photon detectors (SNSPDs) with high efficiency and high time resolution (Conference Presentation). In Quantum Optics and Photon Counting 2019 (Vol. 11027, p. 1102705). International Society for Optics and Photonics.

1. **Chang, J.**, Zadeh, I.E., Los, J.W., Zichi, J. and Zwiller, V., 2019, May. Superconducting Nanowire Single Photon Detector with High Efficiency and Time Resolution for Multimode Fiber Coupling. In CLEO: QELS Fundamental Science (pp. FF1A-2). Optical Society of America.

European Project

1. Zadeh, I.E., **Chang, J.**, Dorenbos, P., Dorenbos, S.N., Krämer, K., Siebbeles, L.D. and Schaart, D.R., 2020. PIZZICATO: Picosecond Scintillator Timing with Superconducting Nanowire Single-Photon Detectors.